



ISSN 1454-8518

**ANNALS
OF THE UNIVERSITY OF
PETROȘANI**
ELECTRICAL ENGINEERING
VOL. 19 (XLVI)

**UNIVERSITAS PUBLISHING HOUSE
PETROȘANI - ROMANIA 2017**

EDITOR OF PUBLICATION

Prof. Ioan-Lucian BOLUNDUȚ Ph.D, Email: ibol@upet.ro

ADVISORY BOARD

Prof. Alexandru BITOLEANU, Ph.D. - University of Craiova, *Romania*; **Prof. Dr. Stanislaw CIERPISZ** – Silesian University of Technology, *Poland*; **Prof. Aurel CAMPEANU** Ph.D, Member of the Academy of Technical Science of *Romania*, *Romania* **Prof. Tiberiu COLOȘI**, Ph.D., - Member of the Academy of Technical Science of *Romania*, President of Cluj Branch; **Dr. Eng. Nicolae DAN** - Dessault Systems Simulia Corp., Providence, *USA*; **Assoc. Prof. Daniel DUBOIS**, Ph.D. - University of Liège, *Belgium*; **Prof. Ion Fotau**, Ph. D. - University of Petrosani, *Romania*; **Eng. Emilian GHICIOI**, Ph.D. - INCD INSEMEX Petrosani, *Romania*; **Prof. Emerit Mircea EREMIA**, Ph.D. – Member of the Academy of Technical Science of *Romania*; **Prof. Dr. Vladimir KEBO** -Technical University of Ostrava, *Cehia*; **Assoc. Prof. dr. Ernő KOVÁCS** - University of Moskolc, *Hungary*; **Prof. Gheorghe MANOLEA**, Ph.D. - Member of the Academy of Technical Science of *Romania*, *Romania*; **Prof. Radu MUNTEANU**, Ph.D. – Member of the Academy of Technical Science of *Romania*, *Vice President*; **Assoc. Prof. Dan NEGRUT**, Ph.D. -University of Wisconsin, Madison, *USA*; **Acad. Prof. Dr. Genadiy PIVNYAK** – National Mining Uninersity Dnepropetrovsk, *Ukraine*; **Prof. Emil POP**, Ph.D - University of Petroșani, *Romania*; **Prof. Flavius Dan ȘURIANU**, Ph.D. – “Politehnica” University of Timișoara, *Romania*; **Prof. Willibald SZABO**, Ph.D. – “Transilvania” University of Brașov, *Romania*; **Prof. Alexandru VASILIEVICI**, Ph.D. – “Politehnica” University of Timișoara, *Romania*.

EDITORIAL BOARD

Editor-in-chief:

Prof. Susana ARAD, Ph.D., University of Petroșani
Assoc. Prof. Liliana Brana SAMOILĂ, Ph.D., University of Petroșani

Associate Editor:

Assoc. Prof. Nicolae PĂTRĂȘCOIU, Ph.D., University of Petroșani
Assoc. Prof. Ilie UȚU, Ph.D., University of Petroșani, University of Petroșani
Assoc. Prof. Olimpiu STOICUȚA, Ph.D., University of Petroșani

Editor Secretary:

Lecturer Dragos PASCULESCU, Ph.D., University of Petroșani
Lecturer Florin Gabriel POPESCU, Ph.D., University of Petroșani

Editorial office address: Ec. Radu Ioan, University of Petroșani, 20 University Street, 332006 Petroșani, Romania, Phone: (40) 254/54.29.94; 54.25.80; 54.25.81; 54.33.82; Fax: (40) 254/54.34.91; 54.62.38,

Contact person: Susana ARAD, e-mail: susanaarad@yahoo.com

This publication is spread in 28 countries.

CONTENTS

1. Gelu Ovidiu Tirian , <i>Smart home automation with arduino</i>	5
2. Leon Pana, Florin Gabriel Popescu , <i>Evaluation of the moments load and maximum allowable voltage drop for overhead and underground power lines</i>	15
3. Leonard Lupu, Florin Adrian Paun, Dan Gabor, Adrian Jurca , <i>Researches regarding determination of the electrical parameters for safe and reliable initiation of the electrical detonators</i>	27
4. Maria Daniela Stochitoiu, Ilie Utu , <i>The benefits of the intelligent production</i>	35
5. Leon Pana, Marius Daniel Marcu , <i>Determination of the maximum length of 20 kV overhead power lines</i>	39
6. Maria Daniela Stochitoiu, Ilie Utu, Liliana Samoila , <i>The modern approachement of power factor</i>	45
7. Marcel Daniel Rad, Mihai Magyari, Sorin Burian, Lucian Moldovan, Dragos Fotau , <i>Verifying the parameters of electric motors acting on fans operating in explosive atmospheres with gases, vapors, mists and dusts</i>	53
8. Tiberiu Csaszar, Sorin Burian, Marius Darie, Cosmin Colda, Adriana Andris , <i>Aspects on testing of galvanic cells for electrical equipment intended for use in potentially explosive atmospheres</i>	63
9. Zhao Qi , <i>Management platform of confucius institute</i>	71
10. Brana Liliana Samoila, Letitia Susana Arad , <i>Virtual instrument for simulating three-phase ac circuits</i>	79
11. Susana Arad, Liliana Samoila , <i>Hydrogen, potential energy source</i>	87
12. Ilie Utu, Maria Daniela Stochitoiu , <i>Modernization of asynchronous motor electric drives supplied by igct static power converters</i>	95
13. Nicolae Patrascioiu, Cosmin Rus, Cecilia Rosulescu , <i>Virtual instrumentation used in study of dynamic regim of the dc motor</i>	103
14. Olimpiu Stoicuta, Lorand Bogdanffy , <i>Simulating the speed and rotor resistance observer in sensorless vector control systems with induction motors</i>	113
15. Olimpiu Stoicuta, Lorand Bogdanffy , <i>Electrical and mechanical parameters estimation of an induction motor</i>	129

SMART HOME AUTOMATION WITH ARDUINO

GELU-OVIDIU TIRIAN¹

Abstract: The paper presents a completely new approach in the field of smart home automation, being a very efficient solution that can also be used in electrical and home appliances. In the work was made a model that is a smart house. The components were assembled so that they could control a house. They can open a door, a garage, detect if someone forces the door at the entrance, light up, pick up and leave the blind, read the level of brightness, and communicate with mobile phone.

The smart house has two servo motors, a light sensor, a temperature and humidity sensor, a power led, a stepper motor, a voltage stabilizer, a bluetooth and an Arduino Mega development board. The house receives command values from the phone and, depending on the values received, it can make decisions through the Arduino Mega command plate. Programming was done using the Arduino software. The order process is to program the components according to the value received from the created application.

The solution proposed represents the modern and efficient method of automation and remote control of smart homes.

Keywords: solar, photovoltaic, energy, conversion, orientation.

1. INTRODUCTION

A smart building is the fusion of technology, design and energy systems. They are well managed, have well-integrated physical and digital infrastructure that provides reliable, cost-effective and sustainable occupancy services. Smart buildings help their owners improve asset reliability and performance, which in turn reduces energy consumption, optimizes how space is used and minimizes the environmental impact of their buildings [1]. Among the properties of a smart building, we mention: it provides data on the performance of the building systems and facilities; monitors in real time and detects errors or deficiencies in construction systems [2]; reports in real time [4] and uses the management of operations, energy and occupant comfort; includes tools, technologies, resources and systems to help conserve energy and environmental sustainability [3].

¹ *PhD., Assistant Eng., Politehnica University Timisoara*

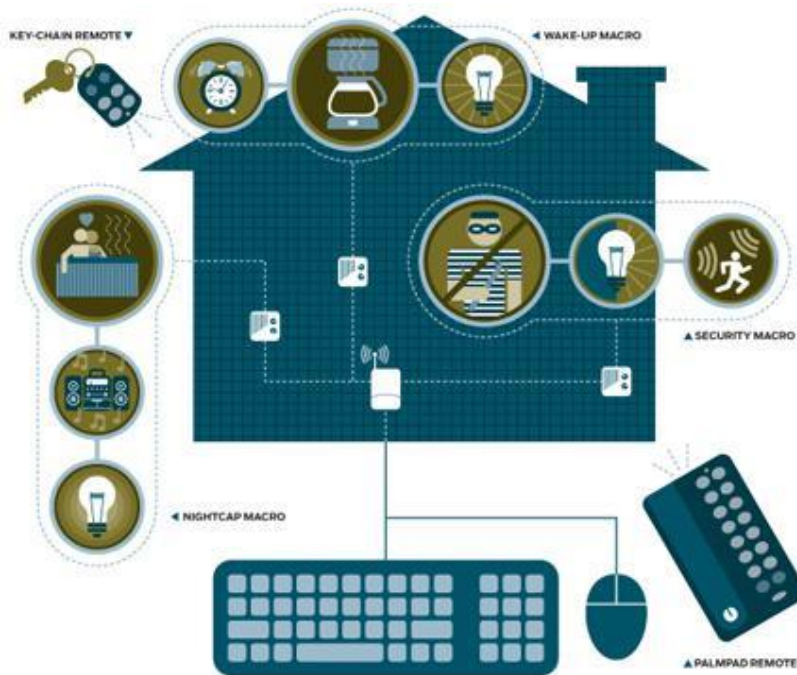


Fig. 1. Control system and monitoring in a smart home

2. FUNCTIONALITY AND STRUCTURE OF A SMART BUILDING

We can look at an smart building as a system that is divided into the following subsystems [4], [12]:

- information and telecommunications technology subsystem
- the security and alarm subsystem
- automated power monitoring and supervision subsystem
- subsystem of power supplies without interruption
- utility subsystems
- supervision and leadership center.

Through the subsystems listed above, the maximization of the following must be ensured:

- comfort for the various occupants' activities
- creativity
- security
- minimizing the costs of the necessary resources.

SMART HOME AUTOMATION WITH ARDUINO



Fig. 2. Functionality of a smart home

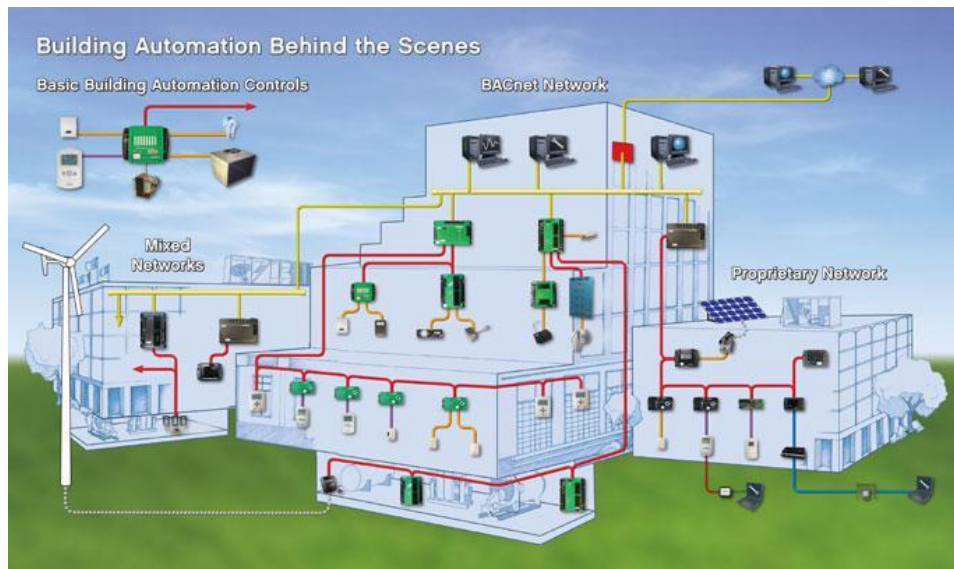


Fig. 3. Building automation controls

When we talk about the structure of a smart building, we talk about its automation network [5]. Intelligent Cloud Automation is a network of centralized hardware and software networks that monitors and controls the environment in commercial, industrial and institutional spaces. While managing different construction systems, the automation system ensures the performance of the building and the safety and comfort of the occupants [6], [7].

Most automation networks consist of a primary and a secondary bus that connect high-level programmable machines (generally specialized for building automation, but can also be generic programmable machines) with lower level controllers, input / output devices, and a user interface (also known as a human-machine interface device). These primary and secondary buses can also be wireless [11].

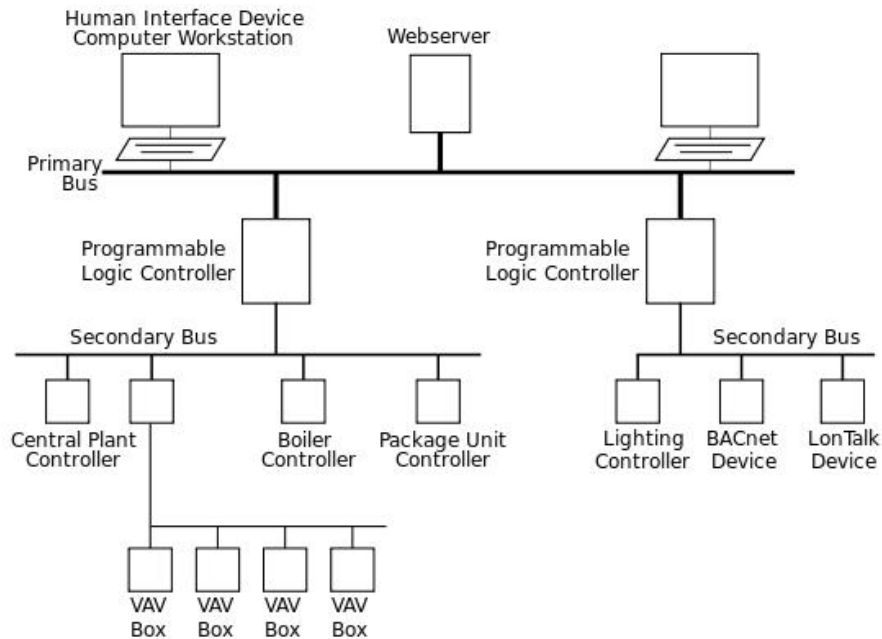


Fig. 4. Automation network in a smart building

3. STRUCTURE AND FUNCTIONALITY OF THE SMART HOME

These are the main components of the system that put the mechanism into operation, due to the properties of each assembled component, helping each other to achieve the communication as well as the functioning of the system. Each component has its specific role and all together form a whole.

The components were assembled so that they could control a house. They can open a door, a garage, detect if someone forces the door on the door, lights up, raises and leaves the blind, reads the level of brightness, and communicates with a cell phone.

The smart house is made of the following components: an Arduino mega control panel, a DTH22 temperature and humidity sensor, two infrared sensors that detect a 3mm led light beam, a TEMT6000 ambient light sensor, a Micro Servo Motor sg90, a servo motor sg5010, female mother-to-father and father-to-father wires, a 28BYJ-48 stepper motor and blue ULN2003 driver, bluetooth HC-06 module and last but not least a CNC machine made of plexiglas laser.

The house receives command values from the phone and, depending on the values received, it can make decisions through the Arduino Mega command plate. To open the entrance door, the application on the phone sends the value 150. After the value has been sent and received by the Arduino mega plate [14],[15], the servo motor is gradually actuated to open the door. After the door is opened, an internal variable passes to 1 to hold in the memory of the programming board that the door is open, and then the control board sends the value 200 to the phone. This value confirms to the phone that the door has been opened and displays it on its "Info Door: Open" Info. If the button on the phone interface is actuated again, after the door has been opened, this loop is repeated with the indication that the internal variable passes to 0 to keep in the memory of the programming board that the door has been closed and the phone a value of 201 is sent to confirm that the door has been closed and "Door Info: Closed" appears on the phone.

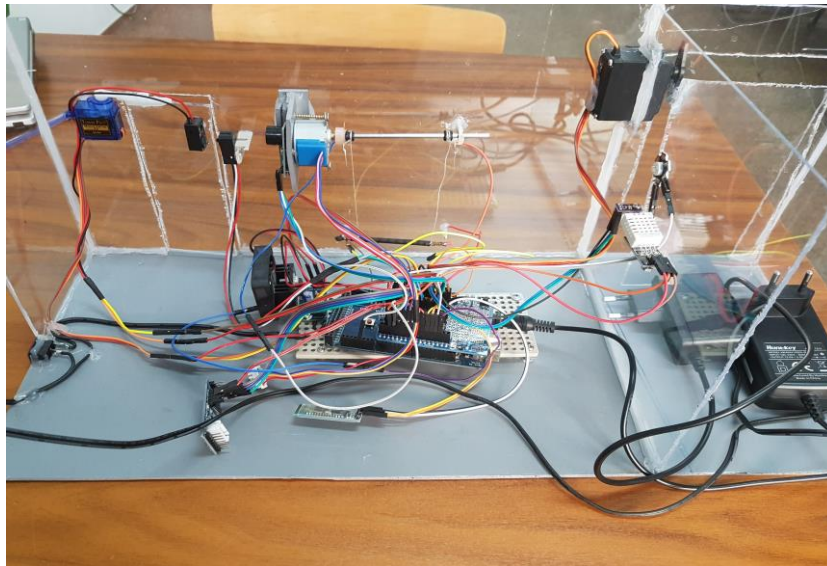


Fig. 5. Smart home structure

To open the garage the application on the phone sends the value 151. Once sent the value and received by the Arduino mega plate [14], gradually the sg5010 servo motor is actuated to open the garage. After the garage is opened, an internal variable passes to 1 to retain in the memory of the programming board that the garage is open, then the control board sends the value 202 to the phone. This value confirms to the phone that the garage has been opened and displays on its "Garage Info: Open" interface as in the case of the entry door, that the values sent to the phone differ. When the garage is closed, 203 is sent to the phone to confirm that the garage was closed and "Garage Info: Closed" appears on the phone.

To raise the curtain or close it, use the same method as opening / closing the door and the garage, only the application on the phone sends the value 152.

Infrared sensors are mounted on the inside of the entrance door. They can detect if the entrance door has been forced to open, that is, without someone opening the door on the phone application.

The temperature and humidity sensor [11] sends the same values to the phone application to display it on the screen. Also a led is positioned next to this sensor. The power light simulates a light bulb inside the house. An additional function is programmed into the system. On screen we have an "Auto" button. If it is pressed, the Arduino Mega programming plate reads the light sensor values constantly. If it reads a weaker light than the read value when the system was started then the door opens, the bulb is lit. It remains lit after the door closes, simulating that we entered the house and stay for a while. The bulb goes out automatically when we open the door once again, simulating that I got out of the house.

4. SOFTWARE IMPLEMENTATION

The first step in smart home programming is to connect the Arduino board to a computer via the USB connection cable for data transmission. Use the programming software for Arduino, which has a program editor provided by www.arduino.cc. The programming language is a common one similar to C ++. The ordering process consists in programming the components according to the value received from the created application. The following window is a programming editor used only for Arduino development boards. For this you must enter the tools menu and choose the plaque you are working with, as well as the selected computer port. The following window is a programming editor used only for Arduino development boards [15]. To do so, you must enter the tools menu and choose the plaque you are working with and the port selected by your computer [8].

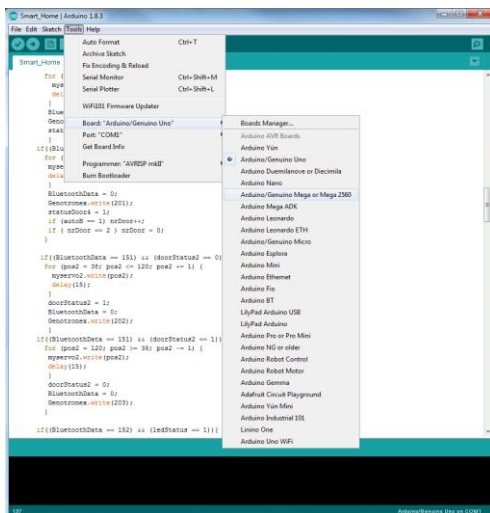


Fig. 6. Choosing the Arduino board

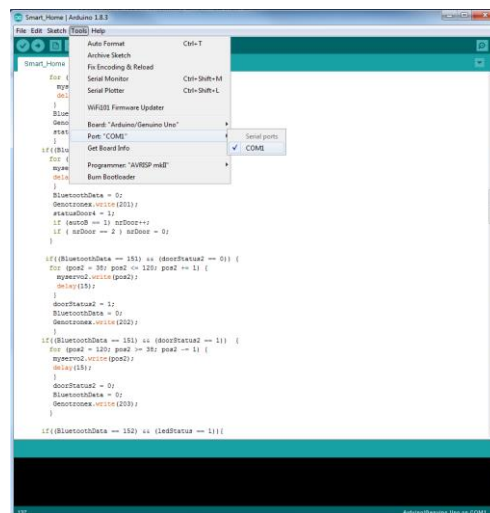




Fig. 7. Port selection

Any code line has to be checked with the button  that will check for errors in the program structure and, once the message “Done compiling” is displayed, the program can be run by pressing the upload button  that sends through port COM3 the instructions to the microcontroller, which processes it and sends it on to the output pins[9],[10].

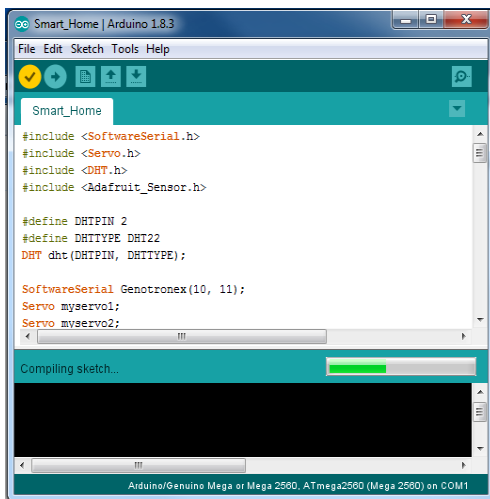


Fig. 8. Program compilation

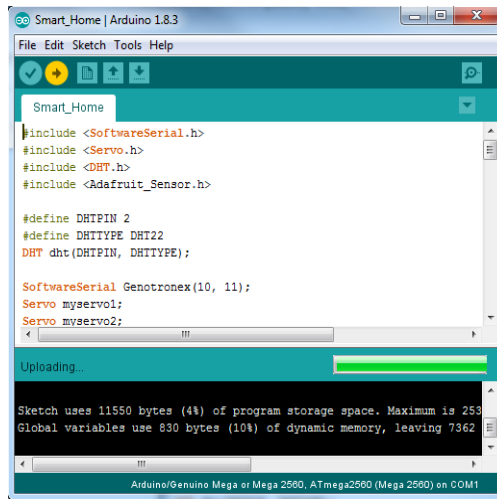


Fig. 9. Program loading

5. PROGRAMMING AND FUNCTIONALITY OF THE SMART HOME IN WORK EDITOR OF MIT APP INVENTOR 2

The first step in smart home programming is to connect the Arduino board to a computer via the USB connection cable for data transmission. Use the programming software for Arduino, which has a program editor provided by www.arduino.cc. The programming language is a common one similar to C ++. The order process is to program the components according to the value received from the created application.

App Inventor is an online program, which means you can create apps right in your web browser. This website provides all the support you need to learn how to create your own apps. The App Inventor software can be accessed at ai2.appinventor.mit.edu[12],[13].

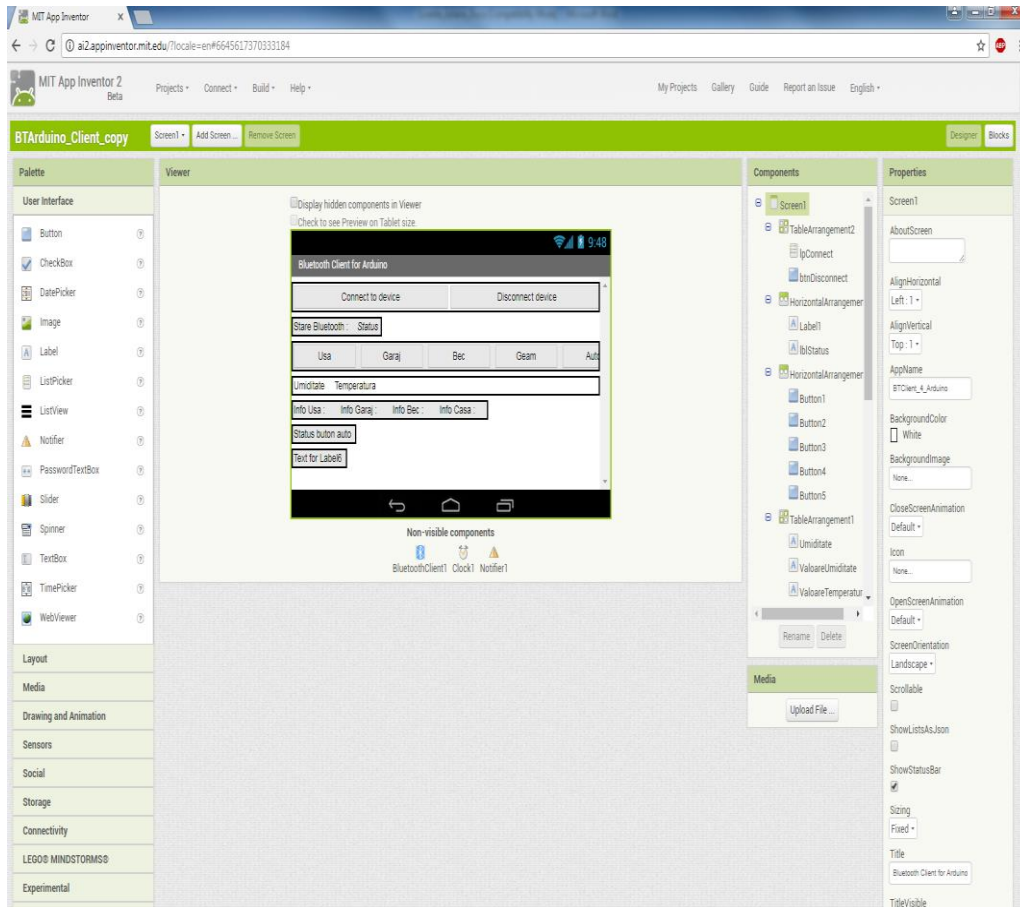


Fig. 10. Work editor of App Inventor software

The above window is a programming editor used by App Inventor software. To create a new application, enter the "Projects" menu and select "Start new project". In this software, it is totally visually programmed so if we want to edit the interface of the editing application on the "Designer" side and when we want to program visually we enter into the Blocks part.

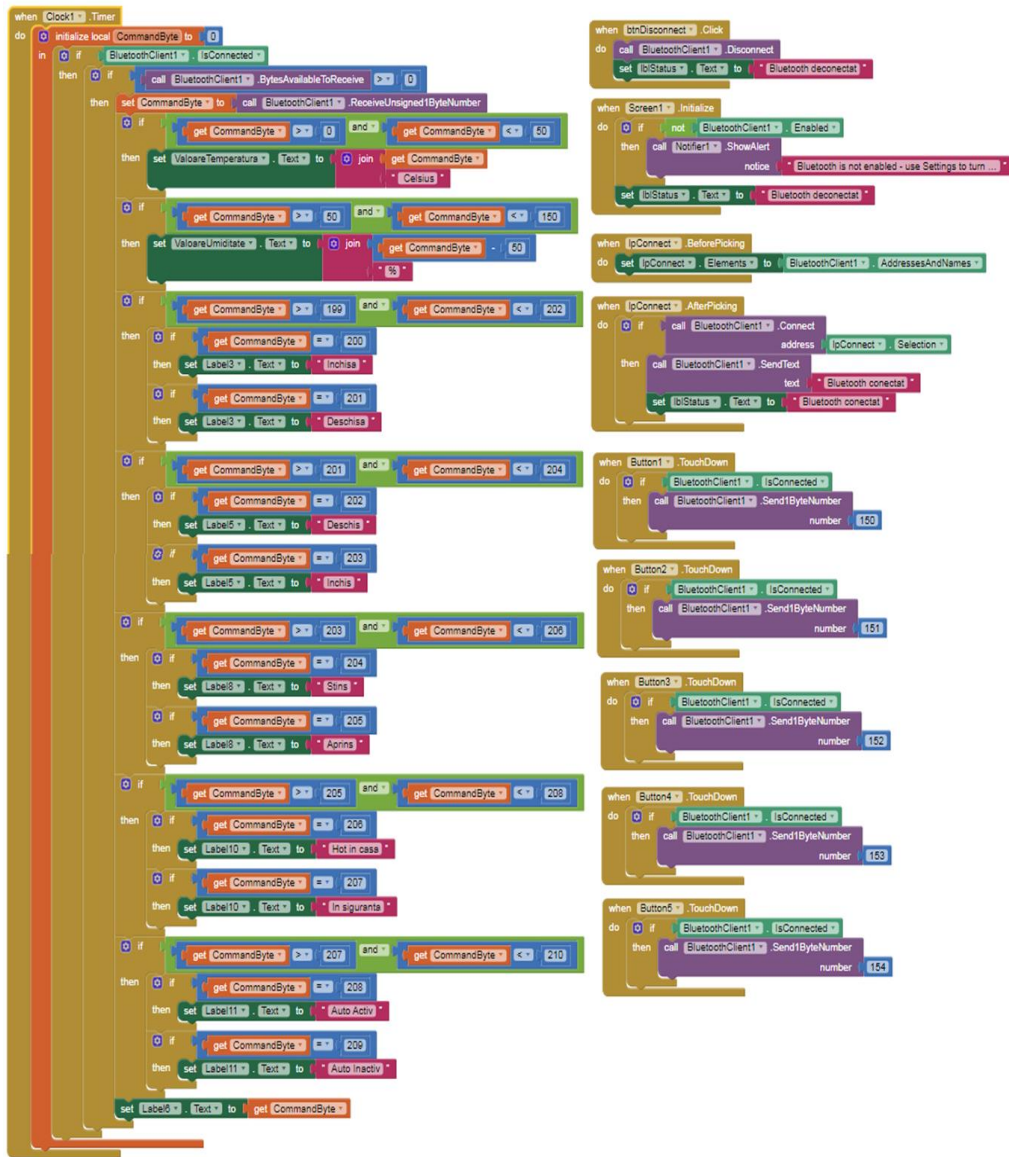


Fig. 11. Blocks Section from software App Inventor

6. CONCLUSIONS

The paper presents a smart home that can be remotely controlled via the mobile phone. The house receives command values from the phone and, depending on the values received, it can make decisions through the Arduino Mega command plate. In order to build the smart home, two servo motors, a light sensor, a temperature and humidity sensor, a power led, a stepper motor, a voltage stabilizer, a bluetooth and an

Arduino Mega development board. The programming was done using the Arduino software, and control with the App Inventor software.

In conclusion, the solution presented can be used for multiple purposes, and many others functionalities can be added to those incorporated at the moment, as required. Basically, a multitude of sensors, monitoring equipment, and so on can be added depending on the purpose for the application.

REFERENCES

- [1]. **Marian I.**, *Mecanizarea în minerit*, Editura Tehnică, București, 1969.
- [2]. **Anghel D.**, *Măsurători electronice și tractoare*, Universitatea „Babes-Bolyai”, Cluj-Napoca, 1996.
- [3]. **Călin S.**, *Reglarea numerică a proceselor tehnologice*, Editura Tehnică, București, 1984.
- [4]. **Daintree Networks**, *Getting Started with ZigBee*, White paper, 2008.
- [5]. **Gacsadi A., Tiponuş V.**, *Sisteme de achiziție de date*, Editura Universității din Oradea, 2005.
- [6]. **Ionel N.**, *Monitorizarea la distanță a proceselor industriale*, Electronica de Azi, Iunie, 2013.
- [7]. **KMC Controls**, *Understanding Building Automation and Control Systems*, White Paper, 2012.
- [8]. **Pintea M.**, *Reglarea automată a parametrilor proceselor tehnologice*, 2009.
- [9]. **Tirian G. O.**, *Automation of a warehouse by means of a robotic arm*, Annals of Faculty Engineering Hunedoara – International Journal of Engineering Tome XI, Fascicule 4, 2013.
- [10]. **Tirian G. O.**, *Maze solving mobile robot*, Annals of Faculty Engineering Hunedoara, International Journal of Engineering, Tomul XIII, Fasc.4, 2015.
- [11]. **Tirian G. O.**, *Robotică*, Editura Politehnica Timișoara, 2013.
- [12]. **Waltenegus Dargie, Christian Poellabauer**, *Fundamentals of Wireless Sensor Networks*, Wiley, ISBN-10: 0470997656, 2010.
- [13]. **Wilson Daniel H.**, *Smart House-Your So-Called Sci-Fi Life*, Popular Mechanics Technology News, Mai 2007.
- [14]. www.ai2.appinventor.mit.edu.com.
- [15]. www.arduino.cc.
- [16]. www.robofun.ro

EVALUATION OF THE MOMENTS LOAD AND MAXIMUM ALLOWABLE VOLTAGE DROP FOR OVERHEAD AND UNDERGROUND POWER LINES

LEON PANA¹, FLORIN GABRIEL POPESCU²

Abstract: Choosing a section of a line section obviously influences the voltage drop across that section. In order for the distribution voltage to remain within certain limits at all points of the electrical network, the voltage drop between the source point and the most disadvantageous point of delivery in this respect must be limited. It is not possible to calculate the voltage drop at the level of a section. In this respect, the influence of the section s on the cumulative voltage drop across the network must be analyzed on all the sections of cascade lines.

Keywords: low voltage, electrical networks, energy, current, power.

1. INTRODUCTION

For the determination of voltage drops in a electrical network distribution it is necessary to know the load circulation (currents or powers) through the elements of the considered network [1, 2, 5, 6].

The main computational hypotheses on distribution networks will be synthesized:

- For short distribution networks, in normal operating mode, consumers are represented by constant currents. Using constant static currents results in close-to-real results.
- The intensities of the transversal currents (both the capacitive and the insulation losses) will be neglected to the conduction current, the equivalent scheme of the lines being considered a bi-port with concentrated parameters.
- Only active power losses in network elements by Joule-Lentz effect will be considered. Determination of reactive losses in these networks is less important because the cost of installations producing a kVAr of losses is (10-15) times lower than the cost of a kW installed in an electric power plant.

¹ *PhD., Lecturer, Eng., University of Petrosani*

² *PhD., Lecturer, Eng., University of Petrosani*

- For power distribution networks, the active power losses are calculated based on the maximum current in each line section.
- The network is considered to operate in symmetrical and sinusoidal mode and does not take into account the imbalances in the distribution networks, especially the low voltage LV, are relatively large.

2. ANALYTICAL MODEL

The voltage drop for a three-phase radiated electric line, expressed in V, which feeds to concentrated consumers, is given by [1, 2, 3, 5, 6]:

$$\Delta U = \frac{r_0 \cdot \cos \varphi + x_0 \cdot \sin \varphi}{U_n \cdot \cos \varphi} \cdot \sum_{i=1}^n P_i \cdot l_i = \frac{r_0 \cdot \cos \varphi + x_0 \cdot \sin \varphi}{U_n \cdot \cos \varphi} \cdot \sum_{i=1}^n p_i \cdot L_i \quad (1)$$

or if to express the voltage drop in relative values, it follows:

$$\Delta U = 10^2 \cdot \frac{r_0 \cdot \cos \varphi + x_0 \cdot \sin \varphi}{U_n^2 \cdot \cos \varphi} \cdot \sum_{i=1}^n P_i \cdot l_i = 10^2 \cdot \frac{r_0 \cdot \cos \varphi + x_0 \cdot \sin \varphi}{U_n^2 \cdot \cos \varphi} \cdot \sum_{i=1}^n p_i \cdot L_i \quad (2)$$

The analytical expressions of the voltage drop in V for the loads expressed as active powers can also be written as follows:

$$\Delta U = \frac{\rho}{s \cdot U_n} \cdot \left(1 + s \cdot \frac{x_0}{\rho} \cdot \operatorname{tg} \varphi \right) \cdot \sum_{i=1}^n P_i \cdot l_i = \frac{\rho}{s \cdot U_n} \cdot \left(1 + s \cdot \frac{x_0}{\rho} \cdot \operatorname{tg} \varphi \right) \cdot \sum_{i=1}^n p_i \cdot L_i \quad (3)$$

respectively in percentage or relative amounts:

$$\Delta U = 10^2 \cdot \frac{\rho}{s \cdot U_n^2} \cdot \left(1 + s \cdot \frac{x_0}{\rho} \cdot \operatorname{tg} \varphi \right) \cdot \sum_{i=1}^n P_i \cdot l_i = 10^2 \cdot \frac{\rho}{s \cdot U_n^2} \cdot \left(1 + s \cdot \frac{x_0}{\rho} \cdot \operatorname{tg} \varphi \right) \cdot \sum_{i=1}^n p_i \cdot L_i \quad (3)$$

in which:

- ΔU is the voltage drop expressed in V or %;
- P_i, p_i the active power on the lines of the line or the active power of the consumers in kW or in MW, depending on the calculated calculation of the voltage drop in V or in%;
- L_i, l_i the length of the line section and the distance between consumers in km;
- ρ the resistivity of the conductive material, in $\Omega \text{ mm}^2 / \text{km}$;
- s conductor section in mm^2 ;
- U_n nominal network voltage or phase voltage equal to line voltage in kV;
- r_0, x_0 specific resistance, specific network response, in Ω / km ;
- $\cos \varphi$ the average power factor of the analyzed electrical network.

EVALUATION OF THE MOMENTS LOAD AND MAXIMUM ALLOWABLE VOLTAGE
DROP FOR OVERHEAD AND UNDERGROUND POWER LINES

In the case of a single-consumer radial power line ($i = 1$), the analytical expressions of the voltage drop in V above are given by the relations:

$$\Delta U = \frac{r_0 \cdot \cos \varphi + x_0 \cdot \sin \varphi}{U_n \cdot \cos \varphi} \cdot P \cdot l = \frac{r_0 \cdot \cos \varphi + x_0 \cdot \sin \varphi}{U_n \cdot \cos \varphi} \cdot p \cdot L \quad (4)$$

respectively as a percentage:

$$\Delta U = 10^2 \cdot \frac{r_0 \cdot \cos \varphi + x_0 \cdot \sin \varphi}{U_n^2 \cdot \cos \varphi} \cdot P \cdot l = 10^2 \cdot \frac{r_0 \cdot \cos \varphi + x_0 \cdot \sin \varphi}{U_n^2 \cdot \cos \varphi} \cdot p \cdot L \quad (5)$$

Analogously, the expressions of the voltage drop in V in the case of a single-consumer radial power line are determined with the relations:

$$\Delta U = \frac{\rho \cdot P \cdot l}{s \cdot U_n} \cdot \left(1 + s \cdot \frac{x_0}{\rho} \cdot \operatorname{tg} \varphi \right) = \frac{\rho \cdot p \cdot L}{s \cdot U_n} \cdot \left(1 + s \cdot \frac{x_0}{\rho} \cdot \operatorname{tg} \varphi \right) \quad (6)$$

respectively the analytical expression of the voltage drop in relative values is:

$$\Delta U = 10^2 \cdot \frac{\rho \cdot P \cdot L}{s \cdot U_n^2} \cdot \left(1 + s \cdot \frac{x_0}{\rho} \cdot \operatorname{tg} \varphi \right) = 10^2 \cdot \frac{\rho \cdot p \cdot L}{s \cdot U_n^2} \cdot \left(1 + s \cdot \frac{x_0}{\rho} \cdot \operatorname{tg} \varphi \right) \quad (7)$$

in which the sizes involved in the aforementioned relations have the above-mentioned meaning.

It is made clear that the hypothesis by which the power transmitted on a three-phase electric line is decomposable in the powers transmitted on each phase is false because the phases, which are inductively and capacitively coupled, do not allow separation surfaces between them [1, 3, 4, 5, 6].

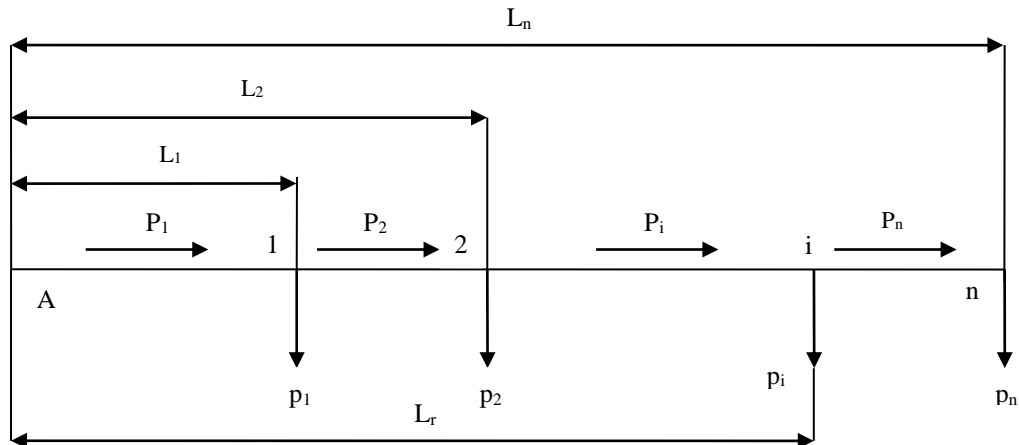


Fig. 1 Determination of reduced length L_r of a radial electrical network with concentrated loads and constant sections

In order to determine the reduced length L_r of a network, analogous theorems from mechanics apply, according to which the sum of moments of forces with respect to any point is equal to the resultant moment in relation to the same point in figure 1.

The total active load of the power line, expressed in kW, is given by:

$$P = \sum_{i=1}^n p_i \quad (8)$$

In this case, forces become electrical loads:

$$\sum_{i=1}^n p_i \cdot L_i = P \cdot L_r \quad (9)$$

The analytical expression of the reduced length L_r is:

$$L_r = \frac{\sum_{i=1}^n p_i \cdot L_i}{\sum_{i=1}^n p_i} = \frac{\sum_{i=1}^n p_i \cdot L_i}{P} \quad (10)$$

In the case of power grids having only active loads, (Figure 2), the network length l_1 and the s_1 section corresponding to the first section can be replaced with a network of length l_2 , section s_2 , in relation to voltage drops, with the relation:

$$l_2 = \frac{l_1 \cdot s_2}{s_1} \quad (11)$$

With the help of the above relations, it is finally determined that the analytical expression of the voltage drop in V in the case of the radial electric networks with loads expressed as active powers according to the reduced length of the electric line is determined based on the relations:

$$\Delta U = \frac{\rho \cdot P \cdot L_r}{s \cdot U_n} \cdot \left(1 + s \cdot \frac{x_0}{\rho} \cdot \text{tg } \varphi \right) \quad (12)$$

respectively the analytical expression of the voltage drop in relative values:

$$\Delta U = 10^2 \cdot \frac{\rho \cdot P \cdot L_r}{s \cdot U_n^2} \cdot \left(1 + s \cdot \frac{x_0}{\rho} \cdot \text{tg } \varphi \right) \quad (13)$$

in which the sizes involved in the aforementioned relations have the above-mentioned meaning.

EVALUATION OF THE MOMENTS LOAD AND MAXIMUM ALLOWABLE VOLTAGE
DROP FOR OVERHEAD AND UNDERGROUND POWER LINES

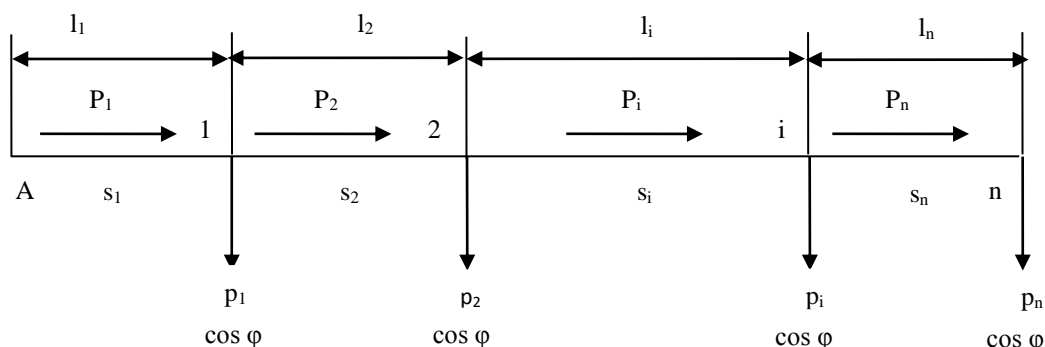


Fig.2. Electricity network with concentrated loads, variable sections and constant load factor

In the above relation the term $10^2 \cdot \frac{\rho \cdot P \cdot L_r}{s \cdot U_n^2} = \frac{\rho \cdot P \cdot L_r}{s \cdot U_n}$ represents the value of the voltage drop in case of neglecting the specific reactance of the power line.

The general term $K_x = \left(1 + s \cdot \frac{x_0}{\rho} \cdot \text{tg } \varphi \right)$ is called the reactance coefficient and takes into account the voltage drops due to the inductive reactance. The reactance coefficient K_x can be defined as the ratio between the total voltage drop and the voltage drop due to the ohmic resistance [1, 3, 4, 5, 6].

The above relation may be in another form:

$$P \cdot L_r \cdot K_x = \frac{s \cdot U_n^2 \cdot \Delta U}{10^2 \cdot \rho} = \frac{s \cdot U_n \cdot \Delta U}{\rho} \quad (14)$$

The product represents the time of electric charge.

The significance of the calculation sizes involved in the above relations is the following:

P is the total active power, in kW or in MW, depending on the calculation relation used.

L_r reduced network length in km

s conductor section in mm²

U_n nominal network voltage or phase voltage equal to line voltage in kV

ΔU voltage drop expressed in relative units

ρ conductivity resistivity in Ω mm² / km

r₀, x₀ specific resistance, specific network response, in Ω / km

cosφ the average power factor of the electrical network.

In a concrete situation, when the section and each of the sections will be optimally calculated "investments plus power or energy losses", it will be equal to the **P₁** active power transit and accepting the approximation that on the section and the voltage drop is inversely proportional to the section, and what is checked if the section

is greater or less than the average value because the reactance is less than the resistance will result in a cumulative voltage drop across all sections and cascades equal in relative value , with:

$$\Delta U = 10^2 \cdot \frac{\rho}{U_n^2} \cdot \sum_{i=1}^n \frac{P_i \cdot l_i}{s_i} \quad (15)$$

respectively, the analytical expression of the voltage drop expressed in V is:

$$\Delta U = \frac{\rho}{U_n} \cdot \sum_{i=1}^n \frac{P_i \cdot l_i}{s_i} \quad (16)$$

and if the relation (17), which makes the connection between P_i and, s_i ,

$$s_{ec} = P \cdot \sqrt{A_3 \cdot T_{PM}^2 + B_3} \quad (17)$$

it follows:

$$\Delta U = 10^2 \cdot \frac{\rho}{U_n^2 \cdot \sqrt{A_3 \cdot T_{PM}^2 + B_3}} \cdot \sum_{i=1}^n l_i \quad (18)$$

or the expression of the voltage drop expressed in V:

$$\Delta U = \frac{\rho}{U_n \cdot \sqrt{A_3 \cdot T_{PM}^2 + B_3}} \cdot \sum_{i=1}^n l_i \quad (19)$$

The maximum voltage drop will, in this case theoretically, be proportional to the total length of cascade line sections.

$$\Delta U = 10^2 \cdot \frac{\rho \cdot L}{U_n^2 \cdot \sqrt{A_3 \cdot T_{PM}^2 + B_3}} = \frac{\rho \cdot L}{U_n \cdot \sqrt{A_3 \cdot T_{PM}^2 + B_3}} \quad (20)$$

where:

$$L = \sum_{i=1}^n l_i \quad (21)$$

l_i is the length of the circuit i the electric line in km

In order to determine the analytical expression of the maximum voltage drop according to the power factor, an electric line of length L is assumed to be supposed to pass through a apparent power S or a current of intensity I.

The analytical expression of the voltage drop across this line, expressed in relative values, is calculated by:

$$\Delta U = 10^2 \cdot \frac{\sqrt{3} \cdot I \cdot L}{U_n} \cdot (r_0 \cdot \cos \varphi + x_0 \cdot \sin \varphi) = 10^2 \cdot \frac{S \cdot L}{U_n^2} \cdot (r_0 \cdot \cos \varphi + x_0 \cdot \sin \varphi) \quad (22)$$

EVALUATION OF THE MOMENTS LOAD AND MAXIMUM ALLOWABLE VOLTAGE
DROP FOR OVERHEAD AND UNDERGROUND POWER LINES

in which:

- S is the apparent cross-sectional power expressed in MVA
 I electric current intensity in kA
 L length of electric line, in km
 U_n nominal voltage of the mains, in kV
 r₀, x₀ resistance, ie line specific response, in Ω / km.

The analytical expressions of the voltage drop, expressed in V, are:

$$\Delta U = \sqrt{3} \cdot I \cdot L \cdot (r_0 \cdot \cos \varphi + x_0 \cdot \sin \varphi) = \frac{S \cdot L}{U_n} \cdot (r_0 \cdot \cos \varphi + x_0 \cdot \sin \varphi) \quad (23)$$

In this relation, the intensity of the current I is given in A, the apparent power S in kVA and the rest of the quantities have the significance shown above.

By canceling the derivative of the above analytical expression with respect to the phase angle, it follows [1, 3, 4, 5, 6]:

- Expression of the power factor for which the voltage drop is maximum relative to the phase angle:

$$\frac{d(\Delta U)}{d\varphi} = 0 \quad \Rightarrow \quad \cos \varphi_{\max} = \frac{r_0}{\sqrt{r_0^2 + x_0^2}} = \frac{r_0}{z_0} \quad (24)$$

- Expression of maximum strain angle drop in relative values for loads expressed as apparent powers:

$$\Delta U_{\max} = 10^2 \cdot S \cdot L \cdot \frac{\sqrt{r_0^2 + x_0^2}}{U_n^2} = 10^2 \cdot S \cdot L \cdot \frac{z_0}{U_n^2} = \alpha_s \cdot S \cdot L \quad (25)$$

in which it was marked with:

$$\alpha_s = 10^2 \cdot \frac{z_0}{U_n^2} \quad \left[\frac{\%}{\text{MVA} \cdot \text{km}} \right] \quad (26)$$

respectively, in the case of loads expressed in currents, the expression of maximum voltage drop in relative values is:

$$\Delta U_{\max} = 10^2 \cdot \sqrt{3} \cdot I \cdot L \cdot \frac{\sqrt{r_0^2 + x_0^2}}{U_n} = 10^2 \cdot \sqrt{3} \cdot I \cdot L \cdot \frac{z_0}{U_n} = \alpha_i \cdot I \cdot L \quad (27)$$

in which it was marked with:

$$\alpha_i = 10^2 \cdot \frac{\sqrt{3} \cdot z_0}{U_n} \quad \left[\frac{\%}{\text{kA} \cdot \text{km}} \right] \quad (28)$$

- Expression of maximum voltage drop in phase V, for stresses expressed as apparent powers:

$$\Delta U_{\max} = \frac{S \cdot L}{U_n} \cdot \sqrt{r_0^2 + x_0^2} = \frac{S \cdot L}{U_n} \cdot z_0 = \alpha_s \cdot S \cdot L \quad (29)$$

in which:

$$\alpha_s = \frac{z_0}{U_n} \quad \left[\frac{\text{V}}{\text{kVA} \cdot \text{km}} \right] \quad (30)$$

respectively, in the case of loads expressed in currents, the expression of the maximum voltage drop in V is:

$$\Delta U_{\max} = \sqrt{3} \cdot I \cdot L \cdot \sqrt{r_0^2 + x_0^2} = \sqrt{3} \cdot I \cdot L \cdot z_0 = \alpha_i \cdot I \cdot L \quad (31)$$

where:

$$\alpha_i = \sqrt{3} \cdot z_0 \quad \left[\frac{\text{V}}{\text{A} \cdot \text{km}} \right] \quad (32)$$

and

$$z_0 = \sqrt{r_0^2 + x_0^2}$$

is the absolute value (modulus) of the specific complex impedance of the electric line, expressed in Ω / km .

The α_s and α_i indicators can be interpreted physically as follows: the specific voltage drop corresponding to a line section having the section s and the unit length through which a load unit is transited.

3. CASE STUDIES

a) Case study 1

For a balanced and concentrated three-phase load at the end of the line and for Table 1. gives the maximum load moments of a cable underground (LEC) and airline, expressed in MW km, with a rated voltage of 6 kV of the network and for the 1% and 5% relative voltage drops.

EVALUATION OF THE MOMENTS LOAD AND MAXIMUM ALLOWABLE VOLTAGE
DROP FOR OVERHEAD AND UNDERGROUND POWER LINES

Table 1. The maximum load times of an LEC, depending on the rated voltage of the mains and the voltage drops of 1% and 5%

The sections [mm ²]	Moment of active electrical load, corresponding to LEC with Cu conductors and PVC insulation. [MW · km]	
	$\frac{\Delta U}{U} = 1\%$	$\frac{\Delta U}{U} = 5\%$
	LEC U _n = 6 kV	LEC U _n = 6 kV
50	0.84	4.21
70	1.12	5.52
95	1.45	7.27
120	1.76	8.84
150	2.12	10.6
185	2.47	12.39
240	2.94	14.70

In order to make a comparison between LEC and LEA, in Table 2 the maximum load moments of an Al, in MW km, are given according to the rated voltage of the mains and the relatively low voltage drops of 1% and 7.5%.

Table 2. The maximum load times of an LEA, depending on the rated voltage of the mains and the voltage drops of 1% and 7.5%.

The section conductors from Al- Al of the LEA s [mm ²]	Moment of active electrical load, corresponding to the LEA with conductors from Al-Al. [MW · km]			
	$\frac{\Delta U}{U} = 1\%$		$\frac{\Delta U}{U} = 7.5\%$	
	LEA U _n = 10 kV	LEA U _n = 20 kV	LEA U _n = 10 kV	LEA U _n = 20 kV
50	2.1	5.1	15.6	39
70	2.6	6.5	19.6	49
120	3.5	8.7	26.5	66
150	4.0	10.0	30.5	76

For underground electrical lines, an appropriate electrical scheme with concentrated or evenly distributed parameters must be appreciated and chosen. In the case of distribution LEAs, which are generally short lines, the transverse currents can be neglected, and the corresponding equivalent scheme is a bi-dimensional dipole with concentrated parameters.

b) Case study 2

In the table 3 shows the values of the specific voltage drop in two variants for loads expressed by currents and respectively for loads expressed as apparent powers. These values were determined both for cables and for power lines in construction used in industry.

The values of the specific voltage drop corresponding to the underground cable lines were calculated for different standardized sections and a unit length through which an active load of 500 kW and an apparent load of 625 kVA corresponding to an average power factor of 0.8 . If the loads on the power lines are expressed by currents, an average value of 100 A has been adopted.

For comparative analysis, analogously using the same relations, the values of the specific voltage drop for the copper conductor cables (6 kV) through which the same load unit is transmitted in both current and apparent power , as in the case of underground cables.

Analyzing the values obtained from the calculations summarized in table 3 for LEC underground mines with copper and PVC conductors, and for normal LEC with copper conductors and PVC insulation, it is observed that they are approximately equal. In the case of the 20 kV (LEA and LEC) rated power lines, a 1.5 MW active load and an apparent load of 1.875 MVA were considered for the specific voltage drop.

The quality of the voltage to the electrical equipment is assessed mainly on the basis of the admissible deviations of the actual value of the voltage from the nominal quantities.

It is also noted that the values of specific voltage losses expressed in relative values for copper and PVC conductors and air needle cables, depending on the maximum length of the power line (1 km) and for different standardized sections, are falls within the permissible limits laid down in STAS 930 technical regulations.

EVALUATION OF THE MOMENTS LOAD AND MAXIMUM ALLOWABLE VOLTAGE
DROP FOR OVERHEAD AND UNDERGROUND POWER LINES

Table 3. **The values for the voltage drop specific for a section of electric section of section s and unit length through which a load unit**

The section s [mm ²]	ΔU_{\max} for different types of power lines			
	$U_n=0.4$ kV		$U_n=6$ kV	
	LEA	LEC	LEA	LEC
a) For calculations with loads expressed by current intensities $\Delta U_{\max} (\%) = \alpha_i \cdot I \cdot L$				
35	0.45	1.5	8.60	8.00
50	0.33	1.03	6.40	5.65
70	0.25	0.69	5.05	4.09
95	0.20	0.58	4.23	3.10
120	-	0.50	3.76	2.53
150	-	0.42	-	2.12
185	-	0.37	-	-
240	-	0.32	-	-
b) For calculations with loads expressed by apparent powers $\Delta U_{\max} (\%) = \alpha_s \cdot S \cdot L$				
35	0.68	0.90	0.29	0.23
50	0.50	0.63	0.18	0.16
70	0.38	0.41	0.14	0.12
95	0.30	0.35	0.12	0.09
120	-	0.30	0.11	0.07
150	-	0.25	-	0.06
185	-	0.22	-	-
240	-	0.19	-	-

3. CONCLUSIONS

In general, the International Electrotechnical Committee (CEI) recommends that the upper and lower limit voltage should not differ by more than $\pm 10\%$ of the rated voltage and, if conditions allow, these limits be reduced to $\pm 5\%$.

A complete calculation must therefore be made on a case-by-case basis, taking into account the structure of the electrical network analyzed, the length of the electrical lines and the distribution of the loads to be fed.

Analyzing the results obtained from the calculations, it is noted that with the apparent (apparent) power increase that transits the respective power lines, the values of the specific voltage losses are also doubled.

The voltage drop from the nominal value to the terminals of the electric power receptacles must be between some nominal voltage values and are regulated by STAS 930, entitled "Electrical networks. Nominal Voltages and Permissible Deviations "and generally range between $\pm 5\%$ and $\pm 10\%$, depending on the type of power supply and the consumer.

REFERENCES

- [1]. **Ionescu G. T., Pop O.**, *Ingineria sistemelor de distribuție a energiei electrice*, Editura Tehnică, București, 1998.
- [2]. **Marcu M.D., Popescu F.G., Pana L.**, *Modeling and simulation of power active filter for reducing harmonic pollution using the instantaneous reactive power theory*. Environmental Engineering and Management Journal, June 2014, Vol.13, No. 6, Pages: 1377-1382.
- [3]. **Marcu M.D., Pana L., Popescu F.G., Slusariuc R.**, *Evaluation the losses power and electrical energy on the basis of the relative load curves, by reference to the basic sizes*. Papers SGEM2014/Conference Proceedings, Vol. Energy and clean technologies, ISBN, 229 - 236 pp, 17-26 June, Albena, Bulgaria, 2014.
- [4]. **Pană, L.**, *Tehnici de optimizare în sistemele electroenergetice miniere*, Editura Focus, Petroșani, 2006.
- [5]. **Pana L., Popescu F.G., Samoilă L., Slusariuc R.**, *Analysis of thermic stability in short circuit regime of electric distribution networks conductor*. 6th International Multidisciplinary Scientific Symposium, SIMPRO 2014, Conference Proceedings, Pages: 331-334, 10-11 Octombrie, Petroșani, 2014.
- [6]. **Popescu F.G., Marcu M.D.**, *Metode moderne de analiză și reducere a armonicilor de curent și tensiune*, Editura Universitas, Petroșani, 2016, pag. 265, ISBN 978-973-741-504-2.

RESEARCHES REGARDING DETERMINATION OF THE ELECTRICAL PARAMETERS FOR SAFE AND RELIABLE INITIATION OF THE ELECTRICAL DETONATORS

LEONARD LUPU¹, FLORIN ADRIAN PAUN²,

DAN GABOR³, ADRIAN JURCA⁴

Abstract: The researches and experiments regarding the electrical parameters of electric detonators are especially important taking into consideration ensuring the safety of life and human health when conducting blasting works. Equipments in special construction for potentially explosive atmospheres should not generate energy sources that could initiate an explosion, and the blasting operations have to take place in reliable and sure conditions.

This paperwork addresses performance improvement of the present testing system of the electric detonators having in view a safe initiation during the blasting works.

Keywords: electric detonators, electric parameters, ignition current.

1. INTRODUCTION

Explosive charges are the amounts of explosives ready to be detonated through electric detonators, for the purpose of mining a certain volume of rock from the mountain. (Fodor D, 1998). The electric detonators have been used on a wide scale within industrial activities as component of the blasting process, both in underground and surface workings. In order to mitigate the explosion risk in these environments - potentially explosive atmospheres generically named "Ex zones", equipment in special construction for potentially explosive atmospheres are to be used, which shall not generate energy sources that could initiate an explosion, and the blasting operations have to take place in reliable and sure conditions.

The field of civil use explosives is represented by the European Directive 93/15/EEC of 5th of April 1993 regarding harmonization of provisions regarding placing on the market and control of civil use explosives.

¹ *Ph. D.Eng., scientific researcher II, INDC-INSEMEX Petroșani*

² *Ph. D.Eng., scientific researcher II, INDC-INSEMEX Petroșani*

³ *Ph. D.Eng., scientific researcher, INDC-INSEMEX Petroșani*

⁴ *Ph. D.Eng., scientific researcher II, INDC-INSEMEX Petroșani*

The electric detonators used in blasting processes have to meet the essential safety requirements addressing their safe and reliable ignition. Testing of electric detonators is of a particular importance taking into consideration the existing explosion risk that has to be minimized in order to ensure safety of human life and health. (Ghicioi E and Părăian M, 2002).

2. RESEARCHES REGARDING DETERMINATION OF ELECTRIC PARAMETERS OF ELECTRIC DETONATORS

Electric detonators operation is based on the heat given by the filament to the flammable paste. The amount of heat developed by the filament can be expressed through the following formula:

$$Q = I^2 \cdot R_f \cdot t \text{ [J]} \quad (1)$$

where: Q - amount of heat;
 I - current [A];
 R_f - electric resistance of filament [Ω];
 t - duration of current passing [s].

From this formula it can be noticed that the main role in developing the heat required to ignite the flammable paste is taken by both current value and duration of its passing through the filament (the value $I^2 \times t$). Thus, when through the filament a high enough current is passing (of a certain value), the amount of heat developed is enough to initiate the pasta burning reaction, thus starting electric detonators operation.

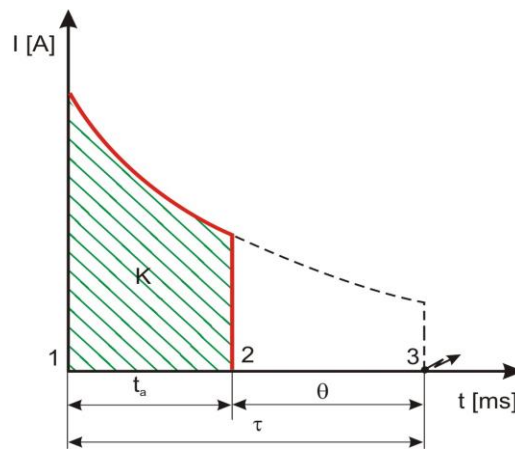


Fig. 1 Diagram of the ignition process in an electric device

For a safe operation of electric detonators it is required to ensure a certain value for the current that passes through the filament, as well as to ensure a certain duration. The ignition time is defined as the time that passes from switching on the electric contact until ignition of the mixture in the igniter's pearl. The transmission time is defined as the time passed from ignition of combustible mixture until detonator's

RESEARCHES REGARDING DETERMINATION OF THE ELECTRICAL PARAMETERS FOR SAFE AND RELIABLE INITIATION OF THE ELECTRICAL DETONATORS

explosion. The performing time is the sum of these two above durations (Ghicioi, E. 2007).

The ignition impulse (k) is the amount of electric energy required by a bridge (filament) having an unit resistance in order to reach the pearl's ignition temperature.

Laboratory experiments to determine electric parameters of electric detonators

In order to perform the experiments the current supply manufactured by AIM TTI, of QPX 1200 S type had been used, to ensure a current output of a maximum value of 50A for voltages in the range of 0 to 60V.

The current supply is provided with an electronic output switch, with current and voltage indicators, with voltage output protections, reversed diode protection for reversed currents of up to 3 A, over-voltage protection in the range of 2V to 65V, overcurrent protection in the range of 2A to 55A, overheating protection.

The supply's operational module is operating at constant voltage or current in automated system on the condition that the power is in the power limits according to the diagram of voltage-intensity-current-ratio (see figure 3).

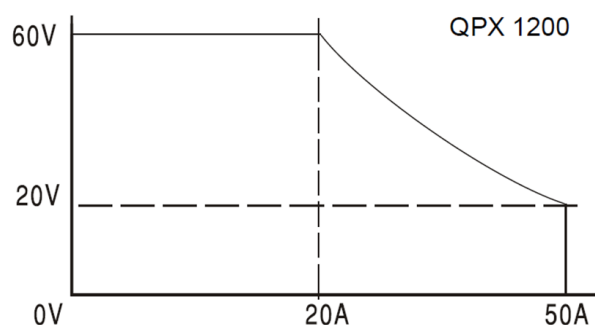


Fig. 3 Voltage - current diagram for the high current supply

The test stand montage for electric safety parameters of electric detonators had been carried out (see figure 4), consisting of three equipment: high current supply, electric signal configuration module and oscilloscope. The first component of this montage, the power supply has the role of generating the electric current covering a wide range both for intensity and voltage.

The second component of the montage, the signal configuration module has the role of transforming the electric signal coming from the high current supply into an altered signal, a step signal which would satisfy the requirements regarding ignition current, determination of non-ignition current or determination of ignition impulse, requirements for the step signal form, requirements regarding the values of the signal delivery duration, as well as values of current intensity. The signal configuration module operates according to the block-scheme (see figure 7) (Lupu, L. 2015).

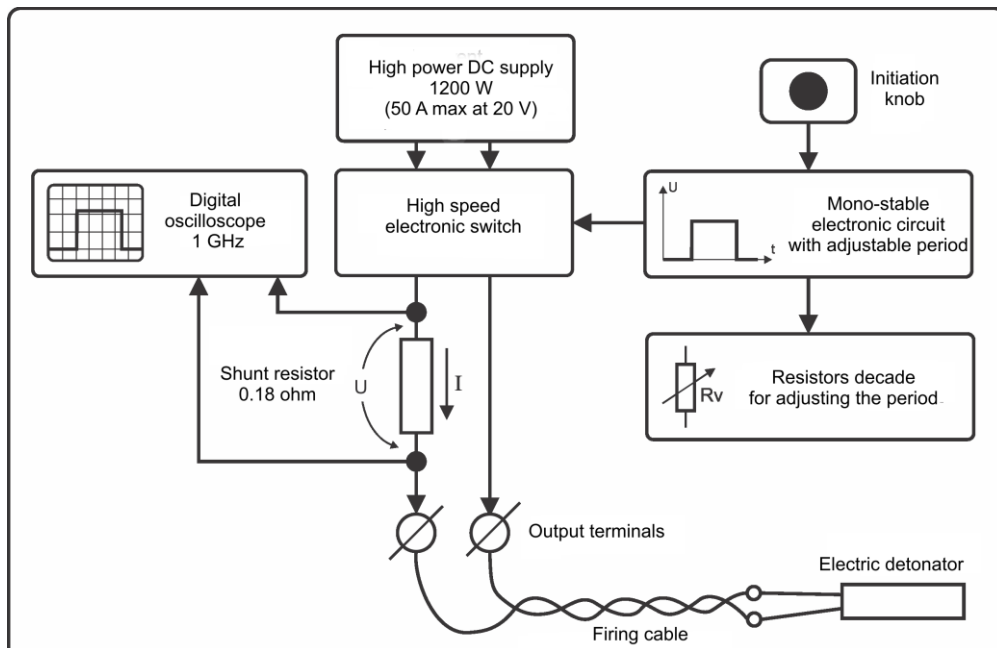


Fig. 4. Block diagram of the signal configuration module

The third component, the oscilloscope allows recording oscillograms which are capacitive electrical discharges with duration of a few milliseconds. A very careful concern was addressed to the accuracy or precision of the oscillograms recording, resulting in the interpretation of data (Lupu et al., 2014).

The testing principle is to measure ignition frequency at defined levels of physical stimuli, i.e. ignition impulse is one of the electric parameters specific to electric detonators. The current impulse recorder had been connected - which is the oscilloscope, and the signal configuration module had been adjusted so as a value two or three times greater than the series ignition current provided by the manufacturer. For the detonators used in tests, the series ignition current provided by the manufacturer is 0,8 A, thus current value in the step signal generated has to be from $2 \times 0,8$ A up to $3 \times 0,8$ A, which is a range from 1,6 A to 2,4 A.

In the step signal oscillogram for determination of ignition impulse (see figure 5) can be noticed the step signal value of 360 mV on cursor a.

RESEARCHES REGARDING DETERMINATION OF THE ELECTRICAL PARAMETERS
FOR SAFE AND RELIABLE INITIATION OF THE ELECTRICAL DETONATORS

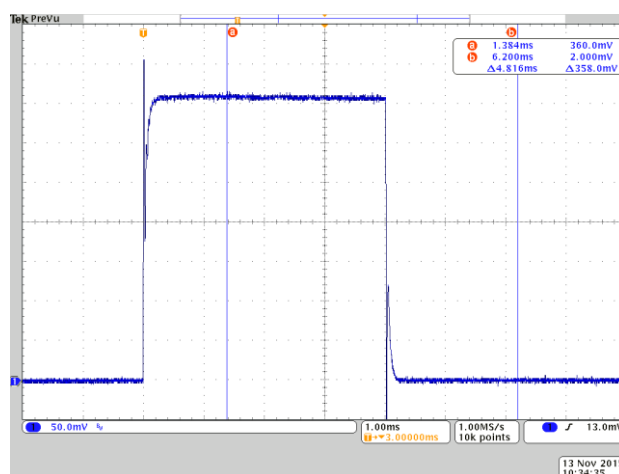


Fig. 5. Oscillogram of the step signal for determination of ignition impulse

The value of 360 mV represents the value of 2 A on the circuit used in our tests, a mean value in the range of 1,6 A to 2,4 A and results in the following calculation:

$$R_{\text{circ}} = 0,18 \Omega \quad U = 360 \text{ mV} = 0,36 \text{ V}$$

$$U = R \cdot I, I = U / R = 0,36 / 0,18 = 2 \text{ A, results the value of } \underline{2 \text{ A}}$$

$$\text{Ignition impulse:} \quad K_{\text{apr}} = I^2 * t = 2^2 * 0,004 = 4 * 0,004 = 0,016 \text{ A}^2\text{s}$$

$$K_{\text{apr}} = 0,016 \text{ A}^2\text{s} = 16 \text{ mJ}/\Omega$$

Configuring the step signal at the above set out values had been followed by performing experimental tests, performing three time initiation on: one instantaneous detonator (step 0), on one step 1 detonator and on one detonator step 10. The results had been positive, which means ignition occurred on all of them, so the detonators responded to the applied physical stimuli (step-type of electric signal) and the duration starting from the moment of signal application until the ignition occurrence had been recorded.

The testing principle is to determine safety in operation for electric detonators when applying the series ignition current declared by the manufacturer, which is one of the electric parameters specific to electric detonators. The current reaction time employed had been 4,2 milliseconds. The current impulse recorder had been connected - i.e. the oscilloscope - and the signal configuration module had been adjusted so as to obtain the value declared by the manufacturer for the ignition current in series, in this case this value is 0,8 A.

In the step signal oscillogramme for determining the ignition current (see figure 6) it can be noticed that the step signal has the value of 144 mV on cursor a.

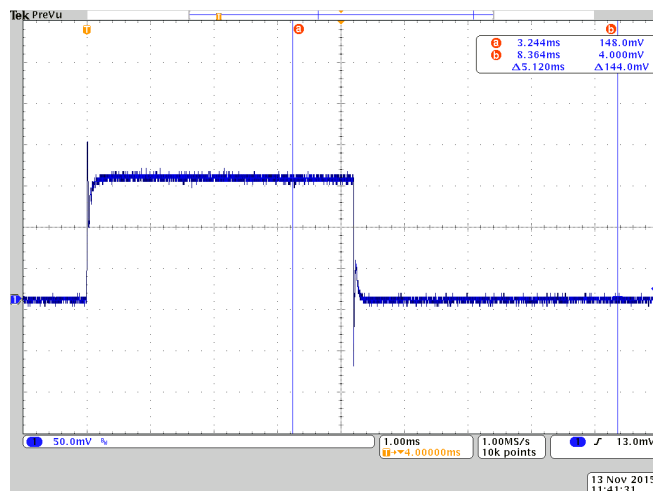


Fig. 6. Oscillogramme of the step signal for determining the ignition current

The value of 144 mV represents the value of 0,8 A on the circuit used for the experiment, resulting from the followin calculus:

$$R_{\text{circ}} = 0,18 \Omega \quad U = 144 \text{ mV} = 0,144 \text{ V}$$

$$U = R \cdot I, I = U / R = 0,144 / 0,18 = 0,8 \text{ A, the value of } \underline{0,8 \text{ A}} \text{ results}$$

After configuring the step signal at the above mentioned values, experimental tests had been performed, which is initiation of 5 electric detonators step 2, in series. The results show constantly that none of the 5 detonators ignited.

The testing principle is to determin the non-ignition current of electric detonators when applying the non-ignition safe current declared by the manufacturer, which is one of the electric parameters specific to electric detonators. For the detonators used in the experiment the safety non-ignition current has the value of 0.18 A. Duration of the squared electric signal is 10 seconds. The current impulse recorder had been connected - i.e. the oscilloscope - and the signal configuration module had been adjusted so as to obtain the value of 0,17 A.

In the step signal oscillogramme for determining the ignition current (see figure 7) it can be noticed that the step signal has the value of 20.4 mV on cursor a.

RESEARCHES REGARDING DETERMINATION OF THE ELECTRICAL PARAMETERS FOR SAFE AND RELIABLE INITIATION OF THE ELECTRICAL DETONATORS

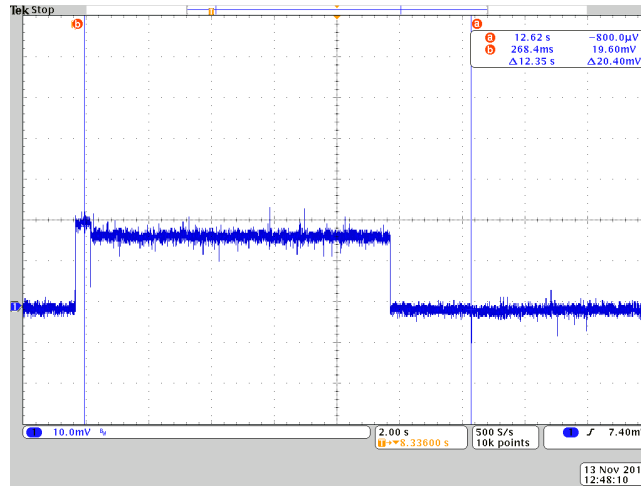


Fig. 7. Oscillograme of the step signal for determining the non-ignition current

The value of 20,4 mV represents the value of 0,17 A on the circuit used in the experiment, resulting from the following calculus:

$$R_{\text{circ}} = 0,12 \, \Omega \quad U = 20,4 \, \text{mV} = 0,0204 \, \text{V}$$

$$U = R \cdot I, I = U / R = 0,0204 / 0,12 = 0,17 \, \text{A}, \text{ results the value of } \underline{0,17 \, \text{A}} \text{ applied}$$

After configuring the step signal at the above mentioned values, experimental tests had been performed, namely two times initiation on a step 8 detonator and on a step 9 detonator. Results show no ignition in any of the two situations.

3. CONCLUSIONS

Testing of electric detonators is of a particular importance taking into consideration the explosion risk and this is the reason why the requirements regarding detonators electric parameters have to be fulfilled aiming to obtain a safe and reliable igniton of detonators.

Analyzing the safety requirements of electric parameters of detonators pointed out a need of improving the testing methods and procedures and to achieve this goal, a power supply should be aquired, capable to generate high currents. Thus, the ability of performing tests on the whole range of electric detonators is extended, from the low intensity ones up to the high intensity electric detonators.

REFERENCES

- [1]. **Fodor D**, *Using explosives in industry*, Publisher INFOMIN Deva, ISBN 973-98552-0-2, 162, 1998.
- [2]. **Lupu L., Ghicioi E., Jurca A., Păun F.**, *Ensuring security and environmental safety at blasting workplaces*, Environmental Engineering and Management Journal, June 2014, 13, no. 6, 1517-1522, 2014.
- [3]. **Ghicioi E.**, *Method for diagnosing electrical detonators*, INSEMEX Publisher House, Petroșani, România , 17, 2007.
- [4]. **Lupu L**, *Study - PN 07 45 02 59 – Researches regarding determination electrical parameters of safe and reliable initiation for detonators*, 16-19, 2015.
- [5]. **Ghicioi, E , Părăian, M** – *Safe Blasting when using electrically initiated explosive materials*. Annals of the University of Petroșani, Mining Engineering, 3, Petroșani 2002.

THE BENEFITS OF THE INTELLIGENT PRODUCTION

MARIA DANIELA STOCHIȚOIU¹, ILIE UȚU²

Abstract: In order to benefit from all the advantages of the intelligent production of tomorrow, the connection between real products and the processes based on digital data are necessary. The basis for this is that the entire construction plan and manufacturing cycle are described digitally. Production is then easily simulated or configured at any time, and can thereby be optimized. The world is changing and it is becoming more digital, intelligent and flexible.

Keywords: quality, LED sources, evolution, competitively, efficient resources.

1. INTRODUCTION

Data exchange as well as the design of the contents to be communicated must fulfill the requirements of the production systems. To be successful in the future, standards and guidelines must be open o development, that means as changing framework conditions and new business models can be provided too.

Consistently digital description

Products and processes are first of all created virtually and are fully transparent. The basis for this is that the entire construction plan and manufacturing cycle are described digitally. Production is then easily simulated or configured at any time, and can thereby be optimized.

Easy to install

The consistent data flow from configuration through to the finished marking label ensures fast, error free installation and manufacturing. The assembled connectors contribute to this, with which distributed devices can be networked with no need for tools.

Communicative and secure

Intelligent mechatronic system communicate across locations and companies using network infrastructure and networks distributed structures and forms the basis for flexible, self optimizing production processes and electrical faults is a key requirement.

¹ *PhD., Associate Professor, Eng., University of Petrosani*

² *PhD., Associate Professor, Eng., University of Petrosani*

Autonomous and adaptable

Unexpected events do not lead to production downtimes or reductions in quality due to intelligent collaboration that work autonomously and safety functions are more important.

Resource efficient

Energy and material usage can be adapted individually and precisely, as all the data required for intelligent management is available. This means that only the energy that is actually required is used [2].

2. QUICK EVOLUTION OF INTELLIGENT PRODUCTIONS

To grow the market share, it is necessary to design, construct and test the different product, and this indeed an expensive and time consuming process.

Although, the enabled benefits applied to products led to the quick evolution of the electrical insulation market. In the middle of 70s years, miniature circuit breakers were properly standardized and this enabled a great increase in the protection of installations and goods. Ten years later, residual current devices become much safer with the help of standardization process, which enhanced the protection of people against electrical shocks. In the middle of 90`s, surge protection against the lighting was standardized and in the middle of 2000`s by energy efficiency and home control, making electrical related products much safer for the end-user. So, the evolution since the mid of 70s until nowadays has enabled improved installation methods and increased people`s safety [6].

2.1. Forecast for the future. New technology to reduce greenhouse gas emissions

The total energy consumption will double between now and until 2030. The urgency about preserving the climate means we've got to halve CO² emissions the next 40 years. So we have got to improve the energy intensity of everything we do by a factor of four [1].

Since the 1975 there was an important growth trend of the different elements of the electrical installation market, develops technologies and solutions to manage energy and process in ways that are safe, reliable, efficient and sustainable in order to sustain innovation.

Also, ensuring the compatibility between LED light sources and controls will help ensure that end users are satisfied with the technology and the risk of arc fault detection is reducing till the circuit protection is worldwide in increasing (fig.1). Satisfied customers are the key to encouraging the mass adoption of LED, reducing energy usage and greenhouse gas emissions. As products and systems become more complex and inter-related such collaboration is the only way to stay ahead of the new market realities [7].

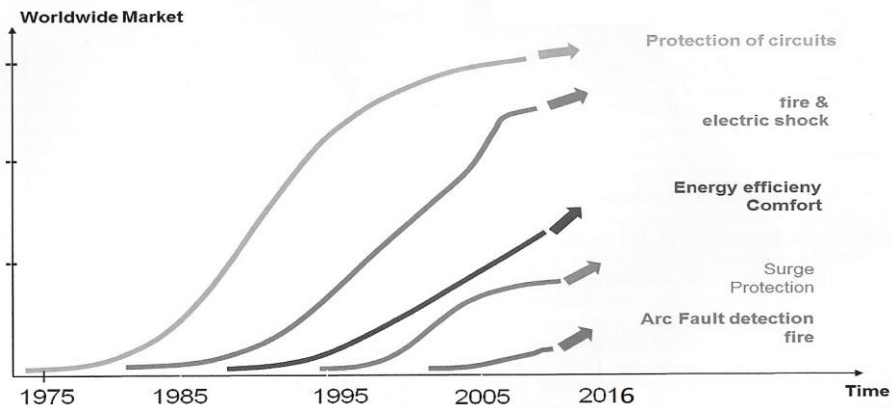


Fig.1. The electrical installation market

2.2. Responding to customers' needs

The local companies are seeking to improve consumer's lives through the development of practical solutions. This enables to offer products to consumers in different regions which are closer to the conditions and reality of their local usage, increases the company's knowledge regarding the technological and regulatory trends, which can lead to product innovation and strengthening of their business model.

Faced with the gradual, global phase – out of incandescent lamps is necessary to adapt the solutions to the evolving market. Light emitting diode (LED) lighting emerged as the preferred replacement; but LED lamps have unique electrical proprieties which mean control devices traditionally used for incandescent lights are not appropriate for LED light control [4].

Customers were faced with new challenges of compatibility and performance issues.

Updated many of products to work with the various LED lamps, the company also realized that the availability for dimming LED lights would make product development easier, product selection less confusing and less risky to the customer, and ultimately result in operational savings across the board.

In the late 1950s, the company's founder, Joel Spira, invented the solid dimmer using a thyristor, which generated less heat, used less energy than the rheostat that is replaced and it could fit into standard wall box. This provided people with the ability to vary the intensity of lights in their homes- something that they would never previously have dreamt of doing [8].

3. INCREASING THE OPERATIONAL COSTS

In order to control systems globally and to ensure the end customer is satisfied with their performance, LED lamps and dimmers will need to meet new specifications, that will help reduce the amount of required compatibility testing for lighting control

and lamp companies alike, reducing costs and accelerating product development for many[3].

The service operators are always looking for cost-effective technological solutions as: quality, maintainability and reliability are also key factors that are considered for all purchases and technology adoptions.

Rather than individuals without the specific knowledge misinterpreting technical requirements, leading to unnecessary requirements being implemented, the improved relationship with suppliers produces collaborative efforts in setting up some guidelines for proper technical requirements [5].

While condition monitoring technologies help to ensure the health of systems, adherence to processes and standards is equally crucial for the company to perform at its optimal level, so adopting international standards, provide a structured manner of defining technical specifications and clear tolerance limits for procured equipments and materials.

4. CONCLUSIONS

Manufacturing companies can use the increasing demands in terms of flexibility, individuality, and efficiency as an opportunity to be competitive over the long time. The system operators need efficient solutions and tools to operate the power systems in such a way to meet the economic and regulatory requirements.

REFERENCES

- [1]. **Leca A.,s.a.** *Managementul energiei*, Editura Agir, Bucuresti 2007.
- [2]. **Stochitoiu M.D** *About the power generating plants demands as energy management feature*, Annals of electrical engineering, University of Petrosani, 2016.
- [3]. www.schneider-electric.com
- [4]. www.mabeinternational.com
- [5]. www.statnett.no/en
- [6]. www.se.com.sa/en-us
- [7]. www.energes.com
- [8]. www.lutron.com

SIMULATION OF THE MAXIMUM LENGTH OF 20 KV OVERHEAD POWER LINES

LEON PANĂ¹, MARIUS MARCU²

Abstract: For any circuit, the cable size selected should not be less than the largest of the sizes calculated to meet the above limitations (this is the smallest size which will meet all of the requirements). In practice, the current-carrying capacity will be found to prevail in short-run/high-current circuits while voltage drop considerations will usually prevail in long-run/low-current circuits. It is unusual for short-circuit temperature requirements to determine the conductor size required for low voltage cable circuits.

Keywords: optimal section, maximum length, surge impedance loading.

1. INTRODUCTION

As power flows along a transmission line, there is an electrical phase shift, which increases with distance and with power flow. As this phase shift increases, the system in which the line is embedded can become increasingly unstable during electrical disturbances. Typically, for very long lines, the power flow must be limited to what is commonly called the Surge Impedance Loading (SIL) of the line.

Surge Impedance Loading is equal to the product of the end bus voltages divided by the characteristic impedance of the line. Since the characteristic impedance of various HV and EHV lines is not dissimilar, the SIL depends approximately on the square of system voltage. Stability limits on power flow can be as low as 20% of the line's thermal limit [1, 3, 4, 5, 6].

In addition to electrical phase shift, voltage magnitude decreases with distance. Generally, for transmission lines, the maximum allowable drop in voltage is limited to between 5% and 10% of the sending end bus voltage. The power flow (in MVA or MW) that corresponds to the maximum allowable decrease in voltage magnitude is called the line's voltage drop limit. As with phase shift, a transmission line's voltage drop limit decreases with transmission distance and is generally higher than the line's thermal limit for short lines but less than the line's stability limit for very long lines.

¹ *PhD., Lecturer, Eng., University of Petrosani*

² *PhD., Associate Professor, Eng., University of Petrosani*

Voltage drop limits on power flow can be as low as 40% of the line's thermal limit. Voltage drop limits may be increased by the addition of shunt capacitors at the end of the line. Such solutions are typically much cheaper than rebuilding the line [1, 3, 4, 5, 6].

2. ANALYTICAL MODEL

For to simplify the comparisons to be made, it is noted with [1, 3, 4, 5, 6]:

P_0 the power for which the section is optimal in terms of investments and losses

P_i the corresponding power at the maximum permissible intensity

P_u the corresponding power at the maximum allowable voltage drop.

In the case of medium voltage electrical networks, in general, for a given section there is the situation: $P_0 < P_i < P_u$. It has been seen in the previous paragraph that the optimum current density at these network categories is in the order of 0.6 to 0.8 A / mm², while the maximum allowable density is in the order of 1.5 to 2 A / mm². For these types of networks, consider the cost of the losses before fixing the conductor sections of an electrical line.

On the main sections of the lines we will have: $P_0 < P_u < P_i$, if the network is radially arbores cent and not too stretched, or $P_u < P_0 < P_i$ otherwise.

In lesser situations encountered in practice, there is the situation that: in the particular case of low-voltage electrical networks.

In order to highlight the above-mentioned aspects, compare P_0 and P_u on a major artery of an air MT departure, having the length L and the s -section. To begin with, it is assumed that the branches are distributed concentrically across the length of the artery. Also, section s being indicated will have to take into account the specific reactance x_0 of the conductor.

Returning to the relation (1), it can be seen that it can be written in the following form:

$$\Delta U = 10^2 \cdot \frac{\rho \cdot P \cdot L}{s \cdot U_n^2} \cdot \left(1 + s \cdot \frac{x_0}{\rho} \cdot \operatorname{tg}\varphi \right) = 10^2 \cdot \frac{P \cdot L}{U_n^2} \cdot \left(\frac{\rho}{s} + x_0 \cdot \operatorname{tg}\varphi \right) \quad (1)$$

In relation (1), the active power is expressed in MW, the length of the line is in km, and the rest of the magnitude has the meaning given in this paragraph.

At the same time, it should be noted that in the case of medium voltage networks of 20 kV, the voltage drop is limited to 7.5% and in the case of 6 kV networks the maximum allowable voltage drop is 5%. By replacing these values in the above relation we finally get:

$$P_u = 0.075 \cdot \frac{s \cdot U_n^2}{(\rho + s \cdot x_0 \cdot \operatorname{tg}\varphi) \cdot L} \quad (2)$$

$$s_{ec} = P \cdot \sqrt{A_3 \cdot T_{PM}^2 + B_3} \quad (3)$$

Taking into account the relation (3), for the main sections of the aerial or underground electric power networks, the following results in the end:

$$P_0 = \frac{s}{\sqrt{A_3 \cdot T_{PM}^2 + B_3}} \quad (4)$$

To determine the maximum length of an electrical line, the condition is: $P_u = P_i$, from where it finally comes:

$$L_{max} = 0.075 \cdot \frac{U_n^2 \cdot \sqrt{A_3 \cdot T_{PM}^2 + B_3}}{\rho + s \cdot x_0 \cdot \operatorname{tg}\varphi} \quad (5)$$

Analogically, the maximum length can be determined in the case of a medium-voltage main artery, in which the derivations are assumed to be evenly distributed throughout the artery length.

In this case, the voltage drop in relative values on the electric line is given by the relation:

$$\Delta U = 10^2 \cdot 0.5 \cdot \frac{\rho \cdot P \cdot L}{s \cdot U_n^2} \cdot \left(1 + s \cdot \frac{x_0}{\rho} \cdot \operatorname{tg}\varphi \right) = 10^2 \cdot 0.5 \cdot \frac{P \cdot L}{U_n^2} \cdot \left(\frac{\rho}{s} + x_0 \cdot \operatorname{tg}\varphi \right) \quad (6)$$

Finally, the expression of the maximum length for an aluminum conductor LEA is:

$$L_{max} = 0.15 \cdot \frac{U_n^2 \cdot \sqrt{A_3 \cdot T_{PM}^2 + B_3}}{\sqrt{3} \cdot (\rho + s \cdot x_0 \cdot \operatorname{tg}\varphi)} \quad (7)$$

In order to concretize the above-described results, an electric conductor line with aluminum conductors is taken into account, with the following data: $\Omega\text{mm}^2/\text{km}$, Ω/km , and kV, the ultimate expression of the maximum length, in km:

$$L_{max} = \frac{30 \cdot \sqrt{75 \cdot T_{PM}^2 + 890}}{31.2 + 0.262 \cdot s} \quad (8)$$

At the same time, determine the optimal section and the optimal current density for the previously analyzed line, and the parameters of the electric line taken from, resulting in:

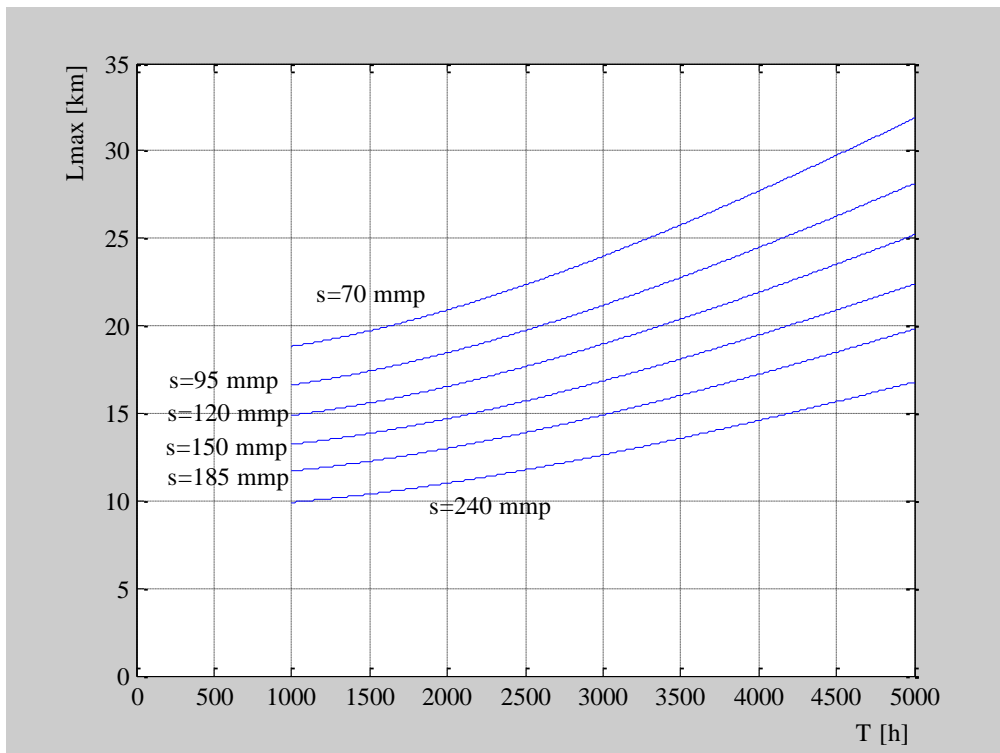
$$s_{ec} = P \cdot \sqrt{75 \cdot T_{PM}^2 + 890} \quad (9)$$

$$j_{ec} = \frac{36.12}{\sqrt{75 \cdot T_{PM}^2 + 890}} \quad (10)$$

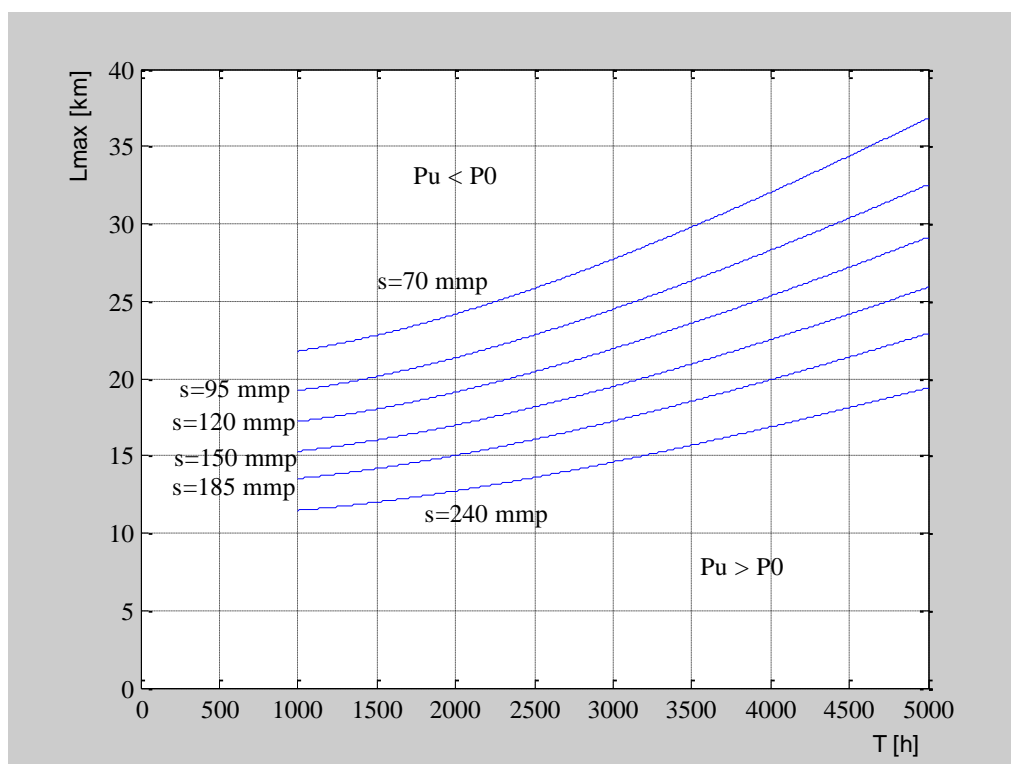
Similarly, the analytical expression of the maximum length in the case of a uniform distributed distribution network is:

$$L_{max} = \frac{60 \cdot \sqrt{75 \cdot T_{PM}^2 + 890}}{\sqrt{3} \cdot (31.2 + 0.262 \cdot s)} \quad (11)$$

In the figure 1 shows the value of the length limit resulting from relations (8) and (11).



a)



b)

Fig.1. The corresponding power at the optimal section and the corresponding power at the maximum voltage drop to a 20 kV LEA
a) LEA AI with uniformly charged loads
b) LEA AI with uniformly distributed tasks

The maximum voltage reached is called critical voltage, which corresponds to the maximum power transported and is also called critical power.

In case of MT derivations for an OHL equipped with conductors of 35 mm^2 OI-Al, it admits a maximum intensity of 135 A, which at 20 kV leads to a transmission capacity of $P_m = 4 \text{ MW}$.

This value of P_m is higher than the required power, generally taking into account local climatic conditions.

3. CONCLUSIONS

In the case of a medium voltage electrical network (LEA), which has the possibility of looping in the event of an incident, the voltage drop in the fault scheme may be higher than in the normal operating circuit, so that for a relatively short time allows to exceed the upper limit of 7.5% indicated above. In the case of electrical networks (LEC 6 kV) the maximum voltage drop is 5%.

In general, for a given electrical network and without taking into account the permissible thermal limit and the maximum allowable voltage drop, there is an active power limit that can be transported and should not be exceeded.

While the maximum power is not reached, the voltage increase in the secondary of the transformer due to the change of the socket is superior to the dimming of the primary voltage due to the decrease of the impedance.

REFERENCES

- [1]. **Ionescu G. T., Pop O.,** *Ingineria sistemelor de distribuție a energiei electrice*, Editura Tehnică, București, 1998.
- [2]. **Marcu M.D., Popescu F.G., Pana L.,** *Modeling and simulation of power active filter for reducing harmonic pollution using the instantaneous reactive power theory*. Environmental Engineering and Management Journal, June 2014, Vol.13, No. 6, Pages: 1377-1382.
- [3]. **Marcu M.D., Pana L., Popescu F.G., Slusariuc R.,** *Evaluation the losses power and electrical energy on the basis of the relative load curves, by reference to the basic sizes*. Papers SGEM2014/Conference Proceedings, Vol. Energy and clean technologies, ISBN, 229 - 236 pp, 17-26 June, Albena, Bulgaria, 2014.
- [4]. **Pană, L.,** *Tehnici de optimizare în sistemele electroenergetice miniere*, Editura Focus, Petroșani, 2006.
- [5]. **Pana L., Popescu F.G., Samoilă L., Slusariuc R.,** *Analysis of thermic stability in short circuit regime of electric distribution networks conductor*. 6th International Multidisciplinary Scientific Symposium, SIMPRO 2014, Conference Proceedings, Pages: 331-334, 10-11 Octombrie, Petroșani, 2014.
- [6]. **Popescu F.G., Marcu M.D.,** *Metode moderne de analiză și reducere a armonicilor de curent și tensiune*, Editura Universitas, Petroșani, 2016, pag. 265, ISBN 978-973-741-504-2.

THE MODERN APPROACH OF POWER FACTOR

MARIA DANIELA STOCHITOIU¹, ILIE UTU², LILIANA SAMOILA³,

Abstract: The electrical equipments are nonlinear loads for a.c. electrical webs. So, some reactive components in absorbed currents and important harmonics are appearing. The reactive components and the harmonics lead to a low power factor, a less efficiency, the electromagnetically interference phenomena for the closer equipments or an overheating of power transformer. Due to aspects, a lot of international agencies have imposed some restrictions above the current harmonics shat by power equipments.

Key words: current harmonics, power factor, distortion effect.

1. INTRODUCTION

The linear loads can have only the diphase current effect due to their reactive components, but the nonlinear loads are causing the absorbed current distortion in first of all and then some diphase eventually. Most of electrical equipments are nonlinear loads so will bring the current harmonics and the degradation of the power factor. It can emphases about the harmonically pollution.[1]

In case of supply with a harmonically voltage, the power factor PF is given by two factors as: the effect of distortion current wave and the effect of current diphase. Harmonics have existed from the earliest days of the industry and were (and still are) caused by the non-linear magnetizing impedances of transformers, reactors, fluorescent lamp ballasts, etc... In addition, power electronic devices have become abundant today because of their capabilities for precise process control and energy savings benefits. However, they also bring drawbacks to electrical distribution systems: harmonics. The definition of the power factor doesn't show the using level of available power in the electrical web in the deformed regime, because the harmonically sources even are the nonlinear receptors not the generators. It is necessary to have in view the electrical energy quality in the interface node of supplier – customer taking in account the extending of nonlinearity of loads.[7] The supplier has the duty to deliver a voltage which has the wave characterized by the true value of power factor of distorting the accepted limit. For the low and average voltage webs the total distorting factor must be under 8% according to the European Standards EN 50160.

¹ *PhD., Associate Professor, Eng., University of Petrosani*

² *PhD., Associate Professor, Eng., University of Petrosani*

³ *PhD., Associate Professor, Eng., University of Petrosani*

The accepted levels of harmonics are prescript by the same standard, too. The supplier requires some limits of perturbation determined on the current wave as the voltage does not be affected and to respect some standards quality indicators. The devices used for monitories an analysis of electrical energy quality are showing two values, one for the fundamental harmonic **DPF** and another one for the total power factor **PF**. Between these values can appear large difference and an uninformed energetic engineering can take wrong decisions for compensation measurements of reactive power using battery of capacitors which can affect the quality energy due to the amplification of harmonics.[2]

$$\lambda_1 \equiv \text{DPF} = \cos \varphi_1 = \frac{P_1}{S_1} \quad (1)$$

PF – the total power factor:

$$\lambda \equiv \text{PF} = \frac{P}{S} = \frac{P}{U \cdot I} \quad (2)$$

The PF includes the influences of harmonics above the active power and the apparent power giving information about the efficiency of the active power. The active power in the no sinus regime is given by the sum of the active powers corresponding of which harmonics:

$$P = \sum_{h=1} U_h I_h \cos(\alpha_h - \beta_h) = \sum_{h=1} U_h I_h \cos(\varphi_h) = P_1 + P_H \quad (3)$$

P_1 - is the fundamental active power

$$P_1 = U_1 I_1 \cos \varphi_1 \quad (3.1)$$

P_H - is the active power of each harmonic

$$P_H = \sum_{h \neq 1} U_h I_h \cos(\varphi_h) \quad (3.2)$$

S_1 - is the apparent power of fundamental $S_1 = U_1 \cdot I_1$

S - is the harmonically apparent power

$$S = (U \cdot I)^2 = (U_1^2 + U_H^2)(I_1^2 + I_H^2) = S_1^2 + S_H^2 \quad (4)$$

The power factor can be defined by introducing the distorting factor **THD** for current and fort the voltage.

$$k_{DI} \equiv \text{THD}_I = \frac{I_H}{I_1} = \sqrt{\frac{\sum_{h \neq 1} I_h^2}{I_1^2}} \quad (5)$$

$$k_{DU} \equiv THD_U = \frac{U_H}{U_1} = \sqrt{\frac{\sum_{h \neq 1} U_h^2}{U_1^2}} \quad (6)$$

So,

$$\lambda \equiv PF = \frac{P}{S} = \frac{P_1 + P_H}{\sqrt{S_1^2 + S_H^2}} = \frac{(P_1/S_1)[1 + (P_H/P_1)]}{\sqrt{1 + (S_H^2/S_1^2)}} = \frac{[1 + (P_H/P_1)] \cdot DPF}{\sqrt{1 + THD_1^2 + THD_U^2 + (THD_1 \cdot THD_U)^2}} \quad (7)$$

The second definition of distortion power factor in (1.7) is suitable for use when $THD_U < 5\%$ and $THD_I > 40\%$, which is true for the majority of the non-linear loads presented in this thesis. However, all DPF values presented are derived from the full definition. From the definitions, it is theoretically possible to improve the true power factor by reducing the phase angle between the voltage and current fundamental components or by lowering the harmonic currents. Due to the distorting residue of the active power is more lower than the fundamental active power $P_H \ll P_1$, so $\frac{P_H}{P_1} \ll 1$. For $THD_U < 5\%$ and $THD_I > 40\%$, the relation between the total power factor and the fundamental power factor is :

$$\lambda \equiv PF = \frac{1}{\sqrt{1 + THD_I^2}} \cdot DPF = \frac{I_1}{I} \cdot \cos\varphi_1 \quad (8)$$

Where: I_1 - is the effective value of fundamental component of current;

I - is the effective value of no sinusoidal current;

φ_1 - is the phase between the fundamental component of the current and the voltage waves [1].

2. THE MEASUREMENT FLUX SOURCES OF POWER FACTOR IN NO SINUSOIDAL STAGE

The quality of value measurement process is assessed through the measurement fluxes. For the power factor the fluxes sources are:

- the nonlinear character of input converter as voltages transformers and the current transformers or amplitude/frequency characteristic of these measurement devices which were designed to work for sinusoidal stages;
- the adoption of measurements ways based on the functional and working basics incompatible with the behave stages. There are a lot of situations when the

power factor is calculated as an average value on a period of time (account period), based on setting down active energy W_a and reactive energy W_r . The errors of reactive energy measurements are increasing even in non sinusoidal operating and sinusoidal operating but unsymmetrical.

$$\lambda_{med} \equiv PF_{med} = \frac{W_a}{\sqrt{W_a^2 + W_r^2}} \quad 0 \leq \lambda_{med} \leq 1 \quad (9)$$

- the improperly choice of tariff period. The power factor persuade using the first relations it is possible do not reflect the real situation where can appear important perturbations, if on the adopted measure period the average power factor fulfill the condition to be equal with the neutral power factor, when the load is varying; the systematically errors of digital measurement devices; the measurement method as using two or three active systems for one digital meter for measurements in three phases circuits can lead to different results; the implementation of different definitions in microprocessors [5].

3. THE CORRECTION METHODS OF POWER FACTOR

The importance of determining the power factor is made by the tariff system for punishing the customer who increases the power losses in the electrical system, necessitating the power factor value in the delimitation point connection and the neutral value of power factor.

The correction capacitors can be used for getting right the the phase angle which determines a low value for power factor. It has to verify if the deforming stage is not emphasizing, some possible resonances can determine overvoltage which provoke the damages of electric components. The energy bill can rise due to operating in capacitive character. If PF is more than 10% of DPF the current harmonics determine the decrease of power factor. If the harmonics level is suggestive it can use the active harmonics conditioners for diminution the deforming stage but there appears an important capacitive power contribution. The increase in nonlinear loads has led to harmonic distortion in electrical distribution systems. Although capacitors do not cause harmonics, they can aggravate existing conditions. Harmonics typically seen on a power system can be subdivided into two distinct categories by the nature of the problems they create and the remedies they usually require [4].

A discussion of power system harmonics is incomplete without discussing the effects of power factor correction capacitors. In an industrial plant containing power factor correction capacitors, harmonic currents and voltages can be magnified considerably due to the interaction of the capacitors with the service transformer. This is referred to as harmonic resonance or parallel resonance. For a typical plant containing power factor correction capacitors, the resonant frequency (frequency at which amplification occurs) normally falls in the vicinity of the 5th to the 13th harmonic. Because nonlinear loads typically inject currents at the 5th, 7th, 11th, and 13th harmonics, a resonant or near-resonant condition will often result if drives and capacitors are installed on the same system [6].

In practice, power factor correction (PFC) techniques will influence both. There are two general forms of PFC, active (a-PFC) and passive (p-PFC). As the name suggests, a-PFC utilizes active electronic components to control the harmonic emissions. Due to the active control, the resulting input current waveform is very close to the ideal sinusoid, with a displacement power factor very close to unity and a very low THD_I [7].

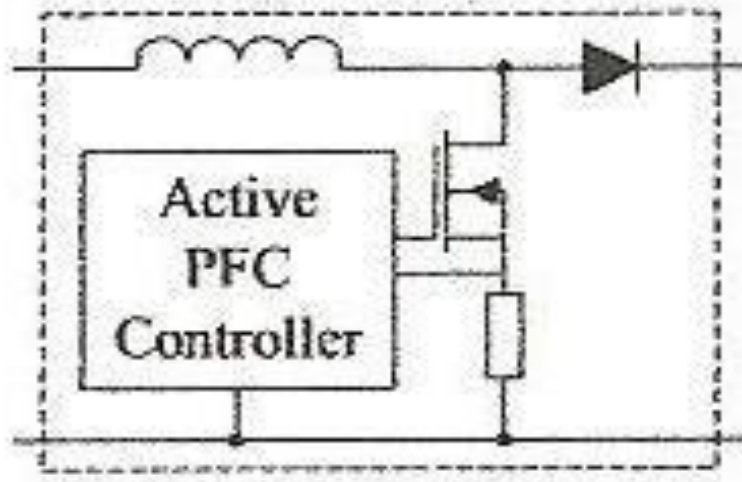


Fig.1. Active power filter correction

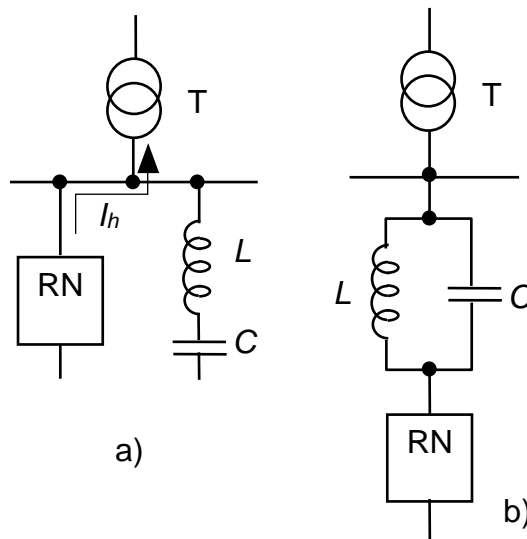


Fig.2. Passive Power Filter correction
a) parallel b) serial

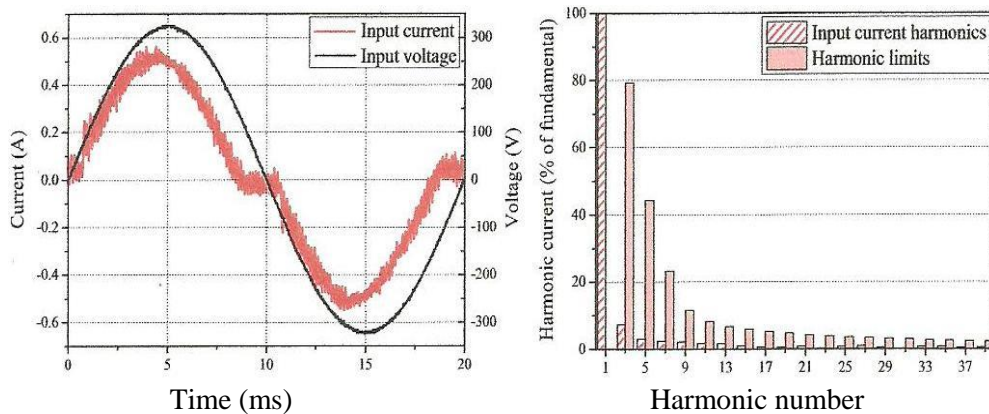


Fig.3. Input current waveform and harmonic content for characteristics Active filter

For stricter harmonic legislation, it may be necessary to include additional passive components in the circuit to satisfy harmonic limits. This is classified as passive-PFC. The most common p-PFC approach in the power electronics load category is to include an additional inductance in the conduction path to reduce the harmonic emissions. As inductors oppose the change of current, this will effectively reduce the rate of change of the current pulse and 'smooth' the input current waveform.

4. CONCLUSIONS

For a typical plant containing power factor correction capacitors, the resonant frequency (frequency at which amplification occurs) normally falls in the vicinity of the 5th to the 13th harmonic. Because nonlinear loads typically inject currents at the 5th, 7th, 11th, and 13th harmonics, a resonant or near-resonant condition will often result if drives and capacitors are installed on the same system.

There are numerous benefits to be gained through power factor correction. These benefits range from reduced demand charges on your power system to increased load carrying capabilities in your existing circuits and overall reduced power system losses. And the benefits of power factor correction aren't just limited to the balance sheet; there are also huge environmental benefits associated with power factor correction, which means your company is reducing its carbon footprint and helping the environment.

REFERENCES

- [1]. **Carmen Ionescu Golovanov** *Masurarea marimilor electrice in sistemul electroenergetic*, Editura Academiei Romane, Bucuresti 2009;
- [2]. **Lucia Dumitriu, s.a.** *Teoria circuitelor electrice*, Editura Matrixrom, Bucuresti 2007
- [3]. **Maria Daniela Orban, s.a.** *Electrotehnica si masini electrice*, Editura Academica Brancusi, Tg Jiu, 2002
- [4]. **Dan Lascu**, *Tehnici si circuite de corectie activa a factorului de putere*, Editura de Vest, Timisoara 2004
- [5]. **Maria Daniela Stochitoiu, Alin Gruber**, *The modern estimation of power factor*, SIMPRO 2012, Petrosani
- [6]. www.sier.ro
- [7]. www.eaton.com

VERIFYING THE PARAMETERS OF ELECTRIC MOTORS ACTING ON FANS OPERATING IN EXPLOSIVE ATMOSPHERES WITH GASES, VAPORS, MISTS AND DUSTS

MARCEL DANIEL RAD¹, MIHAI MAGYARI², SORIN BURIAN³,
LUCIAN MOLDOVAN⁴, DRAGOS FOTAU⁵

Abstract: Where electrical apparatus is to be installed in areas where flammable gases, vapors or mists may be present in the atmosphere, protective measures are applied in order to reduce the likelihood of explosion due to ignition by arcs, sparks or hot surfaces, produced either in normal operation or under specified fault conditions.

Protective measures aim to reduce, to an acceptable level, the likelihood that the electrical installation could become a source of ignition.

Keywords: Electric motors, flameproof enclosure, fans, gas, dust, explosive atmosphere, ventilation, acting.

1. INTRODUCTION

Evaluation of equipment designed to operate in potentially explosive atmospheres, in purpose of certification, represents an important aspect considering the existing explosion risk which has to be minimized in order to ensure people's health and safety, as well as to prevent goods damage and protection of the environment. The evaluation of equipment designed to operate in potentially explosive atmospheres is made by assessment of the technical documentation and tests applied on equipment test samples.

The equipment operating in hazardous explosive atmospheres has to be subjected to certification procedures, according ATEX Directive 2014/34/EU (transposed in Romanian legislation by Government Decision no. 245/2016) (Directive 2014/34/EU, 2014).

¹ *PhD student eng scientific researcher. assistant, INCD INSEMEX Petroșani*

² *PhD eng., IInd degree scientific researcher, INCD INSEMEX Petroșani*

³ *PhD eng., Ist degree scientific researcher, INCD INSEMEX Petroșani*

⁴ *PhD eng., IInd degree scientific researcher, INCD INSEMEX Petroșani*

⁵ *PhD eng., degree scientific researcher, INCD INSEMEX Petroșani*

For the evaluation of explosion-proof characteristics of electrical equipment, the provisions of harmonized standards from the SR EN 60079 series are used. The standards SR EN 60079-0 (Explosive atmospheres. Part 0: Equipment. General requirements) and one or more of the standards containing the specific requirements for the type(s) of protection applied to equipment (ex. SR EN 60079-1 for the type of protection flameproof enclosure "d", SR EN 60079-7 for the type of protection increased safety "e", are used for performing the assessment. For evaluation of explosion-proof electrical equipment, these shall be also subjected to type tests.

In the standard SR EN 60079-0 are indicated the type tests to which all the explosion-proof electrical equipment shall be subjected and the order in which these tests shall be performed.

2. TERMS AND DEFINITIONS

explosive atmosphere

mixture with air, under atmospheric conditions, of flammable substances in the form of gas, vapour, mist or dust, in which after ignition, combustion spreads throughout the unconsumed mixture.

group (of an electrical apparatus for explosive atmospheres)

classification of electrical apparatus related to the explosive atmosphere for which it is to be used.

Electrical apparatus for use in explosive gas atmospheres is divided into two groups:

- group I: electrical apparatus for mines susceptible to firedamp;
- group II: (which can be divided into subgroups): electrical apparatus for places with an explosive gas atmosphere, other than mines susceptible to firedamp
- group III: (which can be divided into subgroups): electrical apparatus for use in places with an explosive dust atmosphere, other than mines susceptible to firedamp

maximum surface temperature

highest temperature which is attained in service under the most adverse operating conditions (but within recognized tolerances) by any part or surface of the electrical apparatus, which would be able to produce an ignition of the surrounding explosive atmosphere

The most adverse conditions include recognized overloads and fault conditions recognized in the specific standard for the type of protection concerned.

The relevant surface temperature may be internal and/or external depending upon the type of protection concerned.

VERIFYING THE PARAMETERS OF ELECTRIC MOTORS ACTING ON FANS
OPERATING IN EXPLOSIVE ATMOSPHERES WITH GASES, VAPORS,
MISTS AND DUSTS

type of protection

specific measures applied to electrical apparatus to avoid ignition of a surrounding explosive atmosphere

flameproof enclosure “d”

type of protection in which the parts which can ignite an explosive atmosphere are placed in an enclosure which can withstand the pressure developed during an internal explosion of an explosive mixture and which prevents the transmission of the explosion to the explosive atmosphere surrounding the enclosure

increased safety “e”

type of protection applied to electrical apparatus in which additional measures are applied so as to give increased security against the possibility of excessive temperatures and of the occurrence of arcs and sparks in normal service or under specified abnormal condition.

3. DEVELOPED TESTING TECHNOLOGIES FOR VERIFYING PARAMETERS OF FANS EQUIPPED WITH ELECTRIC MOTORS

The evaluation of explosion-protected electrical equipment is carried out taking into account the requirements of the reference standards: SR EN 60079-0 (which includes the general requirements for all explosion-protected electrical equipment) and the standards specific to the types of protection involved in the manufacture of the equipment.

For evaluation, as appropriate, explosion-proof equipment must be tested.

Tests and checks to be made to explosion-proof electrical equipment in accordance with SR EN 60079-0 include the verification of the parameters of electric motors acting on a fan.

Verification of fan motor parameters must be applied to fans up to 5 kW, with the fan pad mounted directly on the electric motor, ie the engine is part of the fan.

These requirements apply to fans (eg room fans) with the same EPL inside and outside the fan casing, intended for use in the same area inside and outside the casing. Where ventilation housings are designed to separate a dangerous atmosphere from the interior of the casing to another hazardous atmosphere outside the casing, additional requirements, such as casing tightness requirements, should be considered.

There are no premise ventilators in the Ma, Ga, and Da EPL because these applications are considered to transfer the flammable process environment and not a ventilation function that transfers the air.

The most important nominal parameter for an electric motor that must be observed for its correct choice and operation is the rated voltage, usually denoted U_n and indicated in [V] or [kV]. This is the highest standard voltage value (for DC electric motors) and the highest effective voltage (in the case of AC motors) for which they are designed and built to guarantee their operation long lasting, without damage (of the usual insulation) to disrupt the subsequent operation.

The actual voltage at which an electric motor operates is called a service voltage, usually denoted U_s , at a limit equal to the rated voltage. During the operation of electric motors they are exposed, usually for a limited time, to the action of voltages higher than the nominal voltage, called over voltages, which they must bear without damaging them. Atmospheric overvoltage, but also overvoltage over voltages, can be highlighted by the circuit in which the motor is incorporated and when they occur. In order to withstand these surges, the insulation of the electric motors is characterized by a holding voltage, higher than the nominal voltage, against which even an insulation safety coefficient can be defined. The holding voltage is confirmed by testing of the insulation of the electric motors and distinguishes between the standard voltage pulse and the holding frequency at the industrial frequency.

The block diagram of the bench for parameter checking that meets the test requirements specified in the standard and which will allow the stand to be put into practice is according to Fig. 1.

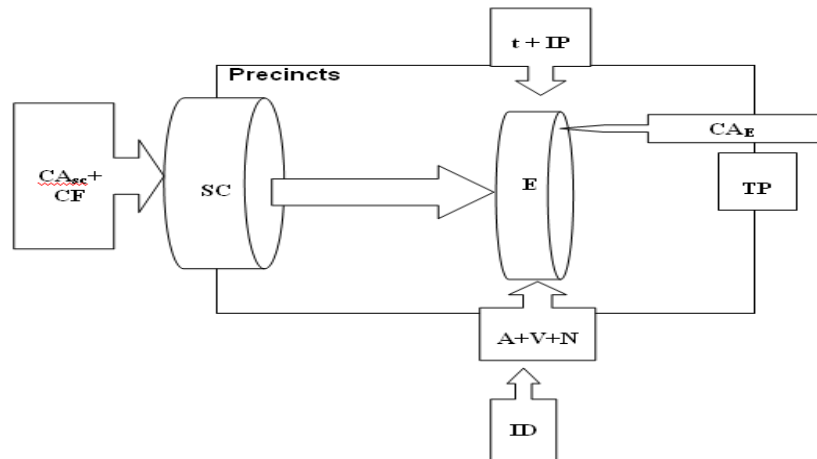


Fig.1. The block diagram of the bench for parameter checking

- SC - backpressure source;
- CAAsc - power source for backpressure;
- CF - frequency converter;
- IP - digital pressure gauge;
- t - temperature indicator;
- A - current indicator;

VERIFYING THE PARAMETERS OF ELECTRIC MOTORS ACTING ON FANS
OPERATING IN EXPLOSIVE ATMOSPHERES WITH GASES, VAPORS,
MISTS AND DUSTS

V - voltage indicator;
N - speed indicator;
TP - pressure transducer;
Data Recording ID;
E - equipment for testing;
CAE - box power equipment for verification.

It should be stressed that the value of the nominal voltage, but also the functionality of the electric motor, decisively influences its gauge.

The nominal voltage values are established by STAS, in line with the regulations of the International Electrotechnical Committee (IEC), so that a typing of the electric motors comes from this point of view. For areas of special use, mining equipment, traction electrical, etc., "abnormal" values of the nominal voltage of the electric motors specific to these installations may occur.

The second important parameter for electric motors is the nominal current, designated I_n and usually indicated in [A]. This is defined as the maximum typed value (maximum effective for AC motors), which passes the current path of the electric masonry according to the expected operation (even for an unlimited period of time), does not produce any heating or other construction components, performs heatings at temperatures exceeding the permissible limits imposed on the design, and therefore does not compromise the subsequent operation of the assembly.

The current paths of the electric motors are actually covered by the service current, denoted I_s , lower, at the limit equal to the nominal current. Under certain operating conditions, the current paths of electric motors are over current, they are over currents, which can be classified by amplitude and duration, for defective situations, such as overcurrent currents or short-circuit currents.

The nominal power P_n , measured in [W] or [kW], is the active power of the motor that it obtains at the shaft when fed to the rated voltage, so that the engine's heating does not exceed the temperature of the its insulation, the engine running for an unlimited time in the service considered and in the specified environmental conditions. It is understood that the nominal P_n power defined above does not mean that the engine has a much lower heating than the corresponding heating for its insulation class

The nominal speed in rpm is the speed immediately below that of the synchronicity when the engine was running in the nominal mode (the synchro cycle speed is given by the relation $n_1 = 60xf_1/p$ and represents the speed with which the stator invasive magnetic field rotates).

The nominal power factor is defined by the factor of the active power absorbed by the motor in the nominal operating mode, considering the voltage and current in the stator as sinusoidal.

The nominal frequency f_n , measured in Hz, is the frequency of the supply voltage of the motor to which it was designed for the purpose of its normal operation.

Following the analysis of the specific requirements for type tests for electrical equipment and fans directly driven by the electric motor shaft, the fan has to be supplied with the rated voltage and, if applicable, with the specified backpressure, and the parameters measured with the test stand to match the nominal fan speeds.

To meet these requirements, a test stand was designed to verify these parameters. The stand for checking the fan parameters driven by an electric motor with the elements specified below is shown in the following figure:



Fig.2. The electric motor with the specified elements

The following components were included in the verification stand:

- a back pressure source which may be a fan capable of generating a minimum pressure;
- Frequency converter required to drive the fan that creates the over pressure given by the manufacturer;
- a control box for supplying the fan to be tested;
- a transparent and insulated enclosure in which the ventilator under test is inserted;
- a digital pressure indicator instrument covering the range of 0-600 Pa;
- a temperature indicator instrument within the limits of 0 to 500 ° C for measuring the surface temperature of the engine operating the fan;
- an instrument for measuring the voltage;
- a current indicator for measuring the current;

VERIFYING THE PARAMETERS OF ELECTRIC MOTORS ACTING ON FANS
OPERATING IN EXPLOSIVE ATMOSPHERES WITH GASES, VAPORS,
MISTS AND DUSTS

- Speedometer indicator instrument;
- a data acquisition system resulting from the test consisting of:
 - a) pressure transducer;
 - b) temperature transducer,
 - c) data acquisition system.

The data acquisition system is used to record test parameter values, but also to raise the fan diagram if necessary.

Verification of the parameters of the electric motor acting on the fan will be done with a three-phase digital multimeter DMM-3T with the following technical characteristics:

DMM-3T - is a microprocessor multimeter designed to monitor the three-phase supply voltage. The multimeter allows high precision measurements of all basic network parameters such as phase voltages and currents, frequency, active, reactive, apparent power and power factor. In addition, the multimeter allows you to completely measure the energy (both input and output) through the four dials.

The monitored measurements and equipment configurations are displayed on the multifunction front panel and LEDs. The multimeter is programmed using the four keypad buttons. The RS485 interface, and the implementation of a MODBUS RTU communication protocol, offers the device communication with equipment from a wide range of hardware and software industries.

Operation:

- direct or indirect (current transformer) measurement of the current for each phase;
- direct or indirect measurement (using current transformer) of the voltage for each phase and the voltage between the phases;
- frequency measurement;
- active, reactive and apparent power measurement;
- power factor measurement;
- quadrant measurement of input and output energy.

Also, another parameter that needs to be checked is the speed of the electric motor that drives the ventilator under test. This parameter will be checked by means of a digital optical speed measurement device, contact

At the same time, during the tests, the maximum surface temperature is also monitored. Maximum surface temperature measurement will be performed throughout the process of checking the parameters of the electric motor operating the fan by means of a PC151HT-0 infrared sensor, temperature 0-500° C.

Verification of fan parameters driven by electric motors

- 1) Check the sample (fan).
- 2) Check that the test stand is not powered on the power grid
- 3) Mount the sample (fan) into the test stand
- 4) connect the sample (fan) to the TCME55 power box
- 5) Check that the electrical connections are correctly made
- 6) engages the stand distribution panel on the electrical network
- 7) the axial helical fan ELICENT IEM 634 T (1IE0604)
- 8) Using the frequency converter the fan speed is adjusted so that the pressure indicated by the differential pressure gauge DT-8890 corresponds to the minimum back pressure or indicated by the manufacturer in the data sheet
- 9) the sample (the fan)
- 10) the maximum parameters (power, current, rotational speed) of the sample (fan)
- 11) compares the maximum parameters measured with the nominal parameters of the sample (fan)

The following screenshots show the steps performed to test the fan motor's parameter controlled by the electric motor.



Fig.3. Testing the fan

VERIFYING THE PARAMETERS OF ELECTRIC MOTORS ACTING ON FANS
OPERATING IN EXPLOSIVE ATMOSPHERES WITH GASES, VAPORS,
MISTS AND DUSTS



Fig.4. Parameters display

4. CONCLUSIONS

The paper aims at studying and evaluating the requirements for checking the parameters of the electric motor driven fan with the "d" flameproof enclosure and the "e" increased security. An analysis has been made of the equipment and components to be purchased

The verification of the mentioned parameters can be performed in compliance with the requirements of the applicable standards (SR EN 60079-1- Protection of the equipment by means of flameproof enclosure "d", SR EN 60079-7 - Protection of the security equipment with increased security "e", which will increase the capacity of the group testing laboratories to perform tests on equipment with a protection type, increased safety "e" and flameproof enclosure "d" for use in potentially explosive atmospheres.

As a result of the analysis of the developed test technology and the developed methodology, it has been shown that all the requirements imposed by the standard SR EN 60079-0: 2013 regarding the testing of parameters of the electric motor driven fans

The works presented their equipment and their technical characteristics, which belong to the company's inspection stand.

The purpose of this paper was to study and analyze the main technical parameters of fans driven by electric motors.

A test procedure has been developed to check the parameters of electric motors powered by fans.

Finalizing and implementing the results of this project will lead to a series of advantages, such as:

- The development of new technologies for the testing of equipment intended for use in explosive atmospheres meeting the requirements of the applicable standards.
- Creating the possibility of carrying out other tests applicable to electrical equipment intended for use in explosive atmospheres with the purchased equipment.

REFERENCES

[1]. EN 60079-0:2013, *Explosive atmospheres* -- Part 0: Equipment - General requirements.

[2]. EN 60079-1:2015, *Explosive atmospheres*. Part 1: Equipment protection by flameproof enclosures “d”.

[3]. EN 60079-7:2007, *Explosive atmospheres*. Part 7: Equipment protection by increased safety “e”.

[4]. Directive 1999/92/EC of the European Parliament and of the Council of 16 December 1999 on minimum requirements for improving the safety and health protection of workers potentially at risk from explosive atmospheres (15th individual Directive within the meaning of Article 16(1) of Directive 89/391/EEC).

[5]. **Bottril G., Chueyne D., Vijayaraghavan G.**, (2005), *Practical electrical equipment and installations in hazardous areas*, Elsevier Publishers, 149-150.

[6]. **Garside R.**, (1995), *Intrinsically safe instrumentation: a guide*, Hexagon Technology Limited, 50-53.

[7]. **Simion S., Baron O., Basuc M.**, (2004) *Explosion Risk*, (in Romanian) Europrint Publishing House, Oradea, Romania.

[8]. Directive 2014/34/EU of the European Parliament and of the Council of 26 February 2014 on the harmonisation of the laws of the Member States relating to equipment and protective systems intended for use in potentially explosive atmospheres.

ASPECTS ON TESTING OF GALVANIC CELLS FOR ELECTRICAL EQUIPMENT INTENDED FOR USE IN POTENTIALLY EXPLOSIVE ATMOSPHERES

TIBERIU CSASZAR¹, SORIN BURIAN², MARIUS DARIE³,
COSMIN COLDA⁴, ADRIANA ANDRIS⁵

Abstract: The explosion protection for electrical equipment designed for operation in potentially explosive atmospheres among other requirements consist of limiting the energy in a circuit. This objective is achieved by the type of explosion protection intrinsic safety, symbolized "i". This type of protection is suitable also for mobile and portable electrical equipment which are supplied from autonomous sources. From point of view of the acceptability of using these types of components in potentially explosive atmospheres, it is underlined that those should be tested in compliance with specific technical standard.

In the introduction is presented the general and specific context of the article demarche. The next two parts is allocated for the underlining the aspects on test procedure and test rig. Pictures included show the rig configuration and its components.

In the part entitled results and discussions is presented graphical time dependence of parameters measured temperature at the middle galvanic cell, current which flows into galvanic cell, voltage across the galvanic cell and ambient temperature. Also in this part is presented the mathematical relations used for inner electrical resistance and stored energy for the tested galvanic cell.

Keywords: intrinsic safety, explosive atmospheres, galvanic cells, maximum surface temperature, inner minimum electrical resistance

1. INTRODUCTION

The explosion protection principle for electrical equipment designed for operation in potentially explosive atmospheres by limiting the energy and temperatures is achieved by the type of explosion protection intrinsic safety. This type of protection is symbolized "i". Also it is suitable for portable electrical equipment which are autonomous sources due to inner energy source. Regarding the acceptability of using these types of equipment in potentially explosive atmospheres, they should be assessed

¹ *PhD. Eng. Researcher I at INSEMEX Petroșani Romania*

² *PhD. Eng. Researcher I at INSEMEX Petroșani Romania*

³ *PhD. Eng. Researcher I at INSEMEX Petroșani Romania*

⁴ *PhD. Eng. Researcher III at INSEMEX Petroșani Romania*

⁵ *Eng. Researcher at INSEMEX Petroșani Romania*

and tested in according to specific technical standards. The autonomous inner sources are based using the primary and secondary galvanic cells.

In order to ensure security of life and health, to prevent damage goods and not the least environmental damages, the process of assessment and testing of the equipment which is part of an explosion protected system plays an important role in order to minimize the explosion risk [3].

The explosion type protection are implemented by using specific requirements. Those requirements are applied to electric equipment in order to prevent ignition of explosive surrounding atmosphere. It could be noticed that the trend increasing of using the wireless connection for data transfer.

For the purpose of applying the intrinsic safety type of protection „i” assessment, the samples provided by the manufacturer are subsequently submitted to a series of tests which have in view the most unfavorable scenarios which could occur. The assessment of explosion protected equipment containing cells is conducted by tests specified in [6] for general requirements and [5] for intrinsic safety specific requirements. Other technical requirements are covered by other specific standards [7] to [12].

All equipment which is part of an explosion protected system used in area endangered by explosions should comply with requirements below listed: to be adequate explosion protected; to maintain explosion protection level for all environment conditions for which was meant; to cope all stress inherent the process of storing, transport, erection and operation.

Intrinsic safety type of protection rely on limitation of energy and temperatures into protected circuit. According to failure scenarios, it is needed to have in view three levels of protection: „ia”, “ib” and “ic”.

2. TEST PROCEDURE

The specific standard for intrinsic safety type of protection mention that are two alternatives for using galvanic cells thus: cells which does not need to be replaced in hazardous area and cells which is needed to be replaced in hazardous area [1].

For first case the cells should be placed in a special closed compartment and other should be encapsulated together with the limitation devices such that just protected circuit parts could be exposed.

For the purpose of spark test ignition of the cells maximum open circuit voltage should be considered. Otherwise, for thermal ignition tests should be used rated voltage (see figures 1 and 2). For the scope of the article will be considered further thermal ignition tests.

According to the standard it is needed to test 10 samples. But before the thermal test it is necessarily to conduct another test for rated cell capacity confirmation. The minimum accepted threshold for capacity is 95% from rated capacity.

ASPECTS ON TESTING OF GALVANIC CELLS FOR ELECTRICAL EQUIPMENT
INTENDED FOR USE IN POTENTIALLY EXPLOSIVE ATMOSPHERE

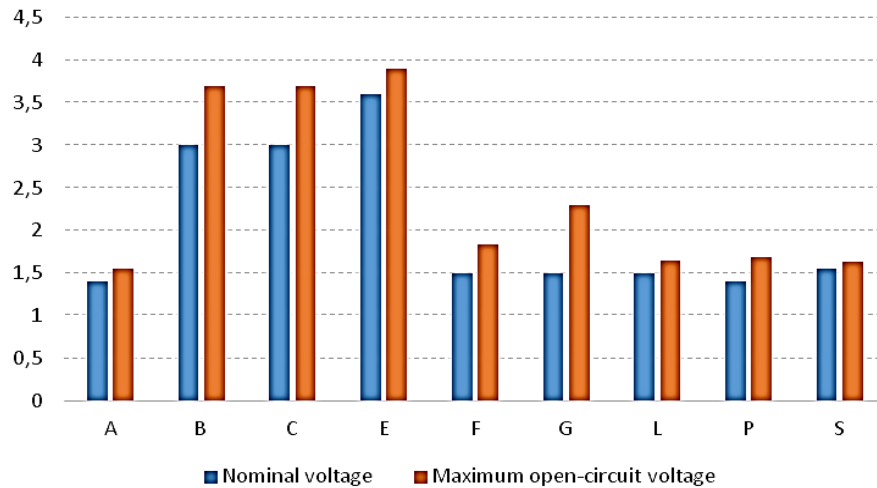


Fig. 1. Nominal and peak voltage for primary cells of types A to S (3)

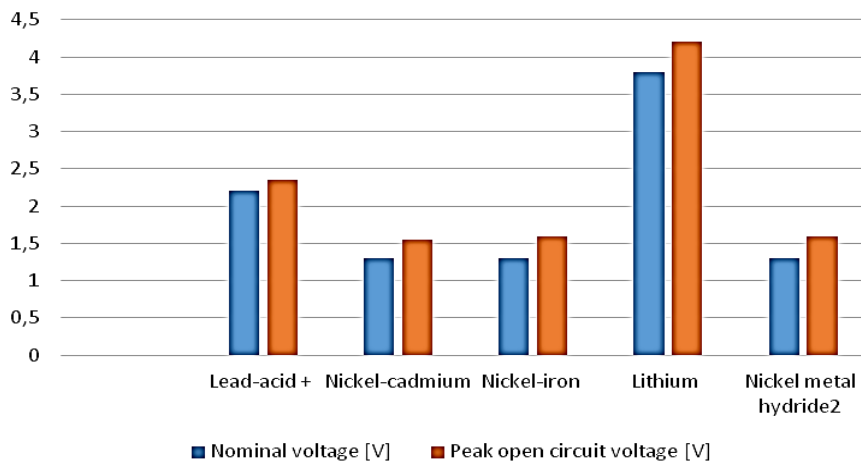


Fig. 2. Nominal and peak voltage for secondary cells of different electrochemical system

3. TEST RIG

In order to test of the cells at INCD INSEMEX Tests Laboratory Group it was created a test rig (see figure 3) [2] and [4].

The achieved test rig rely on monitoring (measurement) system with channels for:

- ambient measured temperature;
- maximum temperature measured at the middle of the cell;
- discharging electrical current of the cell;
- voltage across the cell.

The principal part of the test rig is the device for the electronic short-circuiting of the cell. Additionally for test operator protection the test rig contains a transparent cover having thickness of 20 mm.



Fig. 3. Test rig for maximum surface temperature of the cells

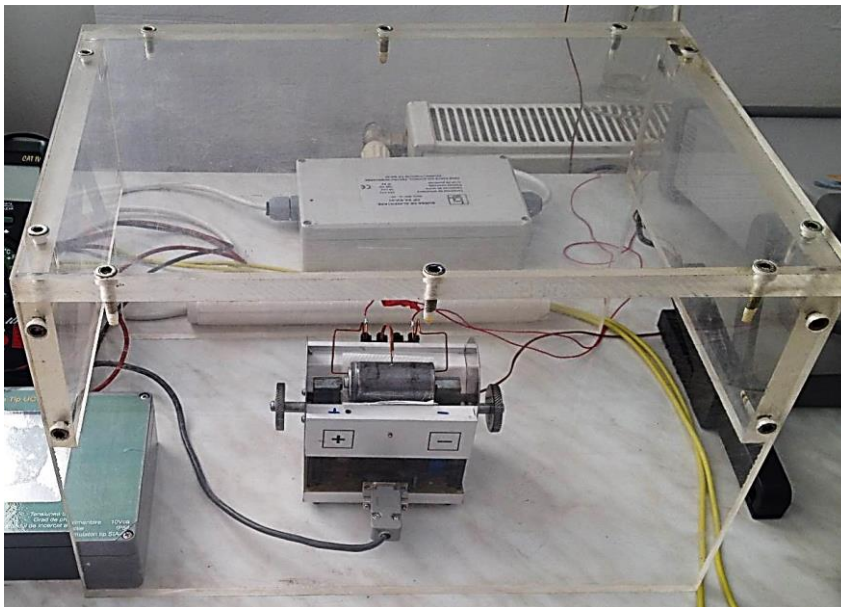


Fig. 4. Zoomed detail of electronic short-circuiting device of test rig

4. RESULTS AND DISCUSSIONS

The test results are shown in figures 5 to 8.

It was tested primary cell type TOSHIBA R20KG SIZE D $U_n=1,5$ V.

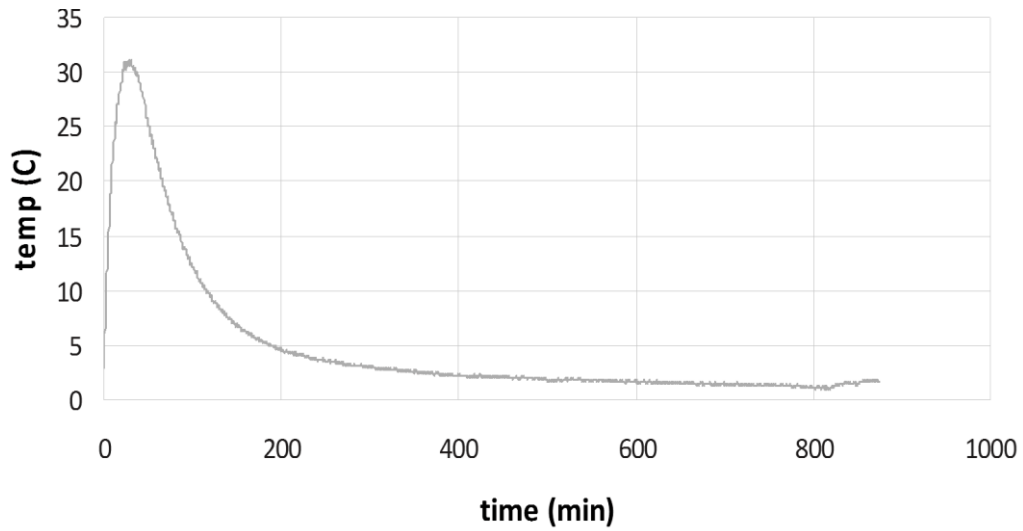


Fig. 5. Measured temperature at the middle of the cell

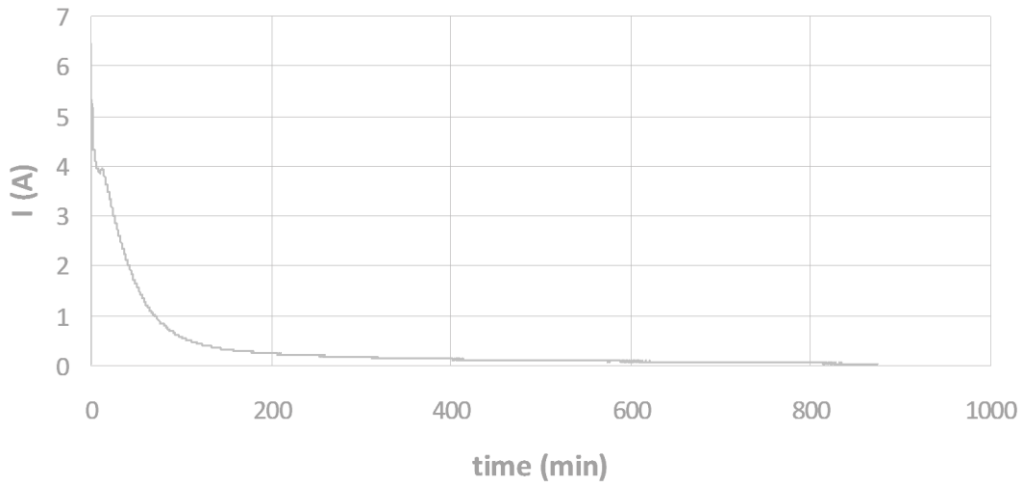


Fig. 6. Electrical current variation across the cell

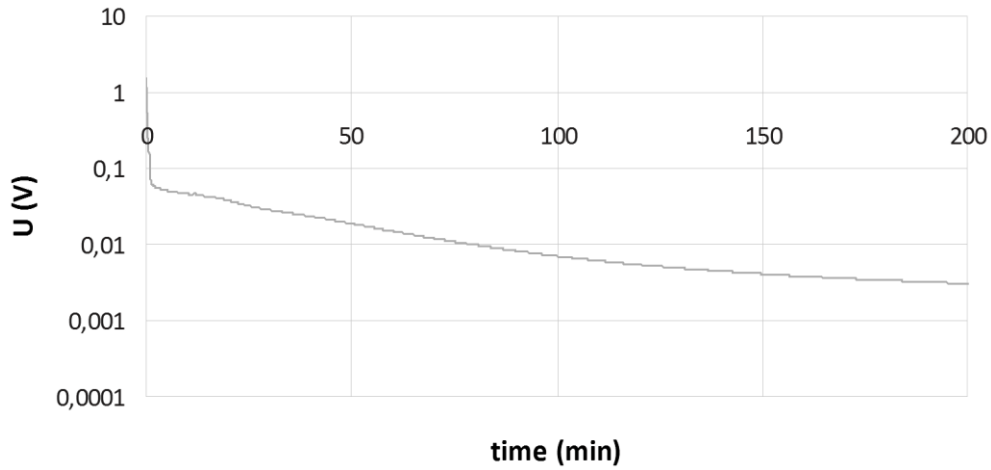


Fig. 7. Voltage across the cell

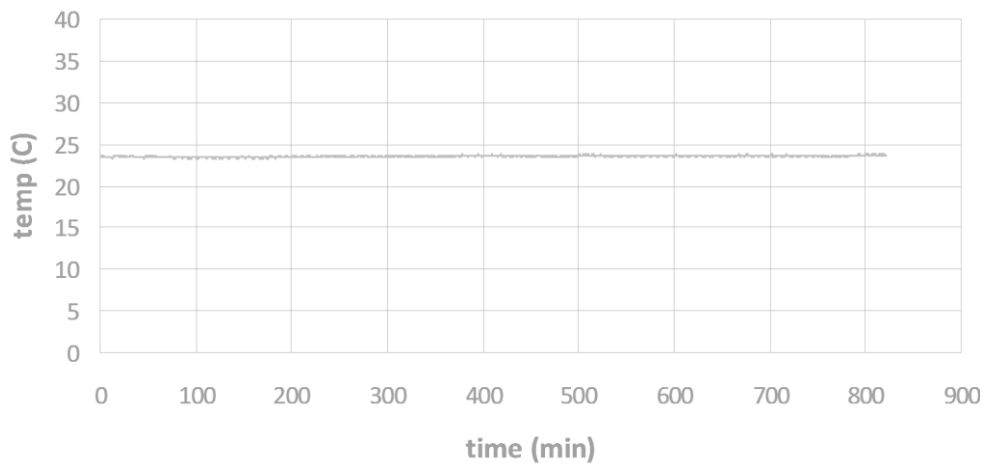


Fig. 8. Ambient temperature

For the purpose of computing the energy delivered by the cell could be used formula (1):

$$W = \int_0^T u(t) \cdot i(t) dt \quad (1)$$

Additional the internal resistance of the cell which is relevant for spark test ignition could be computed with formula (2):

$$r = \frac{\max[u(t)]}{\max[i(t)]} \quad (2)$$

For the tested cell total delivered energy is 624,47 Wh, and minimum internal resistance is 273,77 mΩ

4. CONCLUSIONS

The aim of the article is to underline the importance of galvanic cells test. The principal output of the test is the maximum temperature of external surface of the tested cell and other secondary results are inner minimum electrical resistance and maximum stored energy. At the experimental side of the article the test of type TOSHIBA R20KG SIZE D galvanic cell it was presented. The time needed for completely discharging of the cell was about 14 to 16 hours; the cell maximum surface temperature is 32 °C above the ambient temperature; the electrical current exponentially decrease with respect the time; delivered energy is about: 624,5 Wh; internal minimum resistance is: 273,77 mΩ.

ACKNOWLEDGEMENTS

This article uses the experimental results obtained within the project PN 16 43 01 07 of the „Nucleu” Program developed with the help of ANCSI.

REFERENCES

- [1]. **Csaszar T. A.** - *Theoretical and experimental methods for assessing energy low current circuits for use in potentially explosive atmospheres*, Editura Edyro Press, ISBN 978-973-7718-80-8, 2015.
- [2]. **Csaszar T., Vasilescu D., Burian S., Ionescu J., Darie M.**, *Performing In Safe Conditions the Laboratory Tests in Controlled Explosive Mixtures*, ANNALS of the University of Petrosani – Mining Engineering - , vol.12 (XXXIX), P.272-280, ISSN 1454-9174, UNIVERSITAS Publishing House Petroșani, 2011
- [3]. **Darie M., Ionescu J., Burian S., Csaszar T., Moldovan L.** - *Considerations regarding the assessment of explosive atmospheres ignition probability from low currents electrical installations*, Proceedings of the International symposium SESAM, 5th edition, Sinaia, Romania, 2011.
- [4]. **PN 16 43 01 07** - *Stand and methodology for assessing the ignition potentially explosive atmospheres with spark and the surface temperature of the battery cells and components for electrical equipment with the type of protection intrinsic safety "i"*, 2016.
- [5]. *** IEC 60079-11: 2012 - *Explosive atmospheres -- Part 11: Equipment protection by intrinsic safety "i"*.
- [6]. *** IEC 60079-0: 2011 - *Explosive atmospheres -- Part 0: Equipment - General requirements*
- [7]. *** IEC 60086-1, *Primary batteries – Part 1: General*
- [8]. *** IEC 60622, *Secondary cells and batteries containing alkaline or other non-acid electrolytes – Sealed nickel-cadmium prismatic rechargeable single cells*
- [9]. *** IEC 60623, *Secondary cells and batteries containing alkaline or other non-acid electrolytes – Vented nickel-cadmium prismatic rechargeable single cells*

- [10]. *** IEC 61951-1, *Secondary cells and batteries containing alkaline and other non-acid electrolytes – Portable sealed rechargeable single cells – Part 1: Nickel-cadmium*
- [11]. ***IEC 61951-2, *Secondary cells and batteries containing alkaline and other non-acid electrolytes – Portable sealed rechargeable single cells – Part 2: Nickel-metal hydride*
- [12]. ***IEC 61960, *Secondary cells and batteries containing alkaline or other non-acid electrolytes – Secondary lithium cells and batteries for portable applications*

MANAGEMENT PLATFORM OF CONFUCIUS INSTITUTE

ZHAO QI¹

Abstract: With the booming development of Confucius Institutes around the world, it is urgent to establish a global network education platform to provide a full range of effective service and support. In order to achieve the application of the platform in the global Confucius Institute, based on the Confucius Institute Global VPN line, the design adopts cloud computing concepts and theory, distributed database, middleware design. Platform design includes five sub-module: the literature management system, teacher and student management subsystem, teaching resource management system, personnel information management subsystem, the global secretary interactive teaching system. With the support of the cloud architecture of the platform, each sub-module could achieve three functional requirements which are "unified information coding standards, unified data exchange standards, agreed to identity management", to realize the based on the network teaching process of the new global Confucius Institute teaching management model, to meet the needs of global Confucius Institute teachers and students for real-time interactive teaching and educational management.

Keywords: cloud computing; distributed database; triple-play; resource sharing; mobile terminal.

1. THE NECESSITY OF THE CONSTRUCTION OF CONFUCIUS INSTITUTE MANAGEMENT PLATFORM

At present, there are more than 500 Confucius Institutes and more than 1000 Confucius classrooms all over the world. The conditions, scales and standards are different. The teachers and students are of great mobility and many kinds of teaching materials. The teachers' backgrounds are also diversified. Learning resources sharing requirements are high. And it's lack of complete data for getting some important information from each Confucius Institute and Confucius classroom, and developing support policy; meanwhile, it is also necessary to do the analysis from the aspect of quality for regulating the Confucius Institute teaching process, teaching content and setting up standards. Therefore, it is necessary to build a global teaching management platform which is suitable for remote management and resource sharing. [3], [4]

¹ *Ph.D. Student, University "Lucian Blaga", Sibiu, Chineze Professor Confucius Institute*

This platform can play a certain role in the sharing of quality teaching resources for Chinese as a foreign language.

Platform function analysis

The current problems in the teaching management of Confucius Institutes are as follows: it is impossible to grasp the number of Chinese learners and their changes in the world, and can not accurately control the use of teachers and their changes. They can not grasp the situation of Chinese teachers in the world and can not know well about Chinese institutions all around the world, can not be fully aware of the global Chinese curriculum, can not clearly understand the level of Chinese teaching at all levels, can not keep abreast of the use of learning materials all over the world, can not provide timely teaching management and observation, can not timely share Chinese teaching methods and experience, cannot do analysis on Confucius Institute teachers and students, teaching resources timely.

Confucius Institute's global teaching management platform includes the global Confucius Institute teachers and students library, the global digital interactive teaching system, the global Confucius Institute literature database, the global Confucius Institute teaching resource library, the global Confucius Institute Chinese and foreign language teaching talent library, each function has focus on different aspects (Figure 1).[2]

Among them, the establishment of the global Confucius Institute teachers and students library is conducive to the full access to Confucius Institute students, teachers and institutions and other information; global digital interactive teaching system can be established through the local teaching resources, recording control, synchronized real-time Teaching, video conferencing and other forms, to achieve the monitoring of headquarters of the Confucius Institute on the curriculum, teaching situation. It is conducive to the headquarters' and colleges and universities' effective teaching management to the Confucius Institute all around the world; the establishment of global Confucius Institute teaching resource library helps collecting and making high-quality Chinese language learning resources, electronic materials, etc. in a short time and provide the full service for the Chinese learners world widely; global Confucius Institute Chinese and foreign language teaching talent library is conducive to the realization of outstanding teaching talent, Chinese teaching experience, and other aspects of resource sharing.

In addition, the platform also includes a 7 × 24-hour response center, composed of call center, online message, forum, real-time interactive (IM) several parts. Its function is to monitor the branch of Confucius Institute classroom teaching process, selectivity access to the teaching process to do courseware recording, doing effective management to the recording of the courseware as the Confucius Institute of teaching resources and taking into account video conferencing. [7]

2. PLATFORM CONSTRUCTION TASK ANALYSIS

The platform has the following major construction tasks:

- To establish a global literature database of Confucius Institutes, to collect, collate and classify Chinese literature database on the global scope of Chinese language teaching and Chinese language promotion so as to realize the global sharing of literature databases.
- To establish the basic information of the Confucius Institute and the database of teachers and students, to keep the management on the data of the Confucius Institute enrollment system, students' raw data collection, students' elective situation, students' learning process and graduation, degree and other aspects under their real names.
- To establish the global Confucius Institute teaching resource library, including animation, courses' video, recording and producing of courseware, handouts and other formats.
- To establish Chinese and foreign language teaching and management personnel database of Confucius Institute all over the world, to collect and organize information of Chinese teachers, volunteers, managers, Chinese and foreign language teaching personnel of the global range to support by nationality, gender, age, title, education, teaching age, research direction and other dimensions of the combination of inquiries, so that to achieve global sharing of human resources.
- To establish an education application platform which could support the Chinese language degree education and realize the enrollment management, financial management, educational administration, academic management and examination management for the specialist level, undergraduate level, graduate students and other academic education students.
- To establish a global digital interactive teaching platform, through automatic tracking recording and broadcasting, automatic recording and broadcasting, interactive teaching, distance teaching and monitoring, distance learning resources management, to realize the synchronous reproduction of the scene process between the headquarters and branch, or branch and branch.
- To establish a 7 x 24 hour response center to serve global Chinese learners in the form of forums (BBS), message boards, and instant interaction systems (IM).

2.1. The overall design of the platform

The overall design of the platform should follow the following three principles [1]. First, the principle of reliability: the design of the platform must have a high degree of stability to ensure the continuity of the remote management and the synchronicity of class. Second, the principle of scalability: The platform design should provide sufficient room for expansion in future equipment upgrades and even system upgrades. Third, the principle of maintainability: using the parametric design, dynamic menu, dynamic authorization, the basic data centralized management, so that the maintenance work of system administrator during the operation becomes simple.

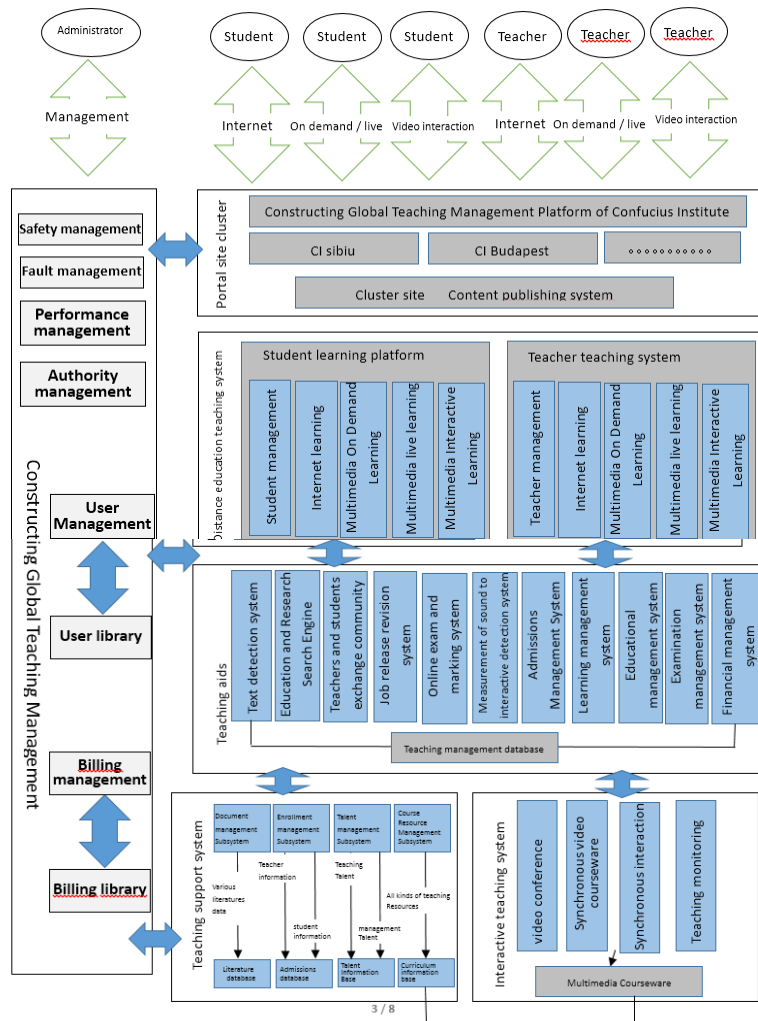


Fig.1. Platform structure block

2.2. Structural design

System structure design directly affects the performance of the entire system. According to the application characteristics of the global Confucius Institute teaching management platform, as well as the existing hardware and software facilities environment, the global teaching support system adopts B/S structure, the global digital interactive teaching system could realize by the way of combining B/S structure with C/S.

2.3. Functional design

The main functions of the platform include collecting and sorting relevant literature, materials, catalogs, indexes and effective preservation of global Chinese teaching and research, and setting up the site search engine according to the catalog and index, and managing the teachers and students' information of the Confucius Institute; at the same time, making the animation, video courseware, notes into possible [3].

The personnel information management subsystem mainly collects and classifies the basic information, resume information, learning experience, Confucius Institute teaching experience of teaching personnel, management service talents, management and maintenance personnel.

Aim of global digital interactive teaching system is mainly to achieve the total classroom teaching scene and the sub-class classroom teaching scene synchronization to reproduce, automatically capture, capture the scene and remote reduction, recording and efficient, secure management courseware and other tasks.

3. PLATFORM CONSTRUCTION APPROACHES

3.1. Construction of massive document

Library Management Subsystem

Literature information acquisition, document management and literature information analysis and utilization, are the three main functions of the subsystem. Therefore, the construction of the mass library management subsystem must seek the appropriate way to obtain the literature information, using the correct literature information editing, deletion, sorting, search, classification and other management methods to achieve the effective analysis of literature information and rational utilization.

Document information acquisition is mainly by three ways through the network search, from the existing library collection and manual entry. Web search refers to the system through the custom engine will transcribe eligible information to the library system; collection from the existing library uses the way of inter-system communication or bulk import, to collect valuable Chinese teaching Papers from

different institutions have included; manual entry refers to the administrator paste, edit, typeset literature resources searching from the web, then collect into a certain directory.

Literature management modes. The management of the literature includes the editing, deletion, sorting, searching and classification of the literature. Analysis and Utilization of Literature Information. [6]

The analysis and utilization of the literature information mainly includes the number of documents according to the catalog statistics, ranking according to the number of times of literature reading, ranking according to the number of downloads of the literature, ranking according to the number of online notes and ranking by the author's nationality.

3.2. The construction of teacher and student management subsystem

The teacher and student management subsystem is managed by the Confucius Institute as a unit, who manages the Confucius Institute of teacher and student information query, analysis, report output. The management mainly contains five functional modules: the enrollment plan management, the registration confirmation management, the admission management, the teacher information management and the statistical analysis Module.

Through the enrollment program management module, the Confucius Institute can set up detailed enrollment plan according to their own situation enrollment batches, entrance examination subjects and test time and set the online test questions strategy. Through the registration confirmation management module, the administrator can check the basic information of students, collect student photos, confirm on the scene or manually confirm the student information after the detailed confirmation of statistical data report. In the admission management module, the system can be based on the number of admission, according to the score line admission and other admission methods for admission, export students have been admitted to the data and reported to the higher authorities, and support the manual set of admission notice, envelope template.

Type admission management. In the teacher information management module, the system can increase, modify and delete the Confucius Institute teacher's nationality, name, gender, professional and technical titles, education, graduation school, date of birth, contact telephone, e-mail, blog address, teacher profile Basic information, and statistical analysis of teachers in the system of teaching and Q & A situation. Statistical analysis module is mainly from the student point of view, statistical analysis of students in the study, graduation, membership, professional distribution and the Confucius Institute enrollment data.

3.3. Construction of teaching resource management system

The system is mainly based on the curriculum website. As shown in Figure 2, the system construction includes eight steps: curriculum resource type management and template settings refers to the curriculum resources in accordance with Flash, PPT, DOC, PDF, RM / RMVB, WMV, SMR, Html and other different types Set the respective storage subdirectories, and set the corresponding fixed template for each type.

3.4. Personnel information management subsystem construction

The construction of the personnel information management subsystem mainly includes the two modules of personnel information management and inquiry. The personnel information management mainly includes the talent in accordance with the management talent, teaching talent two types of classification, the Confucius Institute Dean, management personnel, international Chinese teachers volunteer, foreign Chinese teaching experts and other talents of basic information, work history, educational information, work experience in Confucius Institute, annual assessment information, etc., as necessary to add, edit and delete.

3.5. Construction of global digital teaching interactive system

Global Digital Interactive Teaching System will be the global Confucius Institute through the Internet "link" to form a "master control" and "branch" relationship, and through the teaching resources of local recording, the total control of the recording, synchronization real-time teaching, video conferencing, curriculum resources Value-added use and other forms, to achieve the global sharing of teaching resources and applications. Mainly through the following ways to achieve: First, the design focus is to automatically capture, capture the scene and real-time remote reduction of teaching scenarios, courseware recording, convenient, efficient, security management courseware, remote monitoring and teaching, and remote to give the appropriate assistance.

Second, automatically track the recording and broadcasting system design. The main business of the automatic tracking recording and broadcasting system is the local teaching scene information capturing, collecting and recording courseware. The scene information includes the automatic tracking of the teacher writing the blackboard, automatically tracking the teacher's body language, automatic tracking of the teacher PPT to explain, automatically track the local students to answer questions, automatic tracking shooting students to answer questions.

Interactive teaching system design. Interactive teaching system uses core video and audio and data transmission control protocol control system to support local questions, remote questions, automatic video stream switching, automatic video tracking, automatic courseware recording upload. Interactive teaching system design achieve interactive teaching process of automatic recording and recording and tracking function.

Construction of Distance Teaching Monitoring System. The system mainly completes the remote teaching site real-time monitoring, remote adjustment / configuration digital interactive teaching terminal system parameters, local courseware recording and batch upload, remote courseware recording and batch upload, the implementation of equipment monitoring and other tasks. Remote teaching management system to build distance learning management system is the entire platform supporting and auxiliary system, mainly responsible for courseware user management, rights management and authorization management, courseware storage path management business. Remote digital interactive teaching monitoring and management system using B / S structure development, support Web management, the use of multi-tier architecture.

4. CONCLUSIONS

All above, it is necessary to build a global teaching management platform which is suitable for remote management and resource sharing. This platform can play a certain role in the sharing of quality teaching resources for Chinese as a foreign language which will surely help the Global Teaching Management of Confucius Institutes.

REFERENCES

- [1]. Tylor, E. Seymour-Smith, C. *Macmillan Dictionary of Anthropology*. The Macmillan Press LTD, 1986.
- [2]. James, Paul, Magee, Liam; Scerri, Andy; Steger, Manfred B.. *Urban Sustainability in Theory and Practice: Circles of Sustainability*. London: Routledge. p. 53, 2015.
- [3]. UNESCO, *Universal Declaration on Cultural Diversity*. Retrieved October 14, 2007.
- [4]. UNESCO, *Universal Declaration on Cultural Diversity*, 2001.
- [5]. <http://www.britishcouncil.sg/about/vision-mission>
- [6]. <https://en.unesco.org/post2015/sites/post2015/files/Think%20Piece%20Culture.pdf>
- [7]. 李军、田小红，《中国大学国际化的一个全球试验——孔子学院十年之路的模式、经验与政策前瞻》，《中国高教研究》2015年第04期

VIRTUAL INSTRUMENT FOR SIMULATING THREE-PHASE AC CIRCUITS

LILIANA SAMOILA¹, SUSANA ARAD²

Abstract: The paper presents virtual instruments we achieved in order to simulate the behavior of balanced and unbalanced why and delta connected loads supplied with a symmetrical three phase AC voltage system. The VI-s can be used during educational classes to turn things more clear and allowing the students to experiment themselves with virtual means instead of real devices. These virtual instruments continue our work in providing educational software to help students.

Keywords: virtual instrument, three phase AC, electrical engineering education.

1. INTRODUCTION

In a symmetrical three-phase system feeding a balanced and linear load, the sum of the instantaneous currents of the three conductors is zero.

Comparing to a single-phase AC power supply that uses two conductors, a three-phase supply with no neutral can transmit three times as much power using just 1.5 times as many wires (i.e., three instead of two). [1]

The possible load connections are why and delta, shown in Fig. 1 [6].

When designing a system modeling, it is important to consider a friendly user interface.

LabView is the software package that enables you to create interactive applications. The front panel can be easily designed to simulate the operation of real-world tools, the applications making virtual instruments. [7]

Starting from the facilities offered by the LabView programming environment, the paper presents the simulation of three-phase circuits (why connection, delta connection).

¹ *PhD., Associate Professor, Eng., University of Petrosani*

² *PhD., Associate Professor, Eng., University of Petrosani*

2. VIRTUAL INSTRUMENTS FOR SIMULATING THREE-PHASE AC CIRCUITS

We have built virtual instruments to simulate balanced and unbalanced star and delta connections powered by a symmetrical three-phase voltage system. The load is purely resistive.

In our application, we used numeric controls (NUM CTRL, POINTER SLIDE), numeric indicators (NUM IND, METER, and GAUGE) and TOGGLE SWITCH buttons [3].

2.1 Why-connection simulation

Starting from the theoretical considerations for the circuit shown in Fig. 2 [2], the application simulating the operation of the Y-connection was carried out. The front panel of the VI is shown In Fig. 3, respectively the block diagram in Fig. 4.

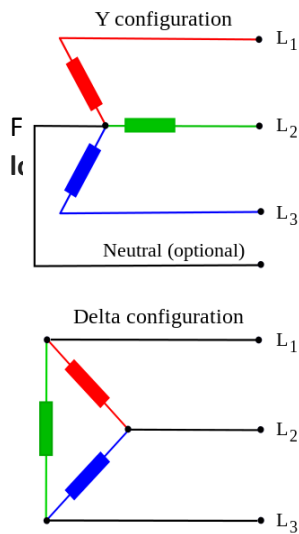


Fig. 1. Three phase load configurations

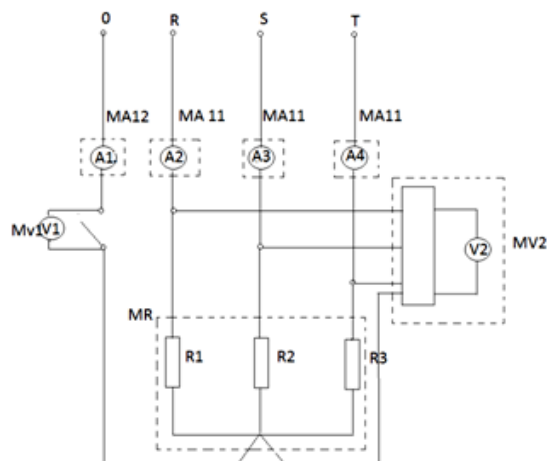


Fig. 2. Y-connection circuit measuring diagram

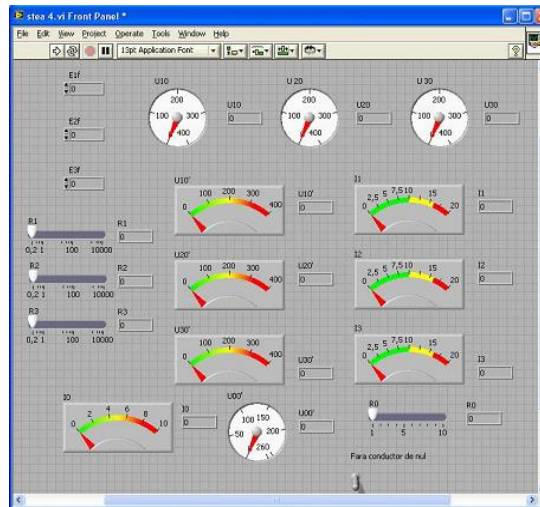


Fig. 3. The „Y-connection” virtual instrument front panel

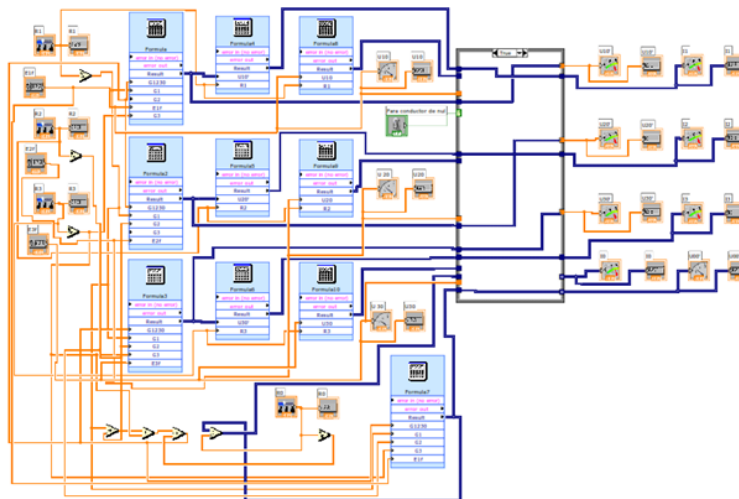


Fig. 4. The „Y-connection” virtual instrument block diagram

The consumer can be balanced or unbalanced.

A. Y-connection balanced load

In the perfectly balanced case all three lines share equivalent loads.

Fig. 5 shows the simulation of a balanced resistive Y-connected load

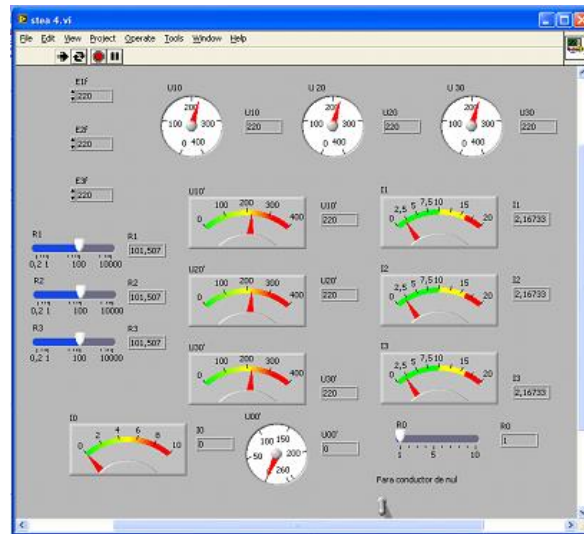


Fig. 5. Simulation of a balanced resistive Y-connection

We can see that, if:

$$\underline{Z}_1 = \underline{Z}_2 = \underline{Z}_3 \quad (1)$$

the currents and the phase voltages are symmetrical, that is they are equal in effective values on the three phases.

$$I_1 = I_2 = I_3 \quad (2)$$

$$U_{10} = U_{20} = U_{30} \quad (3)$$

The line voltages are always the same, no matter the type of connection and the consumer balance, while the power voltages are symmetrical.

B. Y-connection unbalanced load

A load is called unbalanced if the impedances of the three phases differ from one another [5].

There are two situations:

B.1 Unbalanced load with neutral

The simulation of the unbalanced Y-connection with neutral is shown in Fig. 6.

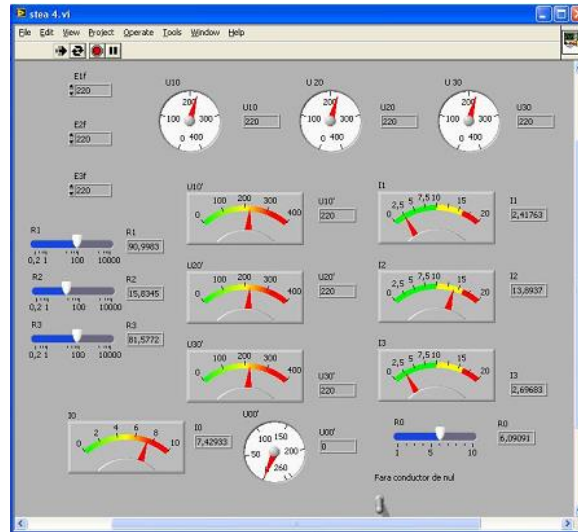


Fig. 6. Y-connection simulation when the load is unbalanced with neutral

As we can see, the currents are no longer equal, but the phase voltages are still symmetrical.

$$I_1 \neq I_2 \neq I_3 \quad (4)$$

$$U_{10} = U_{20} = U_{30} \quad (5)$$

In the null conductor, the current is $I_0 \neq 0$.

B.2 Unbalanced Y-connection without neutral

The simulation of the unbalanced star connection without null conductor is shown in Fig. 7.

If the null conductor is lacking, the currents and the phase voltages are nonequal, a practical undesirable situation.

$$I_1 \neq I_2 \neq I_3 \quad (6)$$

$$U_{10} \neq U_{20} \neq U_{30} \quad (7)$$

Between the null of the symmetric power supply and the load null point there is a neutral displacement voltage $U_{00} \neq 0$.

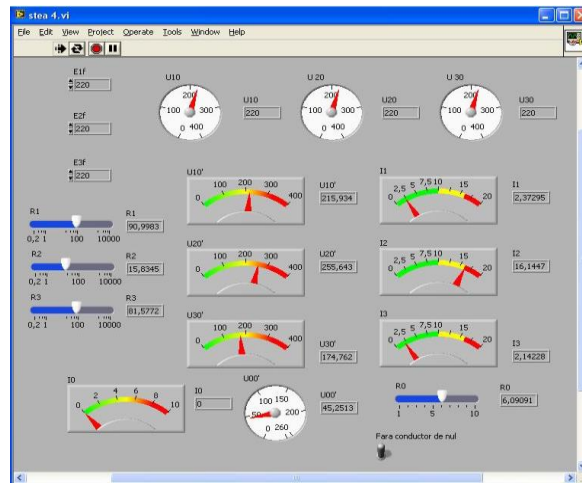


Fig. 7. Simulation of an unbalanced star connection without neutral

3. Delta connection simulation

We made a VI to simulate the behavior of the electric circuit whose diagram is shown in Fig. 8 [2],[4].

The front panel of the VI is presented in Fig. 9 and the block diagram in Fig. 10.

The behavior of a balanced delta-connection load is shown in Fig. 11 and in Fig. 12 is shown the simulation of a non balanced delta-connection.

Comparing the results of the simulations in Fig. 11 and 12, it can be seen that when the load is unbalanced, both the line and the phase currents get asymmetrical but the voltages are the same as the load voltages are equal to the line ones.

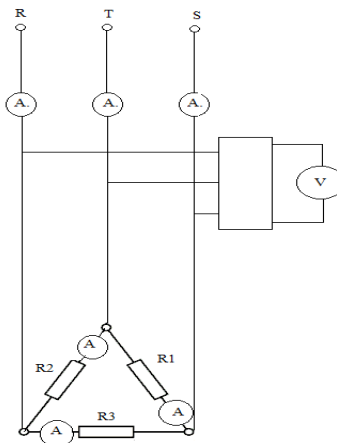


Fig. 8. Delta-connection load digram

VIRTUAL INSTRUMENT FOR SIMULATING THREE-PHASE AC CIRCUITS

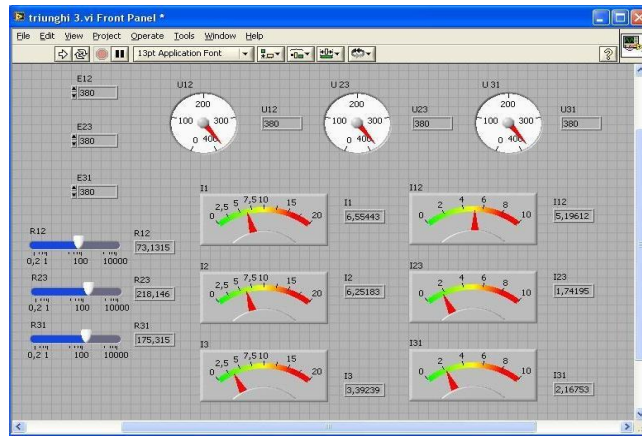


Fig. 9. The front panel of the VI „Delta connection”

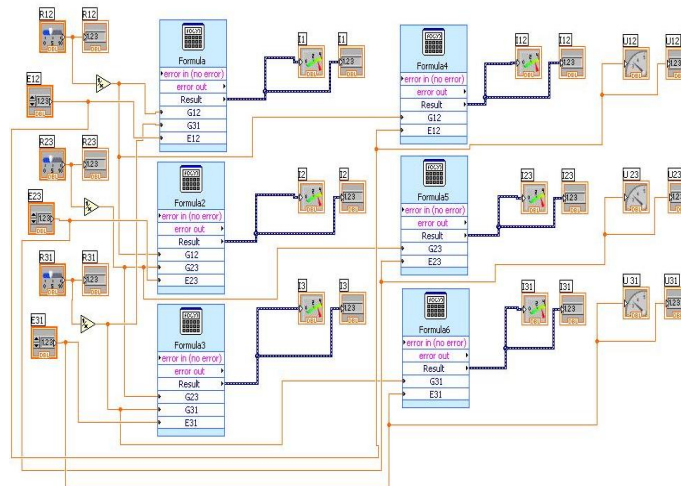


Fig. 10 The block diagram of the VI „Delta connection”

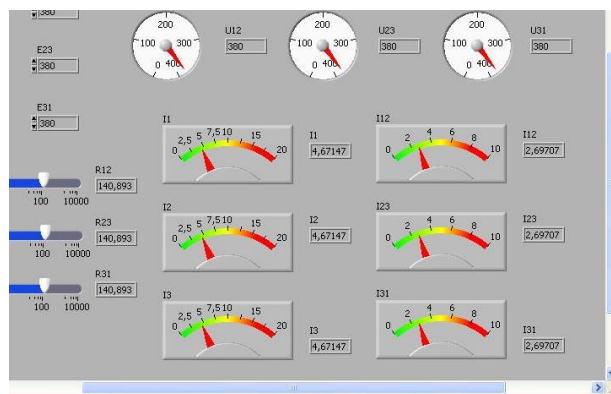


Fig. 11. Simulation of a balanced delta-connected load

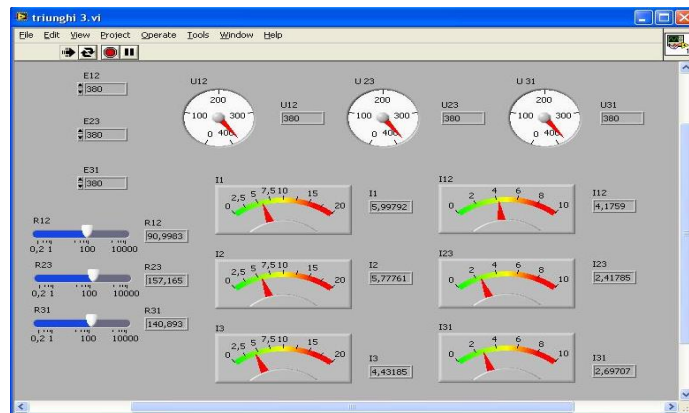


Fig. 12 Simulation of the non balanced delta connected load

4. CONCLUSIONS

The big advantage of the virtual instruments is the possibility of changing the virtual instrument in a short and substantial time, with a better adaptation to the real conditions and requirements.

The applications presented can be integrated into real-time data acquisition systems, being both qualitative and quantitative indicators of three-phase circuits.

Computer-assisted training is an effective way to prepare and perfect the work by modeling, simulating and analyzing electromagnetic processes. The efficiency of the activity is ensured by the way processing and transmitting the information, by the degree of applications flexibility and by the possibility of interactive applications.

Input data is get through the controls in the front panel of the application, then processed on the basis of the algorithm developed and implemented in the block diagram, the results being displayed by means of different types of indicators.

REFERENCES

- [1]. Arad L. S., *Electrotehnica*, Didactic and Pedagogic Publishing House, Bucharest, 2004.
- [2]. Utu I., Samoila L., *Masurarea marimilor electrice*, Universitas Publishing House, Petrosani, 2010
- [3]. Patrascioiu N., *Achizitie de date. Instrumentație virtuala*, Didactic and Pedagogic Publishing House, Bucharest, 2004
- [4]. Uțu I., Marcu M., *Tehnici de masurare. Teorie si aplicatii*. Universitas Publishing House Petrosani,, 2004
- [5]. Uțu I., Marcu M., Orban M. D., *Electrotehnica*, University of Petrosani, 2001
- [6]. https://en.wikipedia.org/wiki/Three-phase_electric_power
- [7]. <http://www.ni.com/ro-ro.html>

HYDROGEN, POTENTIAL ENERGY SOURCE

SUSANA ARAD¹, LILIANA SAMOILA²

Abstract: The paper presents some aspects concerning the production and storage of hydrogen as a power resource. The concept of using hydrogen as a renewable energy source in order to balance the power supply system has to be explained to the students who study Power Engineering at the University of Petrosani as it is an issue of great interest nowadays. Hydrogen generation and storage were studied in laboratory classes with the help of the Renewable Energy Education Set - Horizon, Fuel Cell Technologies. The educational kit can be used to experiment the production of hydrogen with an electrolyzer module supplied by a photovoltaic panel. Using a fuel cell to generate electricity, we powered a LED module, a small fan or a module with a small wheel engine. So, students can see the stages of producing hydrogen and further, electricity.

Keywords: Renewable Energy, Hydrogen, PEM Fuel Cell, Green energy

1. INTRODUCTION

Since the implementation of the 1907 Kyoto Protocol regarding the United Nations Framework Convention about climate change (1992), the renewable energy industry has been pushed towards capitalization on a global renewable energy market. This target can only be reached through a common plan regarding the imperative need to cut down the greenhouse gas emission. Through this Protocol, the developed countries have set the target of reducing by 2012 the greenhouse gas emission by 5.2% from 1990. The 21st Conference of the United Nations Framework Convention on climate change (COP21) was held in Paris in 2015. [1]

The signed intergovernmental agreement succeeds the Kyoto Protocol and it is aimed to make it legally compulsory and applicable to all states starting from January 2021. The document targets to keep the average global temperature rise below 2 degrees in comparison to the pre-industrial age, as it acknowledges that this would significantly reduce the risks and effects of the climate change. [7]

Constant efforts have been made so that as large a proportion of the primary energy production as possible can be achieved from hydrogen and renewable sources. The diagram of an energy system of this kind to use hydrogen and other renewable sources is shown in fig. 1. [3]

¹ *Professor, Eng., PhD, University of Petrosani, Romania*

² *Associate Professor, Eng., PhD, University of Petrosani, Romania*

The European Hydrogen and Fuel cell Technological Platform was launched in 2004 and in 2005 the Platform's board council ratified two important documents: the Strategic Research Agenda which involves major financial contributions over a period of ten years to generate and validate new technologies and the Implementation Strategy according to which applications of hydrogen will be implemented on the market by 2020. [8]

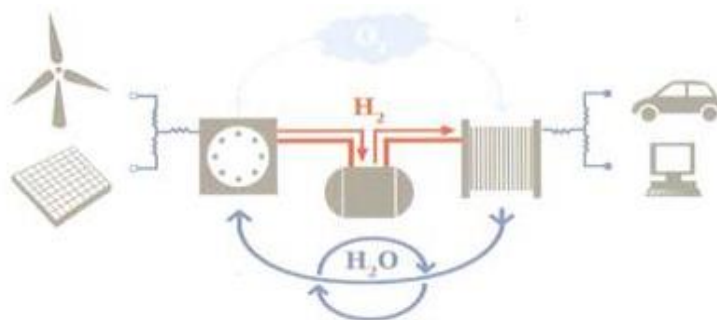


Fig. 1. Renewable energy system

„Fuel cell and Hydrogen” joint Undertaking-FCH JU, (www.fch-ju.eu) partnership have been launched at a European level. This European Union level entity is a public-private partnership. Its objective is to develop a strong, durable and competitive fuel cell and hydrogen sector.

Romania is a country with opportunities which can facilitate the transition from fossil fuel dependency to an energy industry based on hydrogen and renewable sources. A significant electricity percentage is currently being generated by used and old equipment which, at least in theory, have long paid for themselves. [4]

2. USING HYDROGEN IN FUEL CELLS

The flexibility of hydrogen production will have to be combined with adjusting current energy distribution and use systems. Should new sources of energy be discovered and developed, they can also be used to produce hydrogen without affecting the consumer energy system. Since hydrogen can be produced from a wide range of primary energy sources and it can be used in an even larger number of applications, it will become an energy source just like electric energy. Besides being distributed, provided and stored, this energy source can contribute to a rise in energy security stability and it will reduce the energy market vulnerabilities and uncertainties, leading to a competition between the different energy resources, figure 2. [1]

Hydrogen cannot be found freely in nature and since it needs to be produced it cannot be classified as a source of energy but rather an energy carrier (vector). In other words, energy needs to be used in order to produce hydrogen. However once produced, transported and stored, hydrogen can be used especially for fuel cells where it produces electrical energy and heat in the form of hot water or steam. Therefore burning hydrogen is not a polluting process. [4]

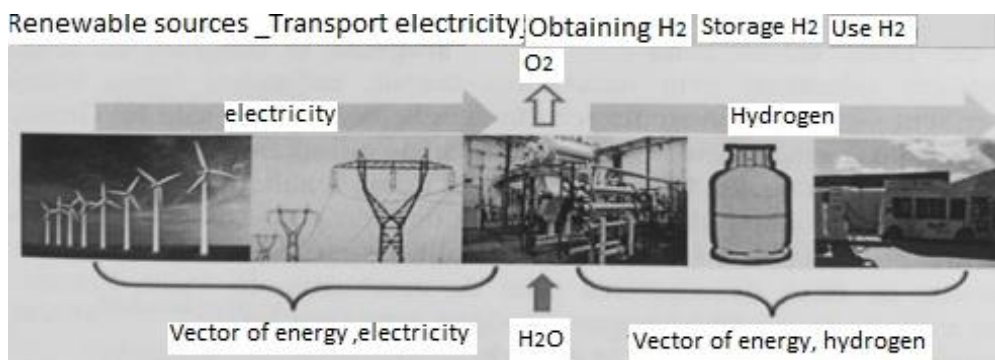


Fig. 2. Hydrogen as an energy vector

With few exceptions (i.e. engines, rockets) hydrogen cannot be directly used to produce energy. It must be converted into electrical energy, for which fuel cells are used.

The most frequently used hydrogen-based fuel cells are PEMFC (Proton Exchange Membrane Fuel Cell), which use a proton changing polymer membrane as an electrolyte. This membrane is an electronic insulator and an excellent proton conductor. The materials used are a fluorocarbon polymeric framework which is similar to Teflon, to which sulfonic acid groups are grafted. The acid molecules are retained inside the polymer, however, the protons from these acid groups are free to move through the membrane. [4]

A fuel cell is a generator which directly turns the internal, chemical energy of a fuel into electrical energy by using a controlled electrochemical procedure. The fuel cell is a system which converts chemical energy into electrical energy, such as electrochemical batteries or heat engines, fig. 3. Unlike a battery, which is a closed system, the fuel cell uses the anode fuel.

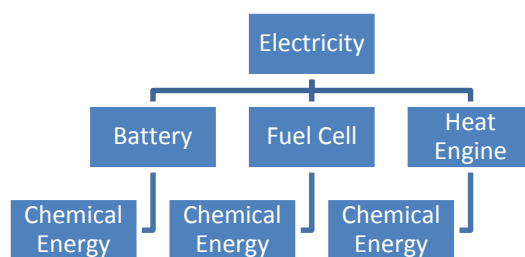


Fig. 3. Different ways to convert chemical energy into electricity

A fuel cell differs from electrochemical batteries in that it can operate continuously without needing recharging or replacing and the reaction products can be constantly removed. In the case of a classical fuel cell, the materials that make it up, the electrodes, are disposable. In time the electrodes wear out (due to anode oxidation and cathode decrease) until the fuel cell is consumed.

The structure of a fuel cell consisting of electrodes, electrolytes, and reactants does not react and it stays, with certain precautions, unchanged in time.

The operating principle of a fuel cell is based on electrochemical conversion. This entails the direct conversion of chemical energy stored in a certain fuel into electrical energy. This kind of conversion is called direct because there is no intermediary stage between the initial and final form of energy. The indirect systems of conversion have multiple conversion stages among which thermal or mechanical energy is compulsory.

To ensure the development of this process a system comprising an anode, a cathode, and an electrolyte has to be set up, that can be directly fuelled with the air that provides the oxygen necessary for the combustion process, fig. 4 [3]. The hydrogen or other fuel (energy source) is fed through the anode and oxygen through the cathode.

When the electrolyte allows the cation exchange, these travel through the electrolyte to get to the cathode. The fuel oxidizes and the oxygen reduces through a redox process. The fuel cell uses the fuel which can be continuously fed through the anode through a process of electrochemical oxidation, thus generating low voltage continuous electricity and heat in the form of hot water or steam.

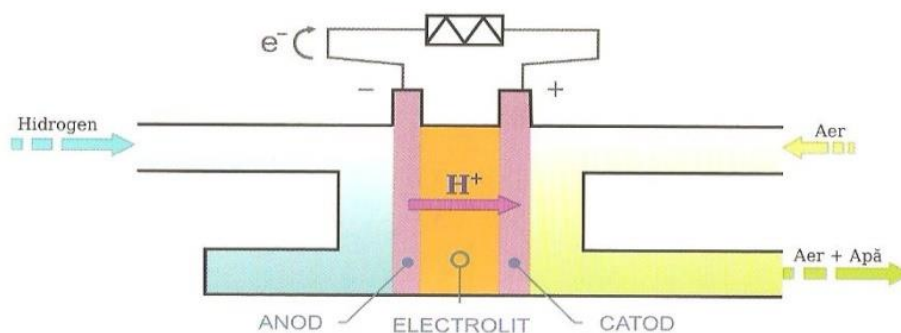


Fig. 4. The functioning principle of a fuel cell

By drawing the typical curve of such fuel cell we can notice the falling tendency of the $U(I)$ character together with an exponential decrease in tension while electricity increases. Diagram $P(I)$ emphasizes that the consumer does not operate within the optimal point, which means that the task is not adapted to the fuel cell. [3]

For low voltage electricity, the generated tension must be 0.9 V, also known as idle. Keeping in mind that electrolysis begins at 1.23 V, for the fuel cell the process is reversed, the generated tension will be lower than 1.23 V due to faulty catalysts, the fuel cell's internal resistance and so on.

Theoretical efficiency is high and the pollution resulted from these fuel cells is low. These arguments are largely accepted by the majority of a scientific community, which leads to the fuel cells becoming a very likely alternative to internal combustion engines (Otto with gas with Diesel fuel). However, the fuel cells cannot operate without mixing a fuel (hydrogen, methanol) with the oxygen from the air.

A comparison between the fuel cells and other fuels is shown in Table 1.

HYDROGEN, POTENTIAL ENERGY SOURCE

Table 1. Comparative elements among different fuels [3]

<i>Combustible</i>	<i>Main Component</i>	<i>Energy density (MJ/Kg)</i>	<i>Ratio H/C</i>
Hydrogen	H ₂	142,0	-
Gas	Ch ₄	55,5	2-2,3
Anaerobic biogas	Ch ₄ ,CO ₂	28-45	0,7-2,0
LPG	C ₃ -C ₄	50,0	2,5-2,7
Methanol	CO ₃ -OH	22,5	4
Ethanol	C ₂ H ₅ -OH	29,5	3
Oil	C ₄ -C ₁₂	45,8	1,6-2,1
Kerosene	Pana la C ₂₅	46,3	1,6-2,0
Diesel	C ₉ -C ₂₄	45,3	1,8-2-3
Biogas from gasification	CH ₄ ,H ₂ ,CO ₂ ,CO	4-14	4

3. EXPERIMENTS REGARDING THE USE OF FUEL CELLS

A range of experiments has been carried out within the Renewable Resources laboratory from the AICEE Department aimed to emphasize hydrogen production and its use as an energy source. The experiments have been carried out using the educational set *Renewable Energy Education Set – Horizon, Fuel Cell Technologies*, fig. 5.



Fig. 5. Renewable Energy Education Set – Horizon, Fuel Cell Technologies [6]

This set provides an excellent opportunity to learn about the exciting prospects of renewable energy, as well basic physics and chemistry principles. It shows how renewable energy can be harnessed, stored, and re-used in all kind of applications and how hydrogen can be the unique link between natural sources of power and power consuming devices - using fuel cell technology.

An electrolyzer module has therefore been set up, fig. 6 (a) from the equipment of this educational set to produce hydrogen by using solar energy through the solar panels available (solar panel with 6V/600mA), wind energy through a wind turbine with power capacity (rotor speed of 200 rpm) of 1W. A battery can also be used to carry out

the electrolysis (when the solar or wind energy sources are not enough) to generate hydrogen using embedded reversible combustion cells Horizon Mini PEM fuel cell, fig. 6 (b), with the following specifications: Output Voltage: 0.6 V DC, Output Current: 0.45 A, Power: 270 mW. Hydrogen consumption will depend on how much power you are drawing out of the fuel cell. At full load (210 mW), the fuel cell will output 360 mA and 0.6V. Fuel cells consume hydrogen at a rate of 7 mL/min/A, therefore this would consume about 2.5 mL/min at full load. Should the solar panel or wind turbines be enough, the system will start producing hydrogen and oxygen in the appropriate cylinders. When bubbles begin to surface in the hydrogen cylinder the cycle is complete. [2]

If the outcome of gas is not enough the electrolysis is repeated. Hydrogen can be produced sustainably from renewable energy systems with no carbon dioxide emissions.



Fig. 6 Electrolyzer Module (a) and PEM fuel cell (b) from Renewable Energy Education Set [6]

An example of such a system is the use of a solar panel, a wind turbine or a micro-hydro generator to convert the radiant energy of sunlight into electrical power, which drives an electrolyzer. The electrolyzer breaks apart water producing hydrogen and oxygen. The hydrogen is stored for use by the fuel cell and the oxygen is released into the atmosphere. Thus when the sun shines, the wind blows or the water flows the electrolyzer can produce hydrogen. A power system incorporating hydrogen from renewable sources and a fuel cell is a closed system, as none of the products or reactants (water, hydrogen, and oxygen) are lost to the outside environment [6]. The water consumed by the electrolyzer is converted into gases. The gases are converted back into the water. The electrical energy produced by the solar panel is transferred to chemical energy in the form of gases. The gases can be stored and transported to be reconverted back into electricity. These systems are truly sustainable, for as long as there is sunlight there can be electrical power, available wherever and whenever required.

One experiment is powering an LED light using a hydrogen fuel cell, after obtaining hydrogen with a solar panel, shown in fig. 7. [2]

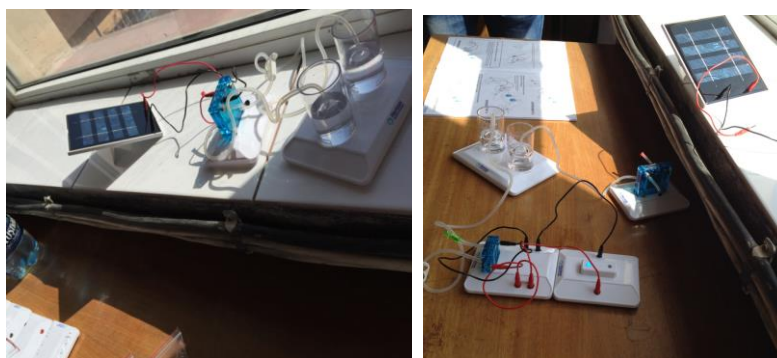


Fig. 7 Using fuel cells to supply a LED module

The reversible PEM Fuel Cell was disconnected from the wind turbine or solar panel and we used the fuel cell to power a small electric fan and the wheel of a small car shown in figure 8. The LED light shows the electricity consumption, the Fuel Cell will use hydrogen from the cylinder and the water level will reflect the changes in the quantity of gas used.

The Renewable Energy Science Kit demonstrates the workings of a clean energy technology system on a miniature scale. We powered an electrical circuit through a solar panel or a wind turbine with profiled blades based on NASA aeronautics. [5]

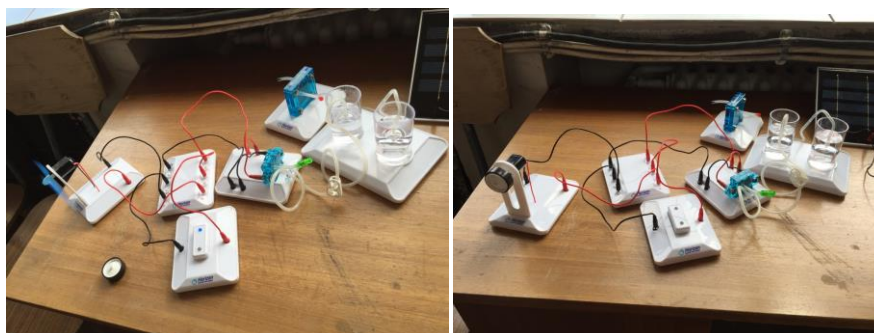


Fig. 8 Using PEM combustion cells to supply a small fan and a small wheel engine

It has generated hydrogen through water electrolysis and converted it into electricity using a PEM fuel cell. Whichever combination of technologies we want to explore, this science kit is a comprehensive introduction to the principles behind renewable micro grids. [5]

CONCLUSIONS

The Renewable Energy Science Kit provides an excellent opportunity to teach students about the exciting prospects of renewable energy, as well as basic physics and chemistry principles. It can be shown how renewable energy can be harnessed, stored and re-used in all kind of applications and how the hydrogen can be the unique link between natural sources of power and power consuming devices - using fuel cell technology.

The Renewable Energy Science Kit demonstrates the workings of a clean energy technology system on a miniature scale. Experiments of such a system were using a solar panel, a wind turbine or a micro-hydro generator to convert the radiant energy of sunlight into electrical power or to control an electrolyzer, which was carried out in Laboratory by students. The electrolyzer breaks apart water producing hydrogen and oxygen. The hydrogen is stored for use by the fuel cell and the oxygen is released into the atmosphere so, when the sun shines, the wind blows or the water flows through the electrolyzer can produce hydrogen.

Due to hydrogen's characteristics, the most adequate storage method is in salt cavities. At an industrial level, the potential users of the underground hydrogen storage systems seem to be the energy sector, through producers, electricity and natural gas operators and the transport sector, seen as a „premium” market in this case.

The concept of using hydrogen in order to balance the electricity supply system is not new. Scientists have been debating this concept with the view to store the excess energy from renewable sources. Hydrogen storage is a key enabling technology for the advancement of hydrogen and fuel cell technologies in applications including stationary power, portable power, and transportation. Hydrogen has the highest energy per mass of any fuel; however, its low ambient temperature density results in a low energy per unit volume, therefore requiring the development of advanced storage methods that have the potential for higher energy density.

REFERENCES

- [1.] Lucian, V., *Surse nepoluante de producere a energiei electrice*, AGIR Press, Bucuresti, 2005
- [2.] Arad, S. *Surse regenerabile. Teorie si aplicatii*, Focus Press, Petrosani, 2015
- [3.] Vadan, I., *Conversia energiei - Lucrari de laborator* UT Press Cluj Napoca, 2008
- [4.] Iordache, I., Gheorghe, A., Stefanescu, I., Iordache M. *Hidrogenul, Vector de energie*, AGIR Press Bucuresti, 2016.
- [5.] <http://www.horizoneducational.com/wp-content/uploads/2014/09/FCJJ-37-datasheet.pdf>
- [6.] <http://www.fuelcellstore.com/manuals/renewable-energy-education-set-2.experiment-guide.pdf>
- [7.] <https://www.iea.org/topics/renewables/>
- [8.] <http://www.renewableenergyworld.com/hydrogen/tech.html>

MODERNIZATION OF ASYNCHRONOUS MOTOR ELECTRIC DRIVES SUPPLIED BY IGCT STATIC POWER CONVERTERS

ILIE UTU¹, MARIA DANIELA STOCHITOIU²

Abstract: The paper studies some aspects regarding asynchronous motor electric drives. In connection with these categories of electric drives, it is proposed to develop a modern electric drive scheme, based on a converter made with the I.G.C.T technology. With such an approach, we aim to increase the functional parameters of the electric drives so that we can achieve a reduction of the electricity consumption and a higher reliability of the installation.

Key words: *Electric drives, asynchronous motor, automatic control, converter, I.G.C.T. technology, power losses.*

1. INTRODUCTION

The asynchronous motor with a squirrel cage rotor are frequently used in electrical drives. The operation of the three-phase asynchronous motor is based on the existence of a spinning magnetic field in the machine's air gap created by the stator windings powered by a three-phase voltage system.

The rotation speed called synchronous speed is determined by the stator current frequency, [5]:

$$n_0 = 60 \cdot \frac{f_1}{p} \quad (1)$$

where:

f_1 - frequency of stator currents;

p - number of pairs of poles.

Defines the sliding:

$$s = \frac{n_0 - n}{n_0} \quad (2)$$

Frequency of rotor currents:

$$f_2 = s \cdot f_1 \quad (3)$$

¹ *PhD., Associate Professor, Eng., University of Petrosani*

² *PhD., Associate Professor, Eng., University of Petrosani*

The electromagnetic torque will be, [5]:

$$M = \frac{m_l \cdot p}{2 \cdot \pi \cdot f_l} \cdot \frac{U_1^2}{(1 + \sigma_s)^2} \cdot \frac{\frac{r_2}{s}}{\left(r_1 + \frac{r_2}{s}\right)^2 + x^2} \quad (7)$$

where:

$$\sigma_s = \frac{x_1}{x_0}$$

and the total leakage reactance is:

$$x = \frac{x_1}{1 + \sigma_s} + x_0 + x_2$$

The critical torque is given by the equation:

$$M_k = \frac{m_l \cdot p}{4 \cdot \pi \cdot f_l} \cdot \frac{U_1^2}{(1 + \sigma_s)} \cdot \frac{I}{r_1 + \sqrt{r_1^2 + x^2}} \quad (8)$$

The critical slip is:

$$s_k = \frac{r_2}{\sqrt{(x_1 + x_2)^2 + r_1^2}} \quad (9)$$

From the relation (3) result the speed control methods: variation of rotor circuit resistance, sliding variation, variation of supply voltage, frequency supply voltage variation, etc. [5].

The most convenient and cheap method would be to adjust the supply voltage. A very good method for speed control a.m. is the variation of the frequency of the supply voltage correlated with the variation of its amplitude, $U/f = \text{const}$.

The induction motors with squirrel cage rotor are classified according to IEC 60034-30:2008 in three efficiency classes:

- a. Standard Efficiency IE1;
- b. High Efficiency IE2;
- c. Premium Efficiency IE3.

In the conductors of the stator winding appear principal and supplementary losses. Starting of T equivalent scheme (fig.1.), parameters are reported to the nominal impedance, and are expressed for slide s through the below relations: so noting r_1 - the stator resistance; r_2 - the rotor resistance (reported to stator); r_0 - the iron losses resistance; x_1 - the stator leakage reactance; x_2 - the rotor leakage reactance and x_0 - the magnetization reactance; p_{wl} - Joule power losses in stator; p_{w2} - Joule power losses in reported rotor; p_0 - the iron losses; p_{mv} - ct., the mechanical and ventilation losses, [4].

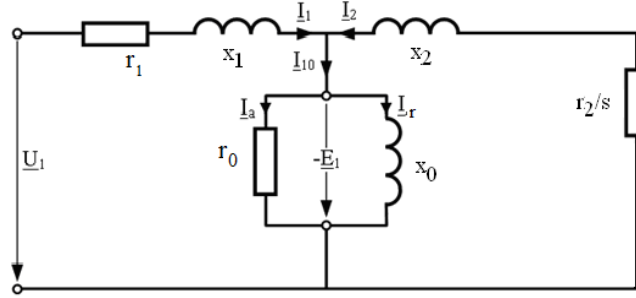


Fig. 1. Asynchronous motor T scheme

$$p_{w1} = \frac{a^2 + b^2}{a^2 + b^2} \cdot \frac{r_1}{\eta_n \cos \varphi_n} \quad (11)$$

$$p_{w2} = \frac{r_0^2 + x_0^2}{c^2 + d^2} \cdot \frac{r_2}{\eta_n \cos \varphi_n} \quad (12)$$

$$p_0 = \frac{\left(\frac{r_2}{s}\right)^2 + x_2^2}{c^2 + d^2} \cdot \frac{r_0}{\eta_n \cos \varphi_n} \quad (13)$$

where:

$$a = r_0 + \frac{r_2}{s} \quad b = x_0 + x_2 \quad (14)$$

$$c = \alpha + \frac{\beta}{s} \quad \alpha = r_0 x_1 - (x_0 x_1 + x_1 x_2 + x_2 x_0) \quad \beta = r_2 (r_0 + r_1) \quad (15)$$

$$d = \gamma + \frac{\delta}{s} \quad \gamma = r_1 (x_0 + x_2) + r_0 (x_1 + x_2) \quad \delta = r_2 (x_0 + x_2) \quad (16)$$

The applied voltage is equal with 1 in the equivalent electrical scheme, written in the relative units, and the current is $i_1(s_n) = 1$ and the power $p_2(s) = 1$ which involve the equality (9). The equation solution drives the load of motor to a nominal load, [4].

The motor efficiency and the power factor can be determined:

$$\eta = \frac{p_2(s)}{p_2(s) + p_{mescv} + p_{w1}(s) + p_{w2}(s) + p_{fe}(s)} \quad (17)$$

$$\cos \varphi = \frac{ac + bd}{\sqrt{(a^2 + b^2)(c^2 + d^2)}} \quad (18)$$

$$a^2 + b^2 = c^2 + d^2 \quad (19)$$

$$p_2(s) = 1 \quad (20)$$

Usually, the asynchronous motor with a squirrel cage rotor requires relatively big starting moments and low starting currents. This requires a certain shape of the rotor notch, which must have a pronounced refutation of the current from the rotor bar, in order to increase the apparent resistance, [4].

The supplementary losses in the core appear both at no load and full load status of the machine. According to the literature, the supplementary losses can reach up to 8-25% from the total losses.

2. INTEGRATED GATE - COMMUTATED THYRISTOR (IGCT)

The **integrated gate-commutated thyristor** (IGCT) is a power semiconductor electronic device, used for switching electric current in industrial equipment. It is related to the gate turn-off (GTO) thyristor (fig.2.). It was jointly developed by Mitsubishi and ABB. Like the GTO thyristor, the IGCT is a fully controllable power switch, meaning that it can be turned both on and off by its control terminal (the gate). Gate drive electronics are integrated with the thyristor device, [3], [6].

The structure of an IGCT is very similar to a GTO thyristor. In an IGCT, the gate turn-off current is greater than the anode current. This results in a complete elimination of minority carrier injection from the lower PN junction and faster turn-off times. The main differences are a reduction in cell size, and a much more substantial gate connection with much lower inductance in the gate drive circuit and drive circuit connection.

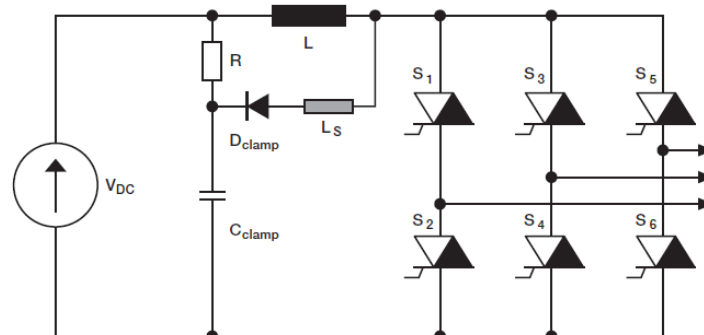


Fig. 2. Basic IGCT inverter circuit

The very high gate currents and fast dI/dt rise of the gate current mean that regular wires cannot be used to connect the gate drive to the IGCT. The drive circuit PCB is integrated into the package of the device. The drive circuit surrounds the device and a large circular conductor attaching to the edge of the IGCT is used. The large contact area and short distance reduce both the inductance and resistance of the connection [7].

The IGCT's much faster turn-off times compared to the GTO's allows it to operate at higher frequencies - up to several kHz for very short periods of time.

However, because of high switching losses, typical operating frequency is up to 500 Hz, [3], [6].

3. INDUSTRIAL APPLICATIONS OF IGCT TECHNOLOGY

These devices can be used for high power converters (100 MW) with the possibility of cascading several devices. The medium-voltage equipment based on this technology is very safe in operation and, for example, we can give the medium voltage frequency converter for 630 kW water pump operation, the 315 kW / 6000 V combustion air fans or the turbochargers up to 3,2 MW.

It is proposed to replace the existing motors with ABB 6 KV motors driven by a medium-frequency static ABB convertor in IGCT technology.

As a medium-voltage static converter, the ACS 5000 Series Converter is chosen because it has been specifically developed with the use of an increasing number of drives of 6KV motors (fig.3.).

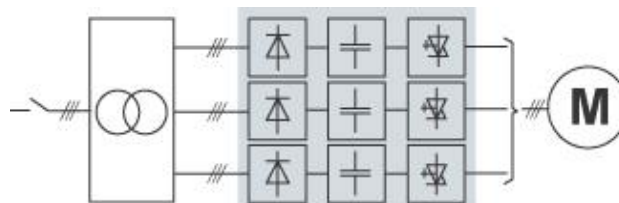


Fig.3. ACS 5000 converter scheme



Fig.4. Connecting motors with local network-connected converters.

The ACS 5000 has a very good performance and low cost, efficiency and increased safety, thanks to the combination of its components and innovative topology.

The ACS 5000 is based on the unique concept that makes it possible to drive motors up to 6.9 kV. Thanks to the VSI-MF (Voltage Source Inverter Multilevel-Fuseless) topology, this converter is used everywhere.

In accordance with our client's needs, ACS can be installed with all the major adapters for smooth integration, monitoring and control of different processes. This converter can also be operated remotely via the local LAN.

In figure 4. we present the scheme of connecting motors with local network-connected converters.

4. CURRENT MEASUREMENTS AT THE MOTOR OPERATION

We will study the case of the electrical drive of an air fan from a power generation group from the Mintia Electric Power Plant. A three-phase asynchronous motor with two speed is used to drive this fan. This motor has the following characteristics (Tab.1):

Table. 1.

Nr. crt.	Function	Motor	Pn [kW]	Un [kV]	In [A]	n [rpm]	cos φ	η [%]
1.	VG-3A speed 1	DAZO 1914-12/16	600	6	90	373	0.7	91
2.	VG-3A speed 2	DAZO 1914-12/16	1400	6	180	497	0.8	92.8

In order to monitor the electric drive of the fans, a series of measurements were performed in various operating modes. When starting the air and gas fans drive motors, the currents were oscillating at both speeds. The measurements were made using Fluke devices (Fig.5 – 9)

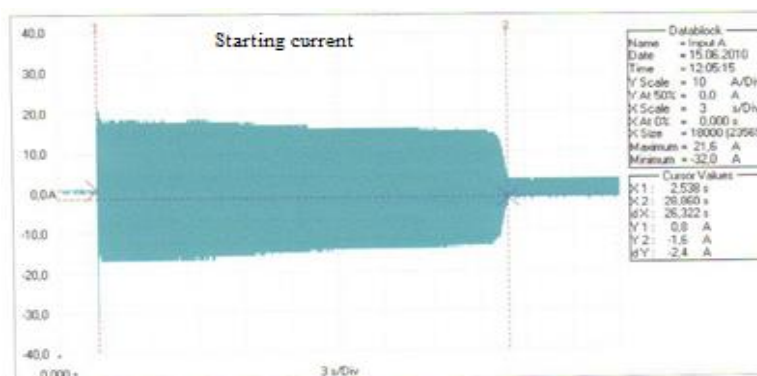


Fig.5. Starting current at first speed

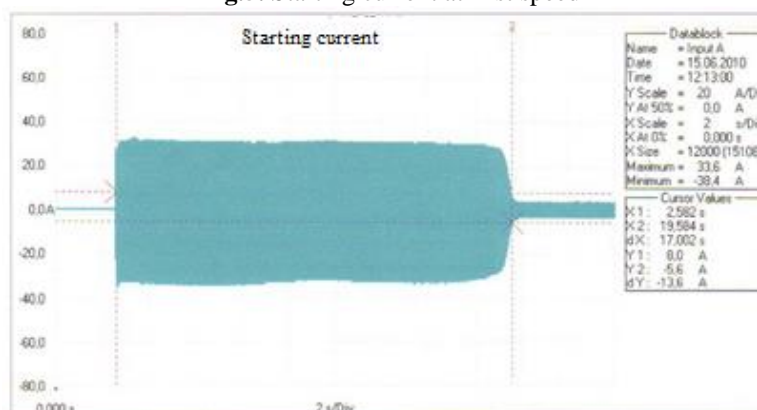


Fig.6. Starting current at second speed

MODERNIZATION OF ASYNCHRONOUS MOTOR ELECTRIC DRIVES SUPLIED BY
IGCT STATIC POWER CONVERTERS

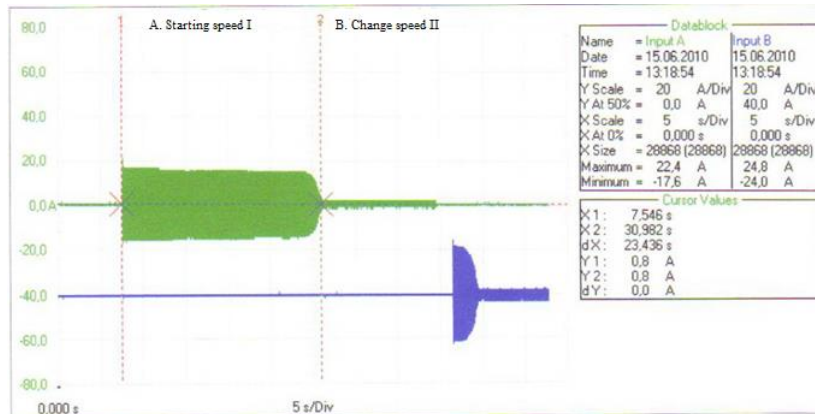


Fig.7. Starting current at first speed and change to second speed

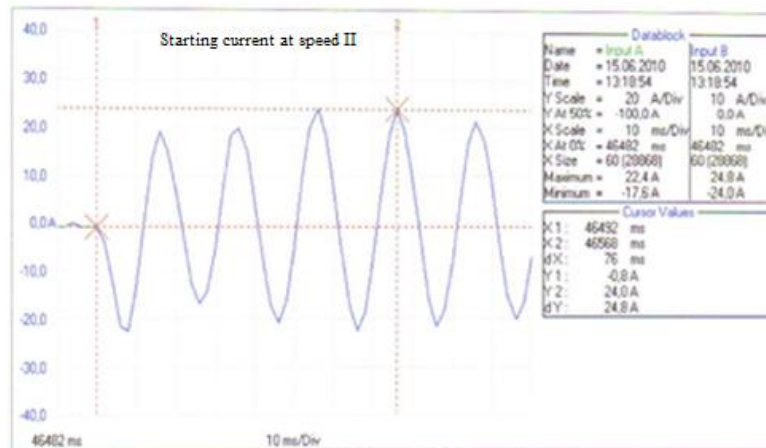


Fig.8. Current value - starting speed II from speed I

As we can see, the current drops from maximum 180 to about 30 amperes.

5. CONCLUSIONS

By applying this proposal, overloads due to engine starting are eliminated, which have the effect of damaging the power cables and the breakouts at the terminals.

The development of the power semiconductor elements has revolutionized the field of electric power control and has permitted the improvement and the diversification of the electric energy converter. As electronic power components improve in reliability and decrease in size, the cost and size of variable drives will continue to decrease.

Usually, the asynchronous motor with a squirrel cage rotor requires relatively big starting moments and low starting currents. This requires a certain shape of the rotor notch, which must have a pronounced refutation of the current from the rotor bar, in order to increase the apparent resistance. The supplementary losses in the core appear both at no load and full load status of the machine.

REFERENCES

- [1]. **Marcu, M., Leon, P., Florin, P., Razvan, S.** *Evaluation the losses power and electrical energy on the basis of the relative load curves, by reference to the basic sizes.* 14th SGEM GeoConference on Energy and Clean Technologies, 2014.
- [2]. **Popescu, F.G., Arad, S., Marcu, M.D., Pana, L.** *Reducing energy consumption by modernizing drives of high capacity equipment used to extract lignite.* International Multidisciplinary Scientific GeoConference: SGEM: Surveying Geology & Mining Ecology Management, 2013.
- [3]. **Peter, I., Scutaru, G., Nistor, C.G.** *Manufacturing of asynchronous motors with squirrel cage rotor, included in the premium efficiency category IE3, at S.C. Electroprecizia Electrical-Motors S.R.L. Sacele.* 14th International Conference on Optimization of Electrical and Electronic Equipment OPTIM 2014.
- [4]. **Stochițoiu, M.D., Uțu, I.** *Some aspects about using the modern high efficiency motors for driving the conveyor belts in lignite open pits.* Proceedings of the 7th International Symposium Occupational Health and Safety, SESAM, Poiana Brasov, octombrie 2015.
- [5]. **Tăbăcaru, T., Uțu, I.** *Mașini electrice și acționări: culegere de probleme.* Editura Universitas, Petroșani, 2012.
- [6]. **Uțu, I., Stochițoiu, M.D.** *Applications of power electronics in electromechanical drives from mining plants.* Annals of the University of Petroșani, Electrical Engineering, Vol. 13, Petroșani 2011.
- [7]. http://www.brown.edu/Departments/Engineering/Courses/ENGN1931F/ABB_Flyer_IGCT_2015.pdf

VIRTUAL INSTRUMENTATION USED IN STUDY OF DYNAMIC REGIM OF THE DC MOTOR

NICOLAE PĂTRĂȘCOIU¹, COSMIN RUS², CECILIA ROȘULESCU³

Abstract: In this paper we propose the algorithms that can be used to determine the values for several parameters that characterize the dynamic regime of operation of a DC motor. These parameters values are determined by simulation based on a state-space model by means of a virtual instrument made in LabView. In this way is possible to observe the dynamic characteristics of the DC motor in different operating conditions.

Keywords: algorithms, state-space mode, simulation, LabView, dynamic system parameters, overturn.

1. INTRODUCTION

One of the solutions for conversion of electrical energy into mechanical energy is represented by the use of electric motors. Of these the most widely used as actuator is the DC motor.

There are several design variants of the DC motor and among them the DC motor with magnetic flux produced by field windings. To this constructive variant the speed can be controlled through variable armature voltage. These electric motors, also called armature voltage controlled DC motors, can be controlled by either through the armature voltage or by controlling the field current [4].

Even if there are several types and constructive versions of the DC motors and their detailed construction is quite complex, it is possible to deduce the operating equations to obtain a satisfactory dynamic model based on fundamental electromagnetic laws. [5].

¹ *PhD., Associate Professor, Eng., University of Petrosani*

² *Ph.D. Student, Eng., University of Petrosani*

³ *Professor, Grigore Geamănu School*

2. MATERIALS AND METHODS

The physical model of an armature controlled DC motor is given in Fig. 1 [3]

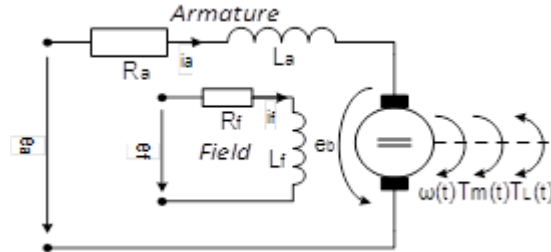


Fig. 1. The physical model of an armature controlled DC motor

where: e_a , i_a – armature supply voltage and current; e_f , i_f – field voltage and current; R_a , L_a – armature winding resistance and inductance; e_b – back electromotive force (e.m.f.); $\omega(t)$ – angular speed; $T_m(t)$ – electromagnetic torque; $T_L(t)$ – load torque.

Based on this physical model the and on functional principles it can build a mathematical model in state-space form expressed by the equations [6]:

$$\begin{pmatrix} \dot{i}_S(t) \\ \dot{\alpha}(t) \\ \dot{\omega}(t) \end{pmatrix} = \begin{pmatrix} -\frac{R_a}{L_a} & 0 & -\frac{k}{L_a} \\ 0 & 0 & 1 \\ \frac{k}{J} & 0 & -\frac{F}{J} \end{pmatrix} \cdot \begin{pmatrix} i_S(t) \\ \alpha(t) \\ \omega(t) \end{pmatrix} + \begin{pmatrix} \frac{1}{L_a} & 0 \\ 0 & 0 \\ 0 & -\frac{1}{J} \end{pmatrix} \cdot \begin{pmatrix} e_a(t) \\ T_L(t) \end{pmatrix} \quad (1)$$

$$y(t) = \begin{pmatrix} 1 & 0 & 0 \\ 0 & 1 & 0 \\ 0 & 0 & 1 \end{pmatrix} \cdot \begin{pmatrix} i_S(t) \\ \alpha(t) \\ \omega(t) \end{pmatrix} + \begin{pmatrix} 0 & 0 \\ 0 & 0 \\ 0 & 0 \end{pmatrix} \cdot \begin{pmatrix} e_a(t) \\ T_L(t) \end{pmatrix} \quad (2)$$

Here we considered the angular displacement $\alpha(t)$, the angular speed $\omega(t)$ and also the armature current $i(t)$ as the output quantities.

The most convenient method for the user to observe the evolution of a quantity is its graphical representation. Thus, for each output quantity, a window will be created in which both the evolution and the parameters characterizing it are highlighted. The parameters that are relevant to this dynamic system are considered the peak value (maximum value) and time of its occurrence, the steady state value and its determining time, rise time, falling time, overshoot. For displacement, it is known that if the load torque is higher than the active torque, the reverse motor movement occurs. In this case a flashing message (OVER TORQUE) and a suitable light indicator will be displayed, also displaying the time of its occurrence to signal this situation.

3. RESULTS AND DISCUSSIONS

Calculation of dynamic system parameters is made by using the LabView libraries or toolkits.

A. The peak value

The peak value that is the maximum absolute value of each of the output variables is computed using Array Max&Min function that returns the maximum and minimum values found in subarrays, along with the indexes for each value [1]. Since the peak value can be positive or negative, depending on the direction of rotation, the maximum value is displayed for a maximum positive value and the minimum value for the maximum negative value. Selection is made through a CASE structure based on comparison of absolute values corresponding to the maximum and the minimum values of displacement. Once determined the maximum value, based on its index, the moment of its appearance is searched.

B. The steady state value

The steady state value S_v and the moment of its appearance TS_v are computed using a SubVI named $Vstat$ whose algorithm is shown in Fig.2.

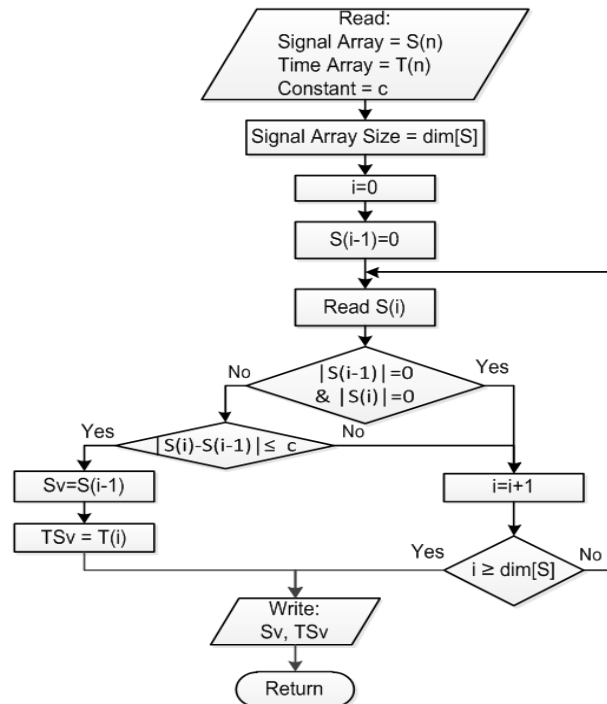


Fig.2. Algorithm used to compute steady state value

This value is determined for each of the three components of output vector. It considers the steady state to be reached if the difference between two consecutive absolute values for outputs variable is less than the constant $c = 10^{-6}$.

This algorithm shown applies to current, to displacement and/or to speed, and each of them can be represented by the subarray $S(n)$. The moment of the steady state value TSv appearance is determined by reading the index i of the S_v in subarray $S(n)$ and with this index the value with the same index i is searched in subarray $T(n)$, which is an array of the time values. Implementation of the algorithm in the virtual instrument structure is made by the SubVI Vstat, and this is shown in Fig.3.

For extracting the values $S(i)$ of the subarray $S(n)$ a while loop is used, whose condition terminal i is incremented until it fulfills the condition:

$$|S(i)| - |S(i-1)| \leq c \tag{3}$$

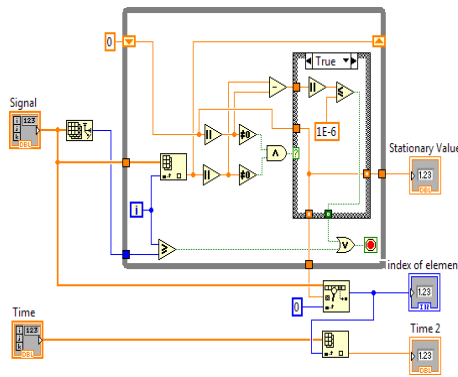


Fig.3. Implementation of the algorithm Vstat

Otherwise, if the condition is not achieved, the algorithm stops after all values in the subarray $S(n)$ are investigated.

C. The rise time

The rise time is computed by the difference between time TSv, when is identified the steady state value, and the time when is generated the proper input variable. The time when is generated the input variable is taken from controls which determine the moment of start through a local variable or Property Node [2] StartS, as shown in Fig.4.

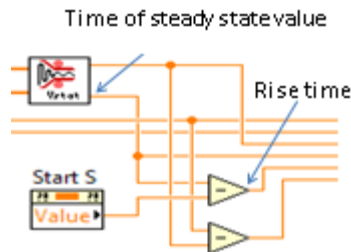


Fig.4. Computation of the rise time

D. The fall time

This value can be calculated, and it will be displayed as well, only for a pulse shape input. To display the value of this variable proper indicators are used, which become visible on front panel only if the input signal type is pulse shape.

To determine this value is used the algorithm shown in Fig.5.

Proper indicators became visible on the front panel only for a pulse shape input, when choosing the value true for the boolean variables *B1* and *B2*, otherwise their values will be false. In the sequence of the time values the index *j* is identified, corresponding to the stop moment *TTs*, so from the sequence of the current and speed values all values that have index greater than *j* are removed. Are thus obtained for both current and speed variables, two sequences of values each with *S* size, and the values in these sequences are reordered starting at index 0.

Determination of fall time of the DC motor response is accomplished by identifying the moment when an absolute value for current or speed is zero (or less than a constant *c*₂, close to zero), according to the relations:

$$|Sc(i)| < c_2 \quad ; \quad |Ss(i)| < c_2 \tag{4}$$

where */Sc(i)/* and */Ss(i)/* represent absolute values extracted from sequences of values for current and respectively, speed.

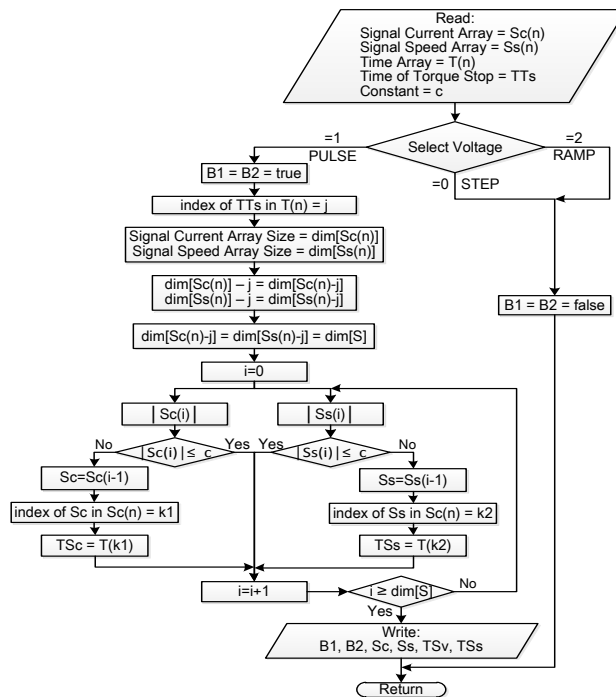


Fig.5. Algorithm used to identify the fall time of the DC motor response

The corresponding indexes c_1 and c_2 are identified for that the conditions (4) are achieved, and based on these indexes the moments TSc and TSs are searched, corresponding to the achievement of these conditions.

Implementing the algorithm in the virtual instrument structure is made by the SubVI Fall, and this is shown in Fig.6.

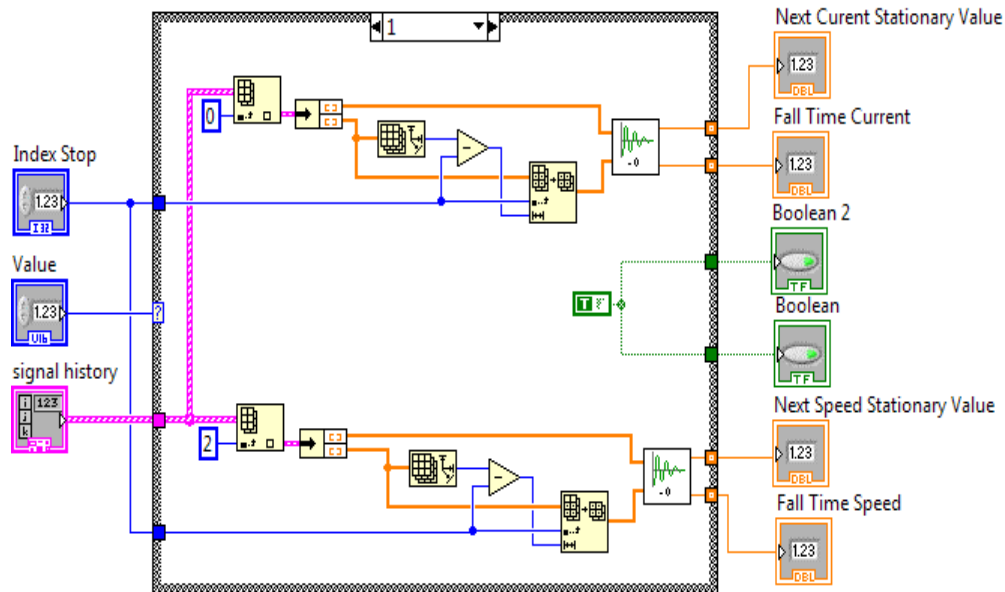


Fig.6. Implementation of the algorithm Fall Time

The algorithm for determining the fall time of the DC motor response is made through a Case structure. The three cases of this structure, corresponding to the three types of signals generated for DC motor command, are selected by controlling the DC Motor Voltage from front panel through the Value signal slide.

As seen in Fig.6, actual implementation of the algorithm takes place only in the sequence 1, which corresponds to a step shape command type for which is possible the compute this parameter of the dynamic regime. In the same sequence, the boolean variables B1 and B2 are set to true. In the other two sequences, only the boolean variables B1 and B2 are set to false.

E. The phenomenon of "overturn"

It is known that, if the load torque exceeds the active torque of the electrical machine, the "overturn" occurs. So it is necessary to be able to determine the overturning moment.

Identifying the phenomenon of "overturn" and overturning moment is achieved using a SubVI named *SENS*, whose algorithm is shown in Fig.7.

VIRTUAL INSTRUMENTATION USED IN STUDY OF DYNAMIC REGIM
OF THE DC MOTOR

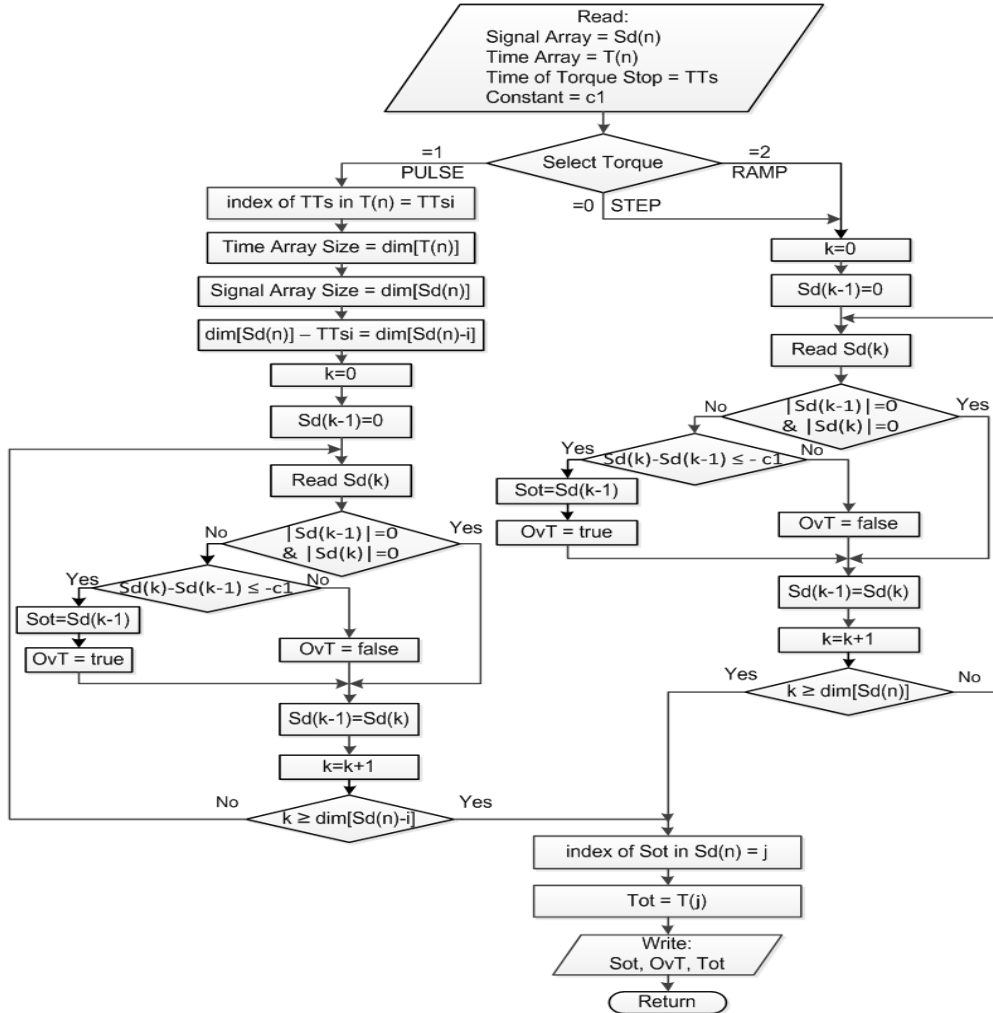


Fig.7. Algorithm used to identify the phenomenon of "overturn" and overturning moment

Identifying the phenomenon of overturn is done by analyzing the sequence of values $Sd(n)$ for angular displacement and the determination of the overturning moment is done by comparing the successive values $Sd(k-1)$ and $Sd(k)$ in the sequence considered. Thus, the phenomenon is considered to occur if:

$$Sd(k) - Sd(k-1) \leq c_1 \quad (5)$$

where $c_1 = -0.01$ is a negative constant used to make the comparison.

If the shape of the torque is pulse, the stop moment TTs is identified in the sequence of time values and through its index number are removed from sequence $Sd(n)$ all values with the index higher than this. Obviously, the comparison is done only if two successive values from the sequence $Sd(n)$ are different from zero.

By fulfilling the condition (5) the value $Sot (=Sd(k-1))$ is identified, corresponding to the overturn, in the sequence of values for angular displacement $Sd(n)$, starting with the appearance of the inversion of rotation. To signal the state of overturn, the value "true" is assigned to the boolean variable Ovt , otherwise the variable receives the value "false".

Indication of the overturning state is made on the front panel by a red color of a LED indicator (that otherwise is green) and by blinking message "OVERTURN", that becomes visible only when this phenomenon occurs.

In cases where the torque is step or ramp shape, considering the fact that these shapes did not have the stop time, it is not necessary to identify this moment in the times sequence values. In these cases, the overturn moment Sot is searched by identifying the condition given by (5) for successive values in sequence of values for angular displacement $Sd(n)$. Completion the algorithm is carried on, as in the case of the torque having pulse shape.

After identifying the value Sot , corresponding to the overturning moment, its index is searched in the sequence of values for angular displacement $Sd(n)$. Based on the index j thus determined, the moment Tot , the moment when overturn occurs in the time array sequence $T(n)$ is searched.

Implementation of the algorithm in the virtual instrument structure is made by the SubVI *Over Torque*, Fig.8, and this is realized through a While Loop that runs until the condition (15) is reached or until all values from the sequence of values for the angular displacement $Sd(n)$ are tested. Depending on the shape of the input signal (Signal Type) one of the three cases is selected, noting that cases 0 and 2 (step and ramp) are the same.

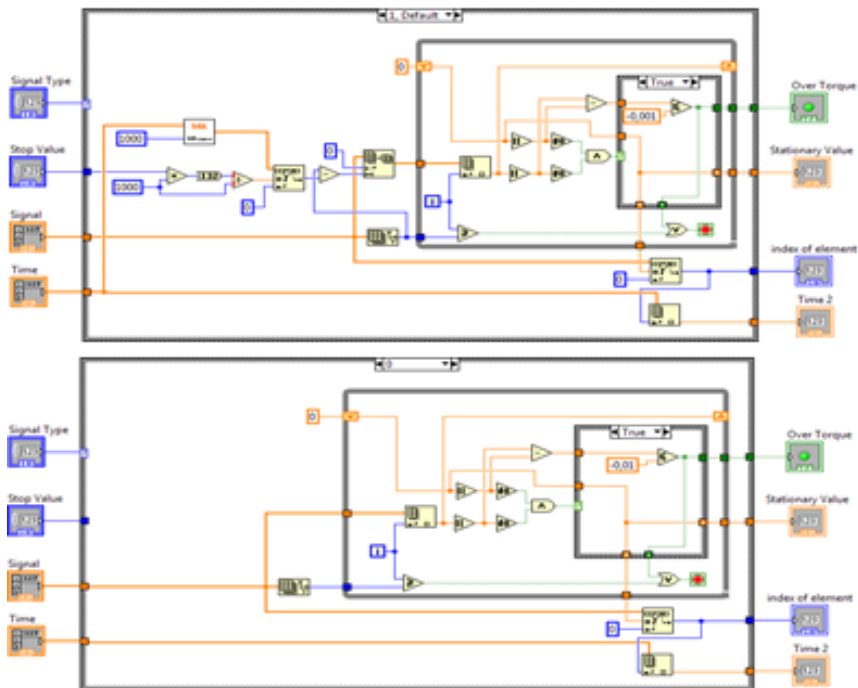


Fig.8. Implementation of the algorithm *Over Torque*

In the execution of the search operation in the array sequences 1D Array Search Function is used, that searches for the element ($Sd(k-1)$) in a 1D array ($Sd(n)$) starting at start index for that is set with 0 value. Because the search is linear, it is no need to sort the array before calling this function and LabVIEW stops searching as soon as the element is found.

To make the index increments after each test for two consecutive values from the sequence array, the iteration (i) terminal of the While Loop is used, that provides the current loop iteration count, which is zero for the first iteration.

F. Stationary value

This value identify the moments in which the absolute values of current and displacement are 0 (or smaller than c_2 , constant very close to zero).

Its operation is similar to determining the stationary value in the SubVI Over Torque and consists in checking the differences between two successive values. For displacement or current and to determine when this difference is zero (or less than constant c_2 whose value is set in this case at 10^{-3}).

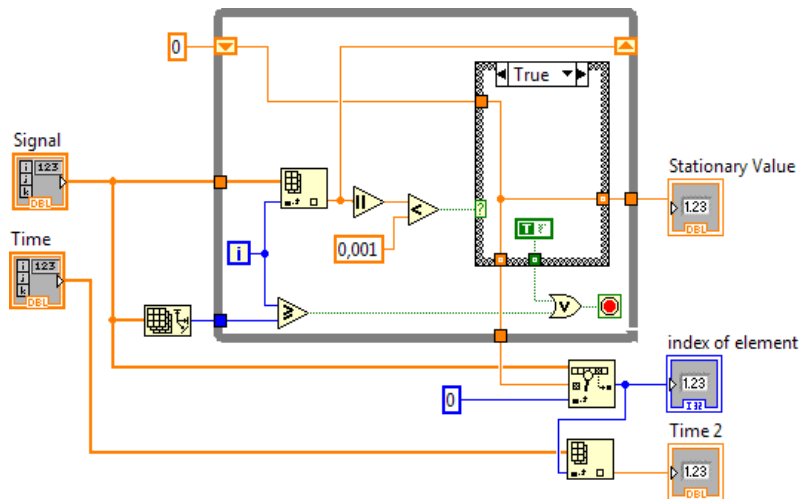


Fig.9. Implementation of the algorithm *Stationary Value*

4. CONCLUSIONS

It is known that computer simulation is an experimental method based on a set of techniques by which operating with virtual things, the functioning of a real system or process is understood.

On the basis of the same principles it is possible and the calculation of values of the parameters which characterize the dynamic regime of a system. Through virtual instrumentation these parameters can be obtained and visualization in interactive mode on the front panel of LabView.

REFERENCES

- [1]. **Beyon J.Y.**, *LabVIEW programming, data acquisition, and analysis*, Prentice Hall, New York (2001).
- [2]. **Bitter R., Mohiuddin T., Nawrocki M.** *LabVIEW. Advanced Programming Technique*. Second Edition. CRC Press, New York (2007).
- [3]. **Richard C. Dorf, Robert H. Bishop**, *Modern Control Systems*, 12th Edition, Prentice Hall (2011).
- [4]. **Fransua Alexandru**, *Machines and electric drives (in Romanian)*, Ed. Tehnica.
- [5]. **Farid Golnaraghi, Benjamin C. Kuo**, *Automatic Control Systems*, 9th Edition, John Wiley & Sons, Inc. (2010).
- [6]. **Patrascoiu N.** *Modeling and Simulation of the DC Motor Using Matlab and LabVIEW*, International Journal of Engineering Education, Vol. 21, No. 1, 2005, pp. 49-54.

SIMULATING THE SPEED AND ROTOR RESISTANCE OBSERVER IN SENSORLESS VECTOR CONTROL SYSTEMS WITH INDUCTION MOTORS

OLIMPIU STOICUTA¹, LORAND BOGDANFFY²

Abstract: The article presents a compensation solution based on the rotor resistance of the extended Gopinath observer used in the simultaneous estimation of the rotor speed and position and mode of the rotor flux phasor. The rotor resistance is estimated based on a relationship deduced from the mathematical model of the induction motor. The dynamic performances of the extended Gopinath observer are highlighted by simulation in Matlab-Simulink.

Keywords: induction motors, modeling and simulation, extended Gopinath observer, speed estimation, rotor resistance estimation, sensorless vector control system.

1. INTRODUCTION

The implementation of sensorless vector control systems raises problems especially with the simultaneous estimation of the speed and rotor resistance of the induction motor. To argue with the above, we recall here the results of the research of H. Kubota [4], [5] and Shinnaka [15]. H. Kubota states that in the vector control systems, in the stationary regime, only the proportionality relation between stator resistance and rotor resistance (R_s/R_r) can be estimated, because it is impossible to separate from the stator state variables, error estimation of the speed of the estimation of the rotor resistance. In other words, in stationary regime the condition of persistence of excitation is not respected [5]. On the other hand, Shinnaka demonstrates that estimating both the speed and the rotor resistance implies a division with zero if the module of the rotor flux phasor is maintained constant [15].

From the above mentioned, it is observed that the provision of excitation persistence, as well as the avoidance of division by zero in the stationary regime, allow the simultaneous estimation of the speed and the rotor resistance of the induction motor.

¹ Associate Professor, Eng., PhD, University of Petrosani, Romania

² Assistant Researcher, Eng., Ph.D, University of Petrosani, Romania

In this context, the paper presents a method of simultaneous estimation of the speed and rotor resistance of an induction motor, from the sensorless vector control system. Within the vector control system, speed and rotor flux of the induction motor are estimated by the extended Gopinath observer [11], [12], [18] and rotor resistance is estimated using a relationship obtained from the mathematical model of the induction motor [3], [10].

In order to eliminate the issue of persistence of excitation, a sinusoidal signal of frequency and amplitude low is used, which is superimposed over the module of the phasor rotor flux reference, and to avoid zero division, the "Fixed Trace" method proposed by T. Pana is used [7], [8], [10].

The dynamic performances of the extended Gopinath observer compensated by the rotor resistance, are analyzed by simulation using the Matlab-Simulink program.

2. THE EXTENDED GOPINATH OBSERVER

This observer is a generalization of the low-order Gopinath observer. The block diagram of the Extended Gopinath Observer is presented in Fig.1.

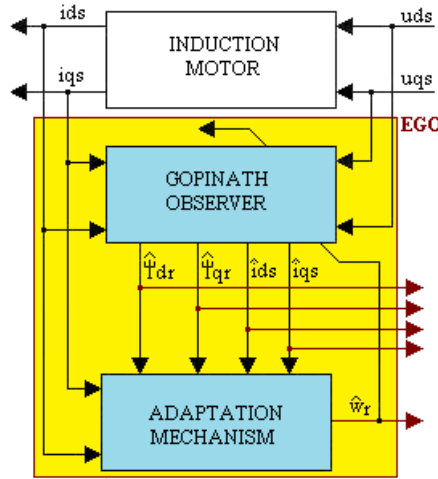


Fig.1. The Extended Gopinath Observer (EGO)

The equations defining the Extended Gopinath Observer (EGO) are [11], [12]:

$$\frac{d}{dt}x = A_a \cdot x + A_b \cdot \dot{x} + B \cdot u + G \cdot C \cdot \frac{d}{dt}e_x \quad (1)$$

where:

$$A_a = \begin{bmatrix} a_a^* & a_{12}^* \\ 0 & a_{22}^* \end{bmatrix}; A_b = \begin{bmatrix} a_b^* & 0 \\ a_{21}^* & 0 \end{bmatrix}; B = \begin{bmatrix} b_{11}^* \\ 0 \end{bmatrix}; G = \begin{bmatrix} 0 \\ g \end{bmatrix}; C = [1 \quad 0]; x = \begin{bmatrix} \underline{i}_s \\ \underline{\psi}_r \end{bmatrix}; \dot{x} = \begin{bmatrix} \dot{\underline{i}}_s \\ \dot{\underline{\psi}}_r \end{bmatrix}; u = \underline{u}_s;$$

$$\underline{i}_s = i_{ds} + j \cdot i_{qs}; \underline{\psi}_r = \psi_{dr} + j \cdot \psi_{qr}; \underline{u}_s = u_{ds} + j \cdot u_{qs}; \dot{\underline{i}}_s = \dot{i}_{ds} + j \cdot \dot{i}_{qs}; \dot{\underline{\psi}}_r = \dot{\psi}_{dr} + j \cdot \dot{\psi}_{qr};$$

$$\begin{aligned}
 e_x &= x - \hat{x}; \quad a_{11}^* = a_a^* + a_b^*; \quad a_{12}^* = a_{13}^* - j \cdot a_{14}^* \cdot z_p \cdot \omega_r; \quad a_{21}^* = a_{31}^*; \quad a_{22}^* = a_{33}^* + j \cdot z_p \cdot \omega_r; \\
 \underline{g} &= g_a + j \cdot g_b; \quad g_a = -k \cdot \frac{a_{31}^* \cdot a_{33}^*}{(a_{33}^*)^2 + (z_p \cdot \omega_r)^2}; \quad g_b = k \cdot \frac{a_{31}^* \cdot z_p \cdot \omega_r}{(a_{33}^*)^2 + (z_p \cdot \omega_r)^2}; \\
 a_a^* &= -\frac{1}{T_s^* \cdot \sigma^*}; \quad a_b^* = -\frac{1 - \sigma^*}{T_r^* \cdot \sigma^*}; \quad a_{13}^* = \frac{L_m^*}{L_s^* \cdot L_r^* \cdot T_r^* \cdot \sigma^*}; \quad a_{14}^* = \frac{L_m^*}{L_s^* \cdot L_r^* \cdot \sigma^*}; \quad a_{31}^* = \frac{L_m^*}{T_r^*}; \\
 a_{33}^* &= -\frac{1}{T_r^*}; \quad b_{11}^* = \frac{1}{L_s^* \cdot \sigma^*}; \quad T_s^* = \frac{L_s^*}{R_s^*}; \quad T_r^* = \frac{L_r^*}{R_r^*}; \quad \sigma^* = 1 - \frac{(L_m^*)^2}{L_s^* \cdot L_r^*}; \quad j = \sqrt{-1}.
 \end{aligned}$$

It can be seen that the matrices A_a and G of the relation (1) are adapted at each moment, depending on the estimated rotor speed.

In the above relations, we marked with „*“, the electrical parameters, determined experimentally, of the induction motor. The positive constant k , is used to increase or decrease the stability degree of the Extended Gopinath Observer [12].

On the other hand, the adaptation mechanism of the extended Gopinath observer is defining the following relationship [11], [12], [18].

$$\hat{\omega}_r = k_r \cdot \varepsilon_a + k_i \cdot \int_0^t \varepsilon_a d\tau \quad (2)$$

where:

$$\varepsilon_a = e_1 \cdot \psi_{qr} - e_2 \cdot \psi_{dr}; \quad e_1 = i_{ds} - \hat{i}_{ds}; \quad e_2 = i_{qs} - \hat{i}_{qs}.$$

In the above relations, k_r and k_i constants are chosen to obtain the desired dynamic regime.

3. ROTOR RESISTANCE ESTIMATION

To determine the mathematical expression that is used in the estimation of rotor resistance, we will present below the voltage equations specific to the squirrel-cage rotor of an induction motor [13].

$$\begin{cases} \frac{d}{dt} \psi_{dr} = -R_r \cdot i_{dr} - z_p \cdot \omega_r \cdot \psi_{qr} \\ \frac{d}{dt} \psi_{qr} = -R_r \cdot i_{qr} + z_p \cdot \omega_r \cdot \psi_{dr} \end{cases} \quad (3)$$

After solving the above system, the rotor speed is given by the following expression:

$$R_r = -\frac{\psi_{dr} \cdot \frac{d}{dt} \psi_{dr} + \psi_{qr} \cdot \frac{d}{dt} \psi_{qr}}{\psi_{dr} \cdot i_{dr} + \psi_{qr} \cdot i_{qr}} \quad (4)$$

On the other hand, the rotor flux equations of the induction motor are [13]:

$$\begin{cases} \psi_{dr} = L_r \cdot i_{dr} + L_m \cdot i_{ds} \\ \psi_{qr} = L_r \cdot i_{qr} + L_m \cdot i_{qs} \end{cases} \quad (5)$$

From (5) we can determine the rotor currents that appear at the denominator of statement (4).

$$\begin{cases} i_{dr} = \frac{\psi_{dr} - L_m \cdot i_{ds}}{L_r} \\ i_{qr} = \frac{\psi_{qr} - L_m \cdot i_{qs}}{L_r} \end{cases} \quad (6)$$

After the introduction of relations (6) into (4), we get the following

$$R_r = -L_r \cdot \frac{\psi_{dr} \cdot \frac{d}{dt} \psi_{dr} + \psi_{qr} \cdot \frac{d}{dt} \psi_{qr}}{\psi_{dr}^2 + \psi_{qr}^2 - L_m \cdot (\psi_{dr} \cdot i_{ds} + \psi_{qr} \cdot i_{qs})} \quad (7)$$

Under these conditions, on the basis of the variables estimated by the Extended Gopinath Observer (EGO), rotor resistance can be estimated as follows:

- *case 1*, in which components d - q of the estimated stator current are used

$$\hat{R}_r = -L_r^* \cdot \frac{\hat{\psi}_{dr} \cdot \frac{d}{dt} \hat{\psi}_{dr} + \hat{\psi}_{qr} \cdot \frac{d}{dt} \hat{\psi}_{qr}}{\hat{\psi}_{dr}^2 + \hat{\psi}_{qr}^2 - L_m^* \cdot (\hat{\psi}_{dr} \cdot \hat{i}_{ds} + \hat{\psi}_{qr} \cdot \hat{i}_{qs})} \quad (8)$$

- *case 2*, in which components d - q of the measured stator current are used

$$\hat{R}_r = -L_r^* \cdot \frac{\hat{\psi}_{dr} \cdot \frac{d}{dt} \hat{\psi}_{dr} + \hat{\psi}_{qr} \cdot \frac{d}{dt} \hat{\psi}_{qr}}{\hat{\psi}_{dr}^2 + \hat{\psi}_{qr}^2 - L_m^* \cdot (\hat{\psi}_{dr} \cdot i_{ds} + \hat{\psi}_{qr} \cdot i_{qs})} \quad (9)$$

From the relations (8) and (9) it is observed that, if desired, we can estimate the inverse of the rotor time constant based on one of the following relations:

- *case 1*, in which components d - q of the estimated stator current are used

$$\frac{1}{\hat{T}_r} = - \frac{\hat{\psi}_{dr} \cdot \frac{d}{dt} \hat{\psi}_{dr} + \hat{\psi}_{qr} \cdot \frac{d}{dt} \hat{\psi}_{qr}}{\hat{\psi}_{dr}^2 + \hat{\psi}_{qr}^2 - L_m^* \cdot (\hat{\psi}_{dr} \cdot \hat{i}_{ds} + \hat{\psi}_{qr} \cdot \hat{i}_{qs})} \quad (10)$$

- *case 2*, in which components d - q of the measured stator current are used

$$\frac{1}{\hat{T}_r} = - \frac{\hat{\psi}_{dr} \cdot \frac{d}{dt} \hat{\psi}_{dr} + \hat{\psi}_{qr} \cdot \frac{d}{dt} \hat{\psi}_{qr}}{\hat{\psi}_{dr}^2 + \hat{\psi}_{qr}^2 - L_m^* \cdot (\hat{\psi}_{dr} \cdot i_{ds} + \hat{\psi}_{qr} \cdot i_{qs})} \quad (11)$$

Given the relationship (1), we can say that estimation errors of stator current and rotor flux components can be compensated either by relations (8) or (9), and by means of relations (10) or (11).

Within this article, the estimation errors of the extended Gopinath observer are offset by the relationship (10). Under these conditions, the coefficients of the extended Gopinath observer, which are calculated according to the inverse of the estimated rotor time constant, are:

$$a_b^* = -\frac{1-\sigma^*}{\hat{T}_r \cdot \sigma^*}; a_{13}^* = \frac{L_m^*}{L_s^* \cdot L_r^* \cdot \hat{T}_r \cdot \sigma^*}; a_{31}^* = \frac{L_m^*}{\hat{T}_r}; a_{33}^* = -\frac{1}{\hat{T}_r} \quad (12)$$

The block diagram of the extended Gopinath observer, adapted to the inverse of the rotor time constant, is shown in Fig.2.

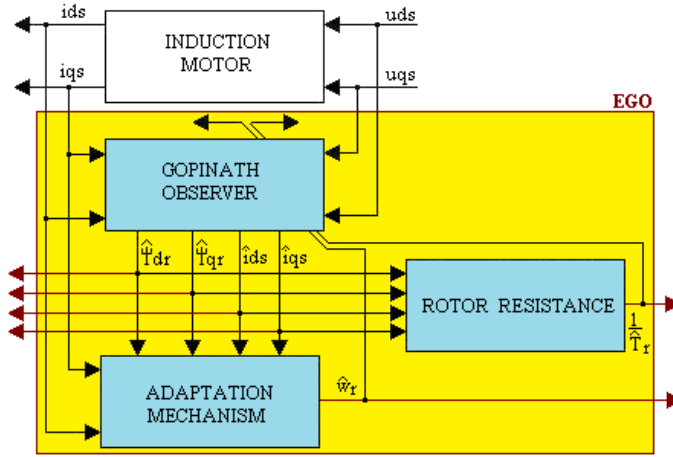


Fig.2. The Extended Gopinath Observer - rotor resistance compensation

In order to implement the relationship (10), we will take into account the results of Shinnaka and T. Pana's research. In this sense, in order to cancel the zero division, which occurs periodically within the above expressions (due to the cancellation of the denominator), even if the rotor flux varies, we will use the Fixed Trace method to effect division of the relationship. In this regard, we will use the following notations:

$$X = -\left(\hat{\psi}_{dr} \cdot \frac{d}{dt} \hat{\psi}_{dr} + \hat{\psi}_{qr} \cdot \frac{d}{dt} \hat{\psi}_{qr} \right) \quad (13)$$

$$Y = \hat{\psi}_{dr}^2 + \hat{\psi}_{qr}^2 - L_m^* \cdot (\hat{\psi}_{dr} \cdot \hat{i}_{ds} + \hat{\psi}_{qr} \cdot \hat{i}_{qs}) \quad (14)$$

Under these conditions, the inverse of the rotor time constant, estimated using the Fixed Trace method, is [7]

$$\frac{1}{\hat{T}_r[m]} = \frac{1}{\hat{T}_r[m-1]} - \frac{\gamma \cdot Y[m]}{1 + \gamma \cdot (Y[m])^2} \left(\frac{Y[m]}{\hat{T}_r[m-1]} - X[m] \right); m = n \cdot T_e; n = 0, 1, \dots \quad (15)$$

where through the forgetting factor γ , which is a positive constant, the noise sensitivity of the estimation increases. Within the relation (15) T_e is the sampling time.

4. VECTORIAL CONTROL SYSTEM

The block diagram of the sensorless vector control system for the induction motor, is presented in Fig.3.

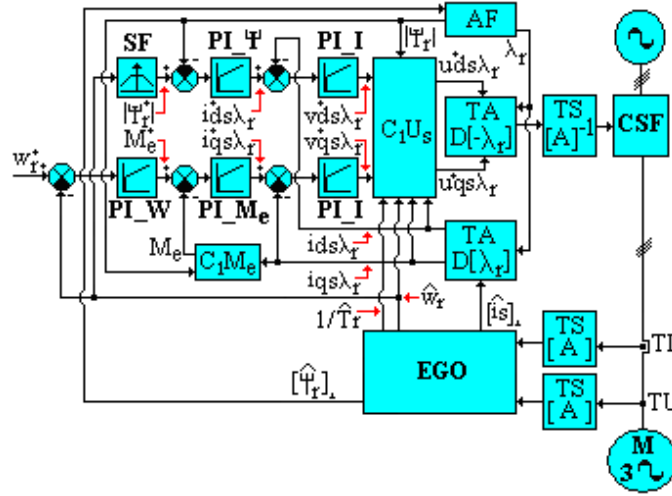


Fig.3. The block diagram of the vector control system [18]

The main blocks within the vector control system are defined by the following equations [18]:

- flux analyzer (AF):

$$\begin{cases} |\hat{\psi}_r| = \sqrt{\hat{\psi}_{dr}^2 + \hat{\psi}_{qr}^2} \\ \sin \lambda_r = \frac{\hat{\psi}_{qr}}{|\hat{\psi}_r|}; \cos \lambda_r = \frac{\hat{\psi}_{dr}}{|\hat{\psi}_r|} \end{cases} \quad (16)$$

- The calculus of the torque block (C_1M_e):

$$M_e = K_a \cdot |\hat{\psi}_r| \cdot \hat{i}_{qs\lambda_r}; K_a = \frac{3}{2} \cdot z_p \cdot \frac{L_m^*}{L_r^*} \quad (17)$$

- stator voltages decoupling block (C_1U_s)

$$\begin{cases} u_{ds}^* = \frac{1}{b_{11}^*} \cdot [b_{11}^* \cdot v_{ds\lambda_r}^* - h_1] \\ u_{qs\lambda_r}^* = \frac{1}{b_{11}^*} \cdot [b_{11}^* \cdot v_{qs\lambda_r}^* + h_2] \end{cases} \quad (18)$$

where:

$$h_1 = a_{13}^* \cdot |\psi_r| + a_{31}^* \cdot \frac{\hat{i}_{qs\lambda_r}^2}{|\psi_r|} + z_p \cdot \omega_r \cdot \hat{i}_{qs\lambda_r};$$

$$h_2 = a_{14}^* \cdot z_p \cdot \omega_r \cdot |\psi_r| + a_{31}^* \cdot \frac{\hat{i}_{ds\lambda_r} \cdot \hat{i}_{qs\lambda_r}}{|\psi_r|} + z_p \cdot \omega_r \cdot \hat{i}_{ds\lambda_r}$$

The coefficients within relation (18) are identical to those in the extended Gopinath estimator, (1) and (12). These coefficients are computed for every moment in time, considering the induction motor rotor constant.

- the field weakening block (SF)

$$|\psi_r^*| = \begin{cases} \frac{U_{\max} \cdot g}{2 \cdot \pi \cdot f_N} & \text{if } |\hat{\omega}_r| \leq \frac{2 \cdot \pi \cdot n_N}{60} \\ \frac{L_m^*}{R_s^*} \frac{U_{\max} \cdot g}{\sqrt{1 + z_p^2 \cdot (T_r^*)^2 \cdot \hat{\omega}_r^2}} & \text{otherwise} \end{cases} \quad (19)$$

where: $g = 1 + A_m \cdot [\sin(\omega_1 \cdot t) + \sin(\omega_2 \cdot t)]$; $\omega_1 = 2 \cdot \pi \cdot f_1$; $\omega_2 = 2 \cdot \pi \cdot f_2$; $U_{\max} = U_N \cdot \sqrt{\frac{2}{3}}$

In the relation (19), by U_N the rated voltage is labeled; f_N is rated frequency; n_N is the rated speed of the induction motor.

The five automatic controllers of the system presented in Fig. 3 are Proportional Integral-type (PI). The parameters of proportionality (K) and the integration times (T) that define the automatic controllers, can be calculated on the basis of the following relations [14]:

- The rotor flux controller (PI $_{\psi}$)

$$K_{\psi} = \frac{T_r^*}{2 \cdot L_m^* \cdot T_{d1}^*}; \quad T_{\psi} = T_r^*; \quad T_r^* = \frac{L_r^*}{R_r^*} \quad (20)$$

where T_{d1}^* is a imposed constant time, and T_r^* is the rotor time constant, initially calculated based on the electrical parameters of the induction motor.

- The torque controller (PI $_{M_e}$)

$$K_M = \frac{2 \cdot \pi \cdot f_N \cdot T_{d1}^*}{K_a \cdot U_{\max} \cdot T_{d2}^*}; \quad T_M = T_{d1}^* \quad (21)$$

where: T_{d2}^* is a imposed time constant, so $T_{d2}^* > T_{d1}^*$.

- the speed controller (PI $_W$)

$$K_{\omega} = \frac{T_4 \cdot (1 + \rho^2)}{2 \cdot K_4 \cdot T_{d2}^*}; \quad T_{\omega} = 4 \cdot \frac{T_{d2}^* \cdot (1 + \rho^2)}{(1 + \rho)^3} \quad (22)$$

where: $\rho = \frac{T_{d2}^*}{T_4}$; $K_4 = \frac{1}{F}$; $T_4 = \frac{J}{F}$; J is moment of inertia of the rotor and F is the coefficient of friction.

- the current controllers (PI_I)

$$K_i = \frac{1}{b_{11}^* \cdot T_{d1}^*}; \quad T_i = -\frac{1}{a_{11}^*} \quad (23)$$

where: $a_{11}^* = -\left(\frac{1}{T_s^* \cdot \sigma^*} + \frac{1 - \sigma^*}{T_r^* \cdot \sigma^*}\right)$; $b_{11}^* = \frac{1}{L_s^* \cdot \sigma^*}$; $T_s^* = \frac{L_s^*}{R_s^*}$; $T_r^* = \frac{L_r^*}{R_r^*}$; $\sigma^* = 1 - \frac{(L_m^*)^2}{L_s^* \cdot L_r^*}$.

From the above, it is noticeable that the current controllers are identical. The proportional coefficients and the integration times of the current controllers are invariant with time being calculated based on the relations (23), taking into account the electric parameters of the induction motor.

The other blocks of Fig. 3, are: current transducers (TI); voltage transducers (TU); static frequency converter (CSF); blocks of transformation of the system (TS) and axis (TA) [13].

5. SIMULATION RESULTS

The EGO observer is validated by simulation, using a 4 [kW] induction motor. The electro-mechanical parameters of the induction motor are presented in Table 1.

Table 1. Induction Motor Parameters

	Name	Value		Name	Value
R_s	Stator resistance	1.405 [Ω]	F	Friction coefficient	0.002985[N·m·s/rad]
R_r	Rotor resistance	1.395 [Ω]	n_N	Rated speed	1430 [rpm]
L_s	Stator inductance	0.178039 [H]	z_p	Number of pole pairs	2
L_r	Rotor inductance	0.178039 [H]	f_N	Rated frequency	50 [Hz]
L_m	Mutual inductance	0.1722 [H]	U_N	Rated voltage	400 [V]
J	Motor inertia	0.0131[kg·m ²]	M_N	Rated torque	27 [N·m]

The transistors within the static frequency convertor with intermediary continuous voltage circuit are considered of ideal commutation.

Within simulation, the CSF disregards the mathematical models of the semiconducting devices.

Within the PWM modulation, the carrier is of isosceles triangle type having a frequency of 5 [kHz]. The modulation technique is based on a modified suboscillation method [1], [16].

The test analyzes the dynamic performance of the sensorless vector control system, which contains an extended Gopinath observer in the loop, of the type shown in Fig. 2.

In simulation test, the induction motor is functioning under load, having at its ax a resistant torque equal to that of the rated torque of the induction motor.

SIMULATING THE SPEED AND ROTOR RESISTANCE OBSERVER IN SENSORLESS
VECTOR CONTROL SYSTEMS WITH INDUCTION MOTORS

The vector control system shown in Fig. 3 is tested taking into account that the speed imposed on the control system is in the form of a two- step speed trapezoidal tachograph.

Are made assuming that the induction motor is preheated. As such, in the initial moment, the rotor resistance is considered with 20% higher than the rated value. After 4 seconds, the value for rotor resistance are abruptly increased by 25% from their rated value.

The rise time from one speed step to another is 0.1 seconds, in the case of the speed imposed. The simulations were made in Matlab – Simulink [2], [6], [9], [13], [17], [19].

In order to solve the differential equations defining the sensorless vector control system, is used the numerical differentiation method of variable order (ode15s), using both an relative and absolute error of the $\varepsilon = 10^{-6}$.

The sampling time used in (15) is $T_e = 1[\mu\text{sec}]$, and initialisation of relation (15), is done by: $\frac{1}{T_r} \Big|_{m=0} = \frac{1}{T_r^*}$. The simulation time is 7 seconds.

The obtained results are presented in the following figures.

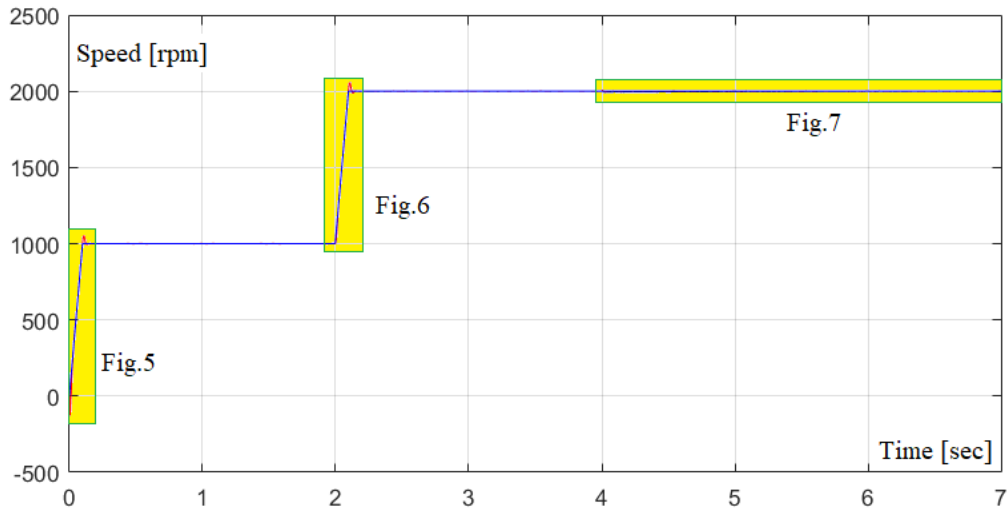


Fig.4. Time variation of imposed speed in tandem with measured speed and estimated motor induction speed.

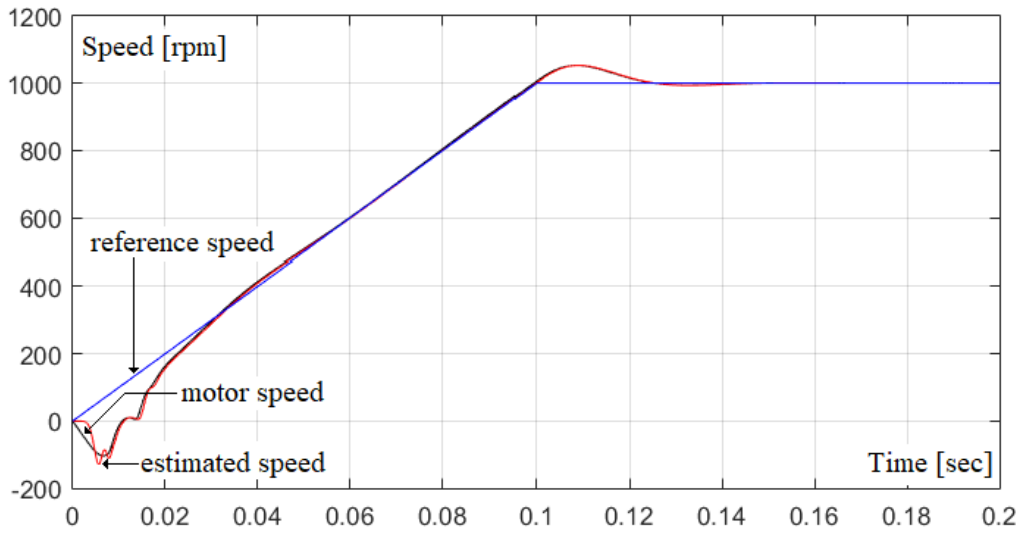


Fig.5. Highlighting the dynamic performance of the vector control system with respect to the time variation of the speed at the start of the induction motor.

In the simulation, stator currents and stator voltages, from the CSF output used in the extended Gopinath observer are filtered by means of second-order Butterworth low-pass filters [16], all of which have a cutting frequency of 500 [Hz].

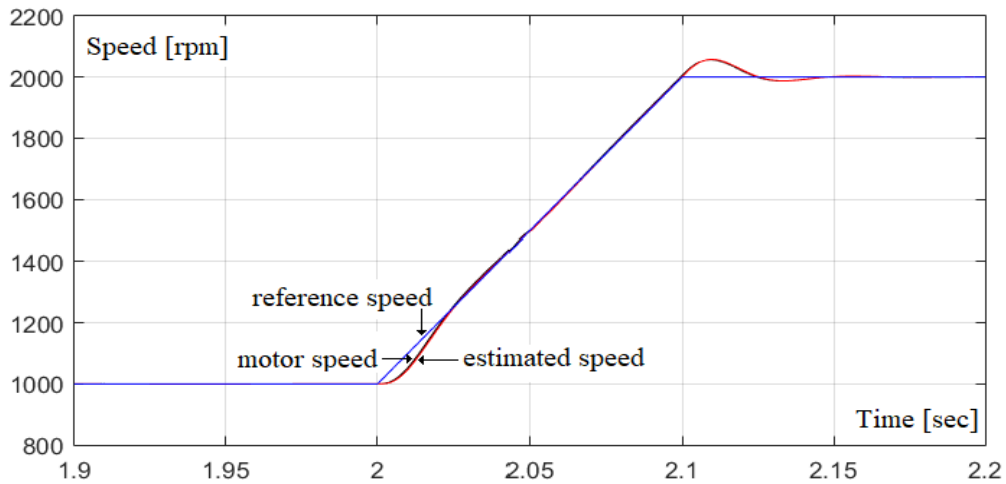


Fig.6. Highlighting the dynamic performance of the vector control system with respect to the time variation of the speed, at the when passing from step 1 to step 2 of the trapezoid speed al tachograph.

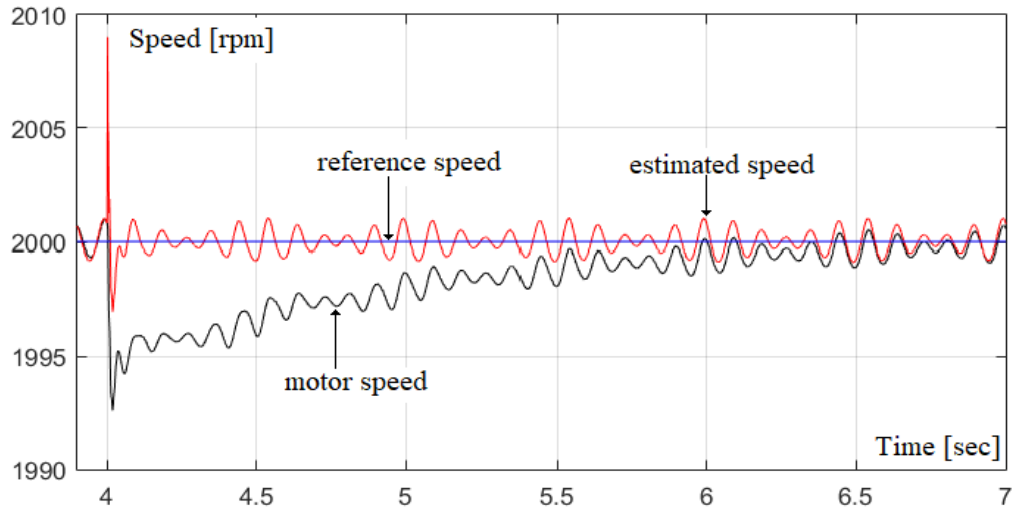


Fig.7. Evidence of the dynamic performance of the vector control system regarding the time variation of the speed, immediately after the sudden variation of the rotor resistance in stationary regime.

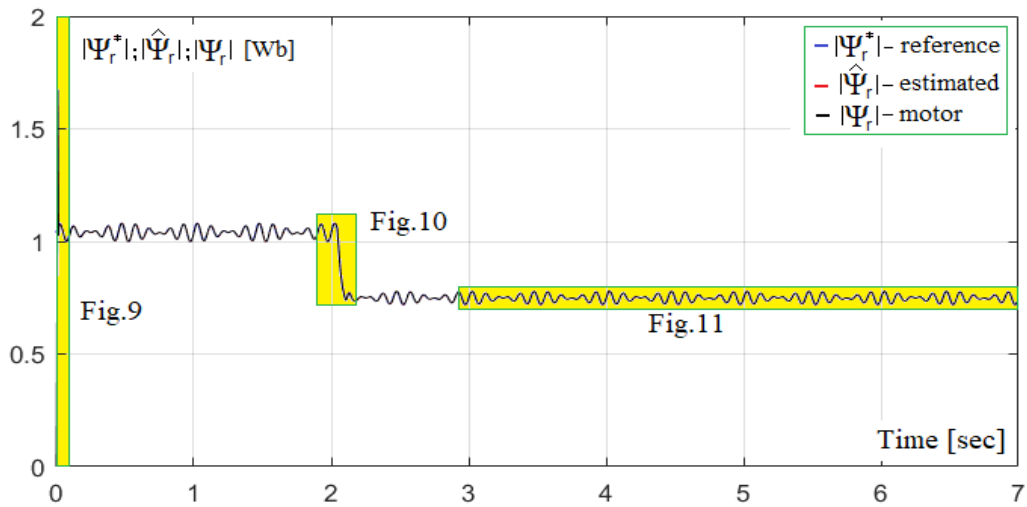


Fig.8. The variation in time of the imposed phasor of the rotor flux, in tandem with the real and estimated rotor flux phasor of the induction motor.

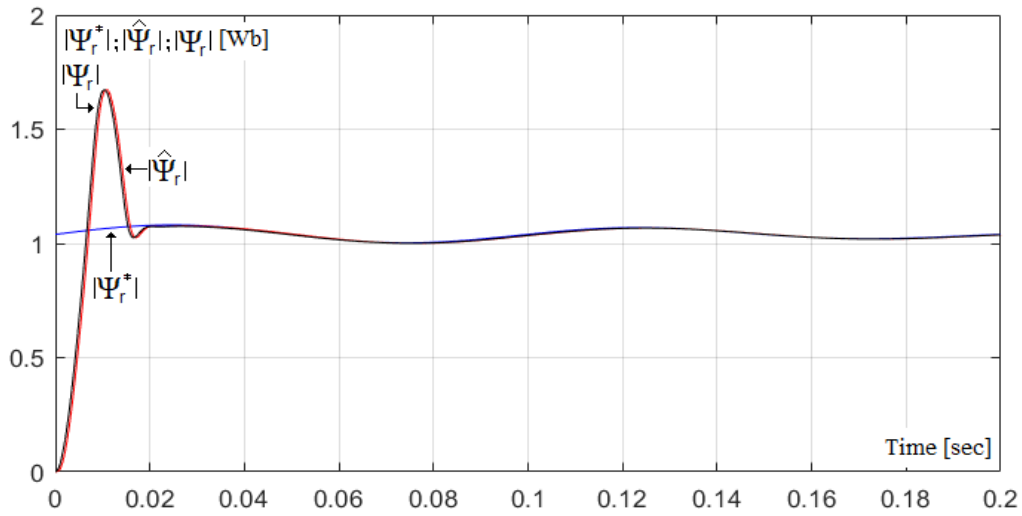


Fig.9. Highlighting the dynamic performance of the vector control system with respect to the time variation of the phasor of the rotor flux, when starting the induction motor.

From Fig. 8 it is observed that when it passing from step 1 to step 2 of the trapezoid speed al tachograph, by means of the SF block within the vector control system of Fig. 3, a rotor flux is reduced (weakening).

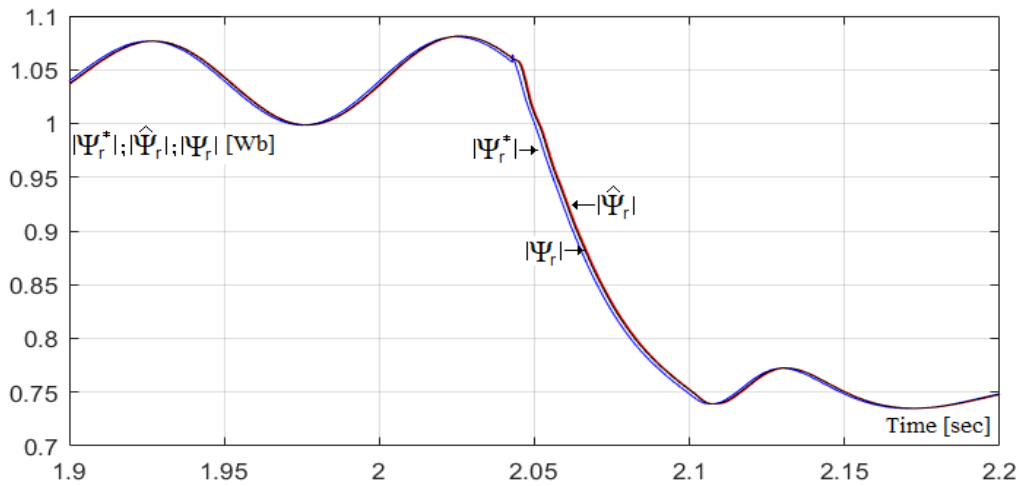


Fig.10. Highlighting the dynamic performance of the vector control system with respect to the time variation of the rotor flux phasor, at the when passing from step 1 to step 2 of the trapezoid speed al tachograph.

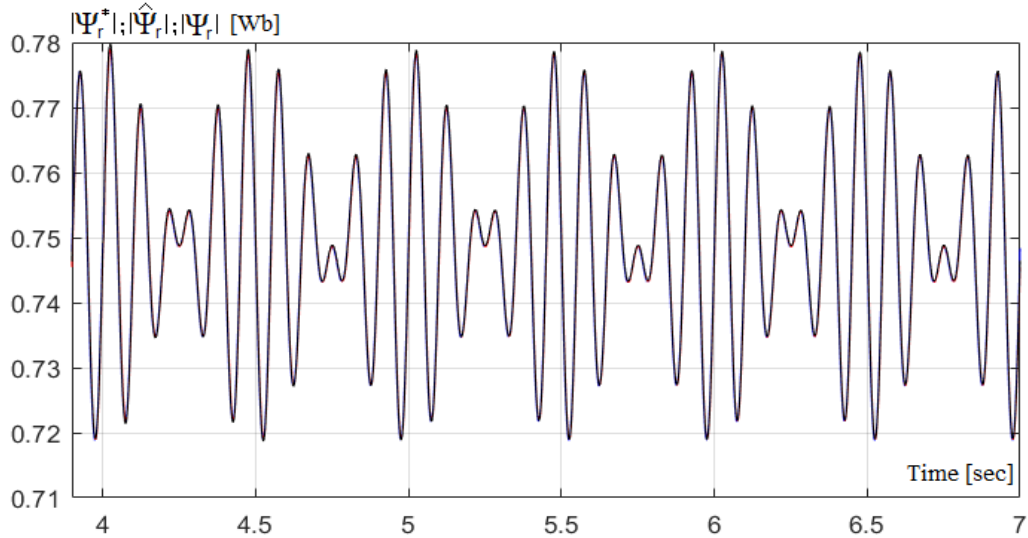


Fig.11. Evidence of the dynamic performance of the vector control system regarding the time variation of the rotor flux phasor, immediately after the sudden variation of the rotor resistance in stationary regime.

At the initial moment, the estimation block of the inverses of the rotor time constant (see Fig. 2) is not used. For 0.02 [sec], the inverse of the rotor time constant is considered to have a value of $9.4[\Omega/H]$, and then the block associated with the rotor time constant inversion estimate is coupled.

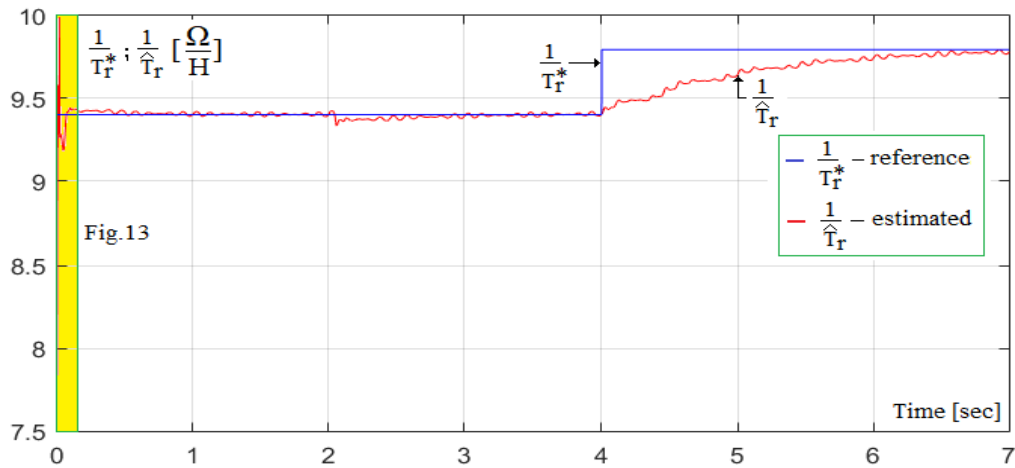


Fig.12. The variation in time of the inverse rotor-time constants - of the reference and estimated.

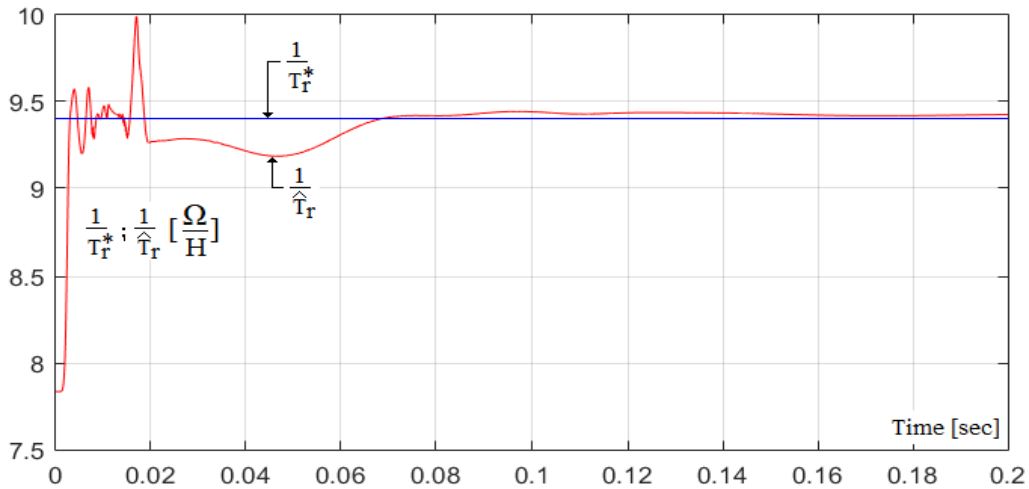


Fig.13. Highlighting the dynamic performance of the vector control system with regard to the time variation of the inverse rotor-time constant, at the start of the induction motor.

From the previously presented graphs we can see that the vector control system, which contains an extended Gopinath observer in the loop, has very good dynamic performance.

On the other hand, it can be seen from Fig. 12 that the estimation of the inversion of the rotor time constant is affected by the speed variation over time (this is observed in Fig. 12 at the time of 2 [sec.]). The effect of the speed variation is canceled after about 1 [sec].

When the rotor resistance suddenly increases to a value 25% higher than the rated resistance (time of 4 [sec]), it can be seen that the inverse of the rotor time constant is estimated correctly after approximately 2.5 [sec] (see Figure 12).

When the inverse of the rotor time constant is estimated correctly, the reference speed overlaps with the estimated speed and the measured speed of the induction motor (this is observed in Fig. 7).

From Figures 8, 9, 10 and 11 it is noticeable that the Gopinath observer, what estimates the d-q components of the stator current as well as the rotor flux, has very good dynamic performances, under the conditions described above.

6. CONCLUSIONS

The compensation solution of the extended Gopinath observer, based on the estimation of rotor resistance using a mathematical relationship deduced from the mathematical model of the induction motor, presents the following advantages:

- the effect of the speed variation on the estimation of the rotor resistance through the deduced relationship from the mathematical model of the induction motor is lower than if the estimation of the rotor resistance is done by means of an adaptive estimator (see [18]);

- the estimator has a very good convergence, with the settling time being less than 2.5 [sec], in the case of a sudden change in rotor resistance;
- reduces errors in estimating speed and rotor flux, so that the dynamic performances of the sensorless vector control systems is much better;
- the parametric stability domain of the sensorless vector control system is much greater than if the extended Gopinath observer is not compensate (see [18]);
- the use of a sensorless vector control system containing an extended Gopinath observer compensated by rotor resistance, allows the elimination of auxiliary ventilation systems of the induction motors.

The main disadvantage of the compensation method of extended Gopinath observer is avoidance to zero division, which occurs in the mathematical relation what defines the rotor resistance estimator.

Given the above, we consider that the proposed observer can be successfully used within industrial applications.

REFERENCES

- [1]. **Holtz J.**, *Pulsewidth Modulation for Electronic Power Conversion*, Proc. of IEEE, vol.82, no.8, pp.1194-1214, 1994.
- [2]. **Ivanov S., Campeanu A., Bitoleanu A., Popescu M.**, *Matlab-Simulink Library for AC Drives Simulation*, Proc. Of Simulation, York, UK, pp. 195-200, 1998.
- [3]. **Kanmachi T., Taahashi I.**, *Sensor-less speed control of an induction motor with no influence of secondary resistance variation*, Proc. of IEEE IAS Annual Meeting, Toronto, Canada, pp. 404-413, 1993.
- [4]. **Kubota H., Matsuse K.**, *DSP-Based Speed Adaptive Flux Observer of Induction Motor*, IEEE Tans. Industry Applications, vol. 29, no. 2, pp.344-348, 1993.
- [5]. **Kubota H., Matsuse K.**, *Speed Sensorless Field-Oriented Control of Induction Motor with Rotor Resistance Adaptation*, IEEE Tans. Industry Applications, vol.30, no. 5, pp.1219-1224, 1994.
- [6]. **Ong C.H.**, *Dynamic Simulations of Electric Machinery: using Matlab/Simulink*, Prentice Hall, 1998.
- [7]. **Pana T.**, *Model based speed and rotor resistance estimation for sensorless vector-controlled induction motor drives using floating point DSP*, Proc. of AMC, Mie, Japan, vol.1, pp.168-173, 1996.
- [8]. **Pana T.**, *Sensorless vector-controlled induction motor drive system with rotor resistance estimation using parallel processing with floating point DSP*, Proc. of IECON, New Orleans, USA, vol.2, pp.948-953, 1997.
- [9]. **Pana T.**, *Matlab Application Toolbox – Electrical Drives – Induction Motor*, Mediamira Publishers, Cluj – Napoca, Romania, 1997.
- [10]. **Pana T., Hori Y.**, *Simultaneous Speed Estimation and Rotor Resistance Identification for Sensorless Induction Motor Drives*, Proc. of IPEC, Yokohama, Japan, pp. 316-321, 1995.
- [11]. **Pana T., Stoicuta O.**, *Small Speed Asymptotic Stability Study of an Induction Motor Sensorless Speed Control System with Extended Gopinath Observer*, Journal of Advances in Electrical and Computer Engineering, vol.11, no.2, pp.15-22, 2011.

- [12]. **Pana T., Stoicuta O.**, *Design of a new adaptive observer for sensorless induction motor drive*, Annals of the University of Craiova – Electrical Engineering, pp.73-78, 2010.
- [13]. **Pana T., Stoicuta O.**, *Stability of the Vector Drive Systems with Induction Motors*, Mediamira Publishers, Cluj –Napoca, Romania, 2016.
- [14]. **Pana T., Stoicuta O.**, *Controllers Tuning for the Speed Vector Control of Induction Motor Drive Systems*, Proc. of AQTR, Cluj-Napoca, Romania, pp.1-6, 2010.
- [15]. **Shinnaka S.**, *A Unified Analysis on Simultaneous Identification of Velocity and Rotor resistance of Induction Motors*, Trans. Institute of Electrical Engineers of Japan, vol.113-D, no.12, pp.1483-1484, 1993.
- [16]. **Stoicuta O.**, *The utilization of the S-Function block in simulation of the Luenberger rotor flux observer for induction motors*, Annals of the University of Petrosani – Electrical Engineering, no.18, pp.31-46, 2016.
- [17]. **Stoicuta O.**, *The modeling and simulation in Matlab-Simulink of the speed control systems of the induction motors*, Universitas Publishing House, Petroșani, Romania, 2012.
- [18]. **Stoicuta O., Pana T., Molnar R.**, *Simultaneous estimation of speed and rotor resistance in the sensorless vector control systems with induction motor, based on Extended Gopinath Observer*, Acta Electrotechnica, vol.57, no.3, pp. 427-432, 2016.
- [19]. ********, *Simulink User's Guide, MathWorks, 2017.*

ELECTRICAL AND MECHANICAL PARAMETERS ESTIMATION OF AN INDUCTION MOTOR

OLIMPIU STOICUTA¹, LORAND BOGDANFFY²

Abstract: The article presents a simple solution for estimating the electrical and mechanical parameters of an induction motor. The estimation methods of induction motor parameters are tested by simulation in Matlab-Simulink.

Keywords: induction motors, modeling and simulation, electrical parameters estimation, mechanical parameters estimation, on-line estimation, extended Gopinath observer.

1. INTRODUCTION

At present, the induction machine is the most used electric machine in various industrial applications. However, one of the most important problems in the implementation of vector control systems is the determination of the electrical and mechanical parameters of the induction machine. Any inconsistency between the determined, identified, or estimated parameters, and the real induction machine parameters, will affect the dynamic performance of the vector control system. On the other hand, it is known that the electrical parameters of the induction machine are affected by temperature, saturation and frequency. For this reason, in many vector control systems is prefer the on-line estimation of the induction machine's electrical parameters, and on the basis of the estimated values, adaptation of the flux observers and controllers in the control system component is made [4],[6]-[8],[13],[14]. Another approach to determining the parameters of an induction machine is based on methods of off-line identification of parameters, when the vector control system is put into operation [1]-[3],[5],[12],[15]. For this purpose either „*DC test*” or „*AC test*” is used.

Taking into account the advantages of on-line estimation methods, this article presents a method of on-line estimation of the parameters of an induction motor, based on an extended Gopinath observer [9]-[11],[13].

¹ Associate Professor, Eng., PhD, University of Petrosani, Romania

² Assistant Researcher, Eng., Ph.D, University of Petrosani, Romania

2. ESTIMATING THE ELECTRICAL PARAMETERS

To determine the mathematical expressions of the electrical parameters observers of an induction motor we will use an adaptation mechanism. The adaptation mechanism processes the errors, obtained in the outputs of two estimators (models), based on the d - q components of the rotor flux and the stator current.

One of the estimators (models) does not contain the estimated parameters and is called *Reference Model* (the induction motor), and the other contains the estimated parameters and is called *Adjustable Model* (the extended Gopinath observer), due to the fact that it is permanently corrected by the last estimated values of the parameters.

From the above, we notice that these types of estimators are adaptive systems based on what is called the *Model Reference Adaptive Systems* (MRAS).

- *Estimation of rotor and stator time constants*

In order to determine these parameters, the *Reference Model* is defined by the model of „stator currents - rotor fluxes”, of the induction motor [11]

$$\frac{d}{dt}x = A \cdot x + B \cdot u \quad (1)$$

where:

$$\begin{aligned} A &= \begin{bmatrix} a_{11} & a_{12} \\ a_{21} & a_{22} \end{bmatrix}; B = \begin{bmatrix} b_{11} \\ 0 \end{bmatrix}; x = \begin{bmatrix} \underline{i}_s \\ \underline{\psi}_r \end{bmatrix}; u = \underline{u}_s; \underline{i}_s = i_{ds} + j \cdot i_{qs}; \underline{\psi}_r = \psi_{dr} + j \cdot \psi_{qr}; \\ \underline{u}_s &= u_{ds} + j \cdot u_{qs}; a_{12} = a_{13} - j \cdot a_{14} \cdot z_p \cdot \omega_r; a_{21} = a_{31}; a_{22} = a_{33} + j \cdot z_p \cdot \omega_r; j = \sqrt{-1}; \\ a_{11} &= -\left(\frac{1}{T_s \cdot \sigma} + \frac{1 - \sigma}{T_r \cdot \sigma} \right); a_{13} = \frac{L_m}{L_s \cdot L_r \cdot T_r \cdot \sigma}; a_{14} = \frac{L_m}{L_s \cdot L_r \cdot \sigma}; a_{31} = \frac{L_m}{T_r}; a_{33} = -\frac{1}{T_r}; \\ b_{11} &= \frac{1}{L_s \cdot \sigma}; T_s = \frac{L_s}{R_s}; T_r = \frac{L_r}{R_r}; \sigma = 1 - \frac{L_m^2}{L_s \cdot L_r}. \end{aligned}$$

On the other hand, the *Adjustable Model* is given by an extended Gopinath observer (EGO), defined by the following relationship [13]

$$\frac{d}{dt}x = \tilde{A}_a \cdot x + \tilde{A}_b \cdot \hat{x} + B \cdot u + \tilde{G} \cdot C \cdot \frac{d}{dt}e_x \quad (2)$$

where:

$$\begin{aligned} A_a &= \begin{bmatrix} a_a^* & a_{12}^* \\ 0 & a_{22}^* \end{bmatrix}; A_b = \begin{bmatrix} a_b^* & 0 \\ a_{21}^* & 0 \end{bmatrix}; B = \begin{bmatrix} b_{11}^* \\ 0 \end{bmatrix}; G = \begin{bmatrix} 0 \\ \underline{g} \end{bmatrix}; C = [1 \quad 0]; x = \begin{bmatrix} \underline{i}_s \\ \underline{\psi}_r \end{bmatrix}; \hat{x} = \begin{bmatrix} \hat{\underline{i}}_s \\ \hat{\underline{\psi}}_r \end{bmatrix}; u = \underline{u}_s; \\ \underline{i}_s &= i_{ds} + j \cdot i_{qs}; \underline{\psi}_r = \psi_{dr} + j \cdot \psi_{qr}; \underline{u}_s = u_{ds} + j \cdot u_{qs}; \hat{\underline{i}}_s = \hat{i}_{ds} + j \cdot \hat{i}_{qs}; \hat{\underline{\psi}}_r = \hat{\psi}_{dr} + j \cdot \hat{\psi}_{qr}; \\ e_x &= x - \hat{x}; a_{11}^* = a_a^* + a_b^*; a_{12}^* = a_{13}^* - j \cdot a_{14}^* \cdot z_p \cdot \omega_r; a_{21}^* = a_{31}^*; a_{22}^* = a_{33}^* + j \cdot z_p \cdot \omega_r; \\ \underline{g} &= g_a + j \cdot g_b; g_a = -k \cdot \frac{a_{31}^* \cdot a_{33}^*}{(a_{33}^*)^2 + (z_p \cdot \omega_r)^2}; g_b = k \cdot \frac{a_{31}^* \cdot z_p \cdot \omega_r}{(a_{33}^*)^2 + (z_p \cdot \omega_r)^2}; \end{aligned}$$

ELECTRICAL AND MECHANICAL PARAMETERS ESTIMATION
OF AN INDUCTION MOTOR

$$a_a^* = -\frac{1}{\hat{T}_s^* \cdot \sigma^*}; a_b^* = -\frac{1-\sigma^*}{\hat{T}_r^* \cdot \sigma^*}; a_{13}^* = \frac{L_m^*}{L_s^* \cdot L_r^* \cdot \hat{T}_r^* \cdot \sigma^*}; a_{14}^* = \frac{L_m^*}{L_s^* \cdot L_r^* \cdot \sigma^*}; a_{31}^* = \frac{L_m^*}{\hat{T}_r^*};$$

$$a_{33}^* = -\frac{1}{\hat{T}_r^*}; b_{11}^* = \frac{1}{L_s^* \cdot \sigma^*}; \sigma^* = 1 - \frac{(L_m^*)^2}{L_s^* \cdot L_r^*}; j = \sqrt{-1}.$$

In the extended Gopinath observer, the A_a , A_b and G arrays are marked with „ \sim ”, because they are adapted at each moment depending on the two estimated parameters.

On the other hand, it can be seen that the matrices A_a and G are adapted at each moment, depending on the rotor speed measured, by an encoder.

In order to determine the mathematical expressions defining the adaptation mechanism, we will use the terminology of asymptotic stability in the Lyapunov sense.

In this regard, the following Lyapunov function is built [13]

$$V_a = e^T \cdot e + \frac{(\Delta T_r)^2}{\lambda_1} + \frac{(\Delta T_s)^2}{\lambda_2} \quad (3)$$

where:

$$\Delta T_r = \frac{1}{\hat{T}_r^*} - \frac{1}{T_r}; \Delta T_s = \frac{1}{\hat{T}_s^*} - \frac{1}{T_s}; e = [e_1 \quad e_2 \quad e_3 \quad e_4]^T;$$

$$e_1 = \hat{i}_{ds} - \hat{i}_{ds}; e_2 = \hat{i}_{qs} - \hat{i}_{qs}; e_3 = \hat{\psi}_{dr} - \hat{\psi}_{dr}; e_4 = \hat{\psi}_{qr} - \hat{\psi}_{qr}.$$

In relation (3), constants λ_1 and λ_2 are arbitrary and positive constants. If the errors of estimation of the rotor flux are neglected, the derivative of function (3) is negative, if the following equations are satisfied [13]

$$\frac{d}{dt} \Delta T_r = \lambda_1 \cdot a_{14}^* \cdot [e_1 \cdot \Delta_\alpha + e_2 \cdot \Delta_\beta] \quad (4)$$

$$\frac{d}{dt} \Delta T_s = -\lambda_2 \cdot b_{11}^* \cdot [e_1 \cdot \hat{i}_{ds} + e_2 \cdot \hat{i}_{qs}] \quad (5)$$

where:

$$\Delta_\alpha = \hat{\psi}_{dr} - L_m^* \cdot \hat{i}_{ds}; \Delta_\beta = \hat{\psi}_{qr} - L_m^* \cdot \hat{i}_{qs}$$

If the variation in time of the estimated variables is in significantly larger than that of the real variables, relations (4) and (5) become:

$$\frac{d}{dt} \left(\frac{1}{\hat{T}_r^*} \right) = k_1 \cdot [e_1 \cdot \Delta_\alpha + e_2 \cdot \Delta_\beta] \quad (6)$$

$$\frac{d}{dt} \left(\frac{1}{\hat{T}_s^*} \right) = -k_2 \cdot [e_1 \cdot \hat{i}_{ds} + e_2 \cdot \hat{i}_{qs}] \quad (7)$$

Within the relations above, constants k_1 and k_2 are chosen to achieve the desired dynamic regime.

Relations (6) and (7) represent the general formulas used in the construction of the adaptation mechanism.

If a much better control of the dynamic performances of the adaptive estimators is desired, the following relationships can be used [13]

$$\frac{1}{\hat{T}_r^*(t)} = k_{i_1} \cdot \varepsilon_a(t) + k_{i_1} \cdot \int_0^t \varepsilon_a(\tau) d\tau \quad (8)$$

$$\frac{1}{\hat{T}_s^*(t)} = - \left[k_{i_2} \cdot \varepsilon_b(t) + k_{i_2} \cdot \int_0^t \varepsilon_b(\tau) d\tau \right] \quad (9)$$

where: $\varepsilon_a(t) = e_1(t) \cdot \Delta_\alpha(t) + e_2(t) \cdot \Delta_\beta(t)$; $\varepsilon_b(t) = e_1(t) \cdot \hat{i}_{ds}(t) + e_2(t) \cdot \hat{i}_{qs}(t)$.

From relations (8) and (9), we can see that the adaptive estimators have every two coefficients (one of proportionality „ k_r ” and one integration coefficient „ k_i ”) by means of which the dynamic performances are controlled.

- *Estimation of rotor and stator resistances*

For the simultaneous estimation of rotor and stator resistances, the same strategy is adopted as in the previous case. The Lyapunov function chosen for this case is

$$V_b = e^T \cdot e + \frac{(\Delta R_r)^2}{\lambda_3} + \frac{(\Delta R_s)^2}{\lambda_4} \quad (10)$$

where:

$$\begin{aligned} \Delta R_r &= \hat{R}_r^* - R_r; \Delta R_s = \hat{R}_s^* - R_s; e = [e_1 \quad e_2 \quad e_3 \quad e_4]^T; \\ e_1 &= \hat{i}_{ds} - \hat{i}_{ds}; e_2 = \hat{i}_{qs} - \hat{i}_{qs}; e_3 = \psi_{dr} - \psi_{dr}; e_4 = \psi_{qr} - \psi_{qr}. \end{aligned}$$

In relation (10), the constants λ_3 and λ_4 are arbitrary and positive constants. If errors of estimation of the rotor flux are neglected and assumed that the variation in time of the estimated variables is significantly larger than that of the real variables, the mathematical expressions on the basis of which the rotor and stator resistances are estimated are:

$$\hat{R}_r^*(t) = k_{i_3} \cdot \varepsilon_a(t) + k_{i_3} \cdot \int_0^t \varepsilon_a(\tau) d\tau \quad (11)$$

$$\hat{R}_s^*(t) = - \left[k_{i_4} \cdot \varepsilon_b(t) + k_{i_4} \cdot \int_0^t \varepsilon_b(\tau) d\tau \right] \quad (12)$$

where: $\varepsilon_a(t) = e_1(t) \cdot \Delta_\alpha(t) + e_2(t) \cdot \Delta_\beta(t)$; $\varepsilon_b(t) = e_1(t) \cdot \hat{i}_{ds}(t) + e_2(t) \cdot \hat{i}_{qs}(t)$;
 $\Delta_\alpha(t) = \hat{\psi}_{dr}(t) - L_m^* \cdot \hat{i}_{ds}(t)$; $\Delta_\beta(t) = \hat{\psi}_{qr}(t) - L_m^* \cdot \hat{i}_{qs}(t)$.

ELECTRICAL AND MECHANICAL PARAMETERS ESTIMATION
OF AN INDUCTION MOTOR

In this case, the extended Gopinath observer is also defined by relation (2), but the matrices A_a , A_b and G are adapted at each moment according to the estimated values of the rotor and stator resistances.

The coefficients of the matrices in the extended Gopinath observer component, adapted to the estimated values of rotor and stator resistances, are:

$$\begin{aligned} a_{11}^* &= a_a^* + a_b^*; & a_{12}^* &= a_{13}^* - j \cdot a_{14}^* \cdot z_p \cdot \omega_r; & a_{21}^* &= a_{31}^*; & a_{22}^* &= a_{33}^* + j \cdot z_p \cdot \omega_r; \\ \underline{g} &= g_a + j \cdot g_b; & g_a &= -k \cdot \frac{a_{31}^* \cdot a_{33}^*}{(a_{33}^*)^2 + (z_p \cdot \omega_r)^2}; & g_b &= k \cdot \frac{a_{31}^* \cdot z_p \cdot \omega_r}{(a_{33}^*)^2 + (z_p \cdot \omega_r)^2}; \\ a_a^* &= -\frac{1}{\hat{T}_s^* \cdot \sigma^*}; & a_b^* &= -\frac{1 - \sigma^*}{\hat{T}_r^* \cdot \sigma^*}; & a_{13}^* &= \frac{L_m^*}{L_s^* \cdot L_r^* \cdot \hat{T}_r^* \cdot \sigma^*}; & a_{14}^* &= \frac{L_m^*}{L_s^* \cdot L_r^* \cdot \sigma^*}; & a_{31}^* &= \frac{L_m^*}{\hat{T}_r^*}; \\ a_{33}^* &= -\frac{1}{\hat{T}_r^*}; & \hat{T}_s^* &= \frac{L_s^*}{\hat{R}_s^*}; & \hat{T}_r^* &= \frac{L_r^*}{\hat{R}_r^*}; & \sigma^* &= 1 - \frac{(L_m^*)^2}{L_s^* \cdot L_r^*}. \end{aligned}$$

- *Estimation of rotor and stator inductances*

To achieve simultaneous estimation of rotor and stator inductances, are used both the extended Gopinath observer for estimating inverse rotor and stator time constants, as well as the extended Gopinath observer used to estimate rotor and stator resistances.

In these conditions, the following relationships are used for the determination of the rotor and stator inductances:

$$\begin{cases} L_r^* = \hat{T}_r^* \cdot \hat{R}_r^* \\ L_s^* = \hat{T}_s^* \cdot \hat{R}_s^* \end{cases} \quad (13)$$

Due to the remarkable robustness of the extended Gopinath observer at the variations of the rotor and stator inductances, it is not adapted to these estimated values.

- *Estimation of mutual inductance*

In order to determine the mutual inductance, we will use the extended Gopinath observer used in estimating the inversion of the rotor time constant, as well as the estimated values of the d-q components of the rotor flux and the stator current, given by this observer.

To determine the mutual inductance, we will use the equations of the mathematical model of „stator currents - rotor fluxes”, of the induction motor. Under these conditions, mutual inductance is determined on the basis of the following relationship [11]:

$$\hat{L}_m^* = \frac{\hat{T}_r^* \cdot \frac{d|\hat{\psi}_r|^2}{dt} + |\hat{\psi}_r|^2}{\hat{\psi}_{dr} \cdot \hat{i}_{ds} + \hat{\psi}_{qr} \cdot \hat{i}_{qs}}; \quad |\hat{\psi}_r|^2 = \hat{\psi}_{dr}^2 + \hat{\psi}_{qr}^2 \quad (14)$$

As in the previous case, due to the remarkable robustness of the extended Gopinath observer, it is not adapted to this estimated value.

The block diagram of the observer, used in estimating all the electrical parameters of the induction motor is shown in Fig. 1.

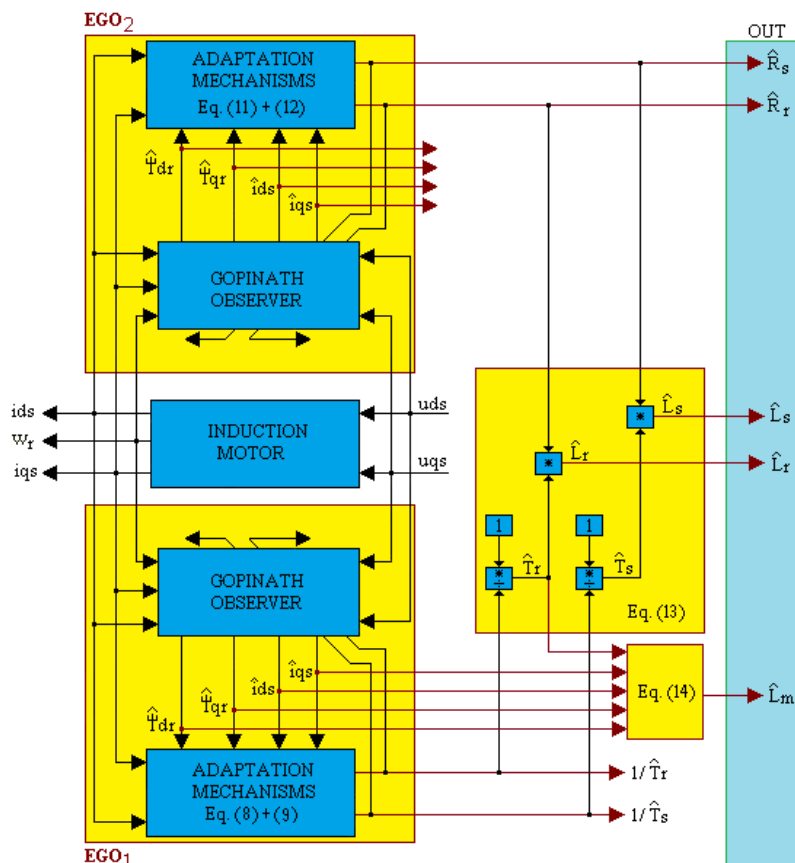


Fig.1. Block diagram of the electrical parameters observer of the induction motor

3. ESTIMATION OF MECHANICAL PARAMETERS

The estimated mechanical parameters are the inertia moment (J), the viscous friction coefficient (F) and the dry friction torque (M_f). The estimation method presented in this article does not require rotor removal.

In order to estimate the mechanical parameters we will use the following equation of motion [11]

$$J \cdot \frac{d\omega_r}{dt} = M_e - F \cdot \omega_r - M_f - M_r \quad (15)$$

where: M_e is the electromagnetic torque given by the induction motor, and M_r is the resistant torque given by the working machine.

Taking into account the estimated values provided by the observer shown in Fig. 1, the electromagnetic torque developed by the induction machine can be estimated based on the following relationship [11]:

$$\hat{M}_e = \frac{3}{2} \cdot z_p \cdot \frac{\hat{L}_m^*}{\hat{L}_r^*} \cdot (\hat{\psi}_{dr} \cdot \hat{i}_{qs} - \hat{\psi}_{qr} \cdot \hat{i}_{ds}) \quad (16)$$

From the above we can see that the estimation of the mechanical parameters can be made very easy in the conditions when we do not have a working machine coupled to the induction motor shaft. In these conditions the resistant torque is null and the relation (15) can be written as follows:

$$J \cdot \frac{d\omega_r}{dt} + F \cdot \omega_r + M_f = M_e \quad (17)$$

In order to determine the mechanical parameters, the relation (17) is discretized by the Euler method . In these conditions we get the following mathematical expression:

$$J \cdot \Omega(m \cdot T_e) + F \cdot \omega_r(m \cdot T_e) + M_f = \hat{M}_e(m \cdot T_e) ; m=0,1,2,\dots \quad (18)$$

where: $\Omega(m \cdot T_e) = \frac{\omega_r((m+1) \cdot T_e) - \omega_r(m \cdot T_e)}{T_e}$, T_e is the sampling time.

Under these conditions, the equation presented above can be written as such

$$y(m) = \psi^T(m) \cdot \theta(m) + e(m); m=0,1,2,\dots \quad (19)$$

where: $e(m)$ is the error of approximation of the derivative; $y(m) = \hat{M}_e(m \cdot T_e)$;

$$\psi(m) = [\Omega(m \cdot T_e) \quad \omega_r(m \cdot T_e) \quad 1]^T ; \theta(m) = [J(m \cdot T_e) \quad F(m \cdot T_e) \quad M_f(m \cdot T_e)]^T .$$

It can be noticed that the mechanical parameters of the induction motor are obtained from the optimal solution of the system (19). In order to solve the system we will use a Kalman filter.

The Kalman filter algorithm, used in solving the system (19) is

$$\left\{ \begin{array}{l} \hat{\theta}(m) = \hat{\theta}(m-1) + K(m) \cdot (y(m) - \psi^T(m) \cdot \hat{\theta}(m-1)); m=0,1,2,\dots \\ K(m) = \frac{P(m-1) \cdot \psi(m)}{R_2 + \psi^T(m) \cdot P(m-1) \cdot \psi(m)} \\ P(m) = P(m-1) + R_1 - K(m) \cdot \psi^T(m) \cdot P(m-1) \end{array} \right. \quad (20)$$

where: R_1 is the drift matrix of the Gaussian white noise vector that affects the vector of the mechanical parameters, and R_2 is the error variant $R_2 = var(e)$, and P is the covariance matrix indicating the parameter errors.

The algorithm proposed above requires the following initializations

$$\hat{\theta}(m-1)\Big|_{m=0} = \theta_0; P(m-1)\Big|_{m=0} = P_0 \quad (21)$$

and an appropriate choice of both the covariance matrix R_1 and the variant R_2 .

The block diagram of the observer used in estimating all the electrical and mechanical parameters of the induction motor is shown in Fig. 2.

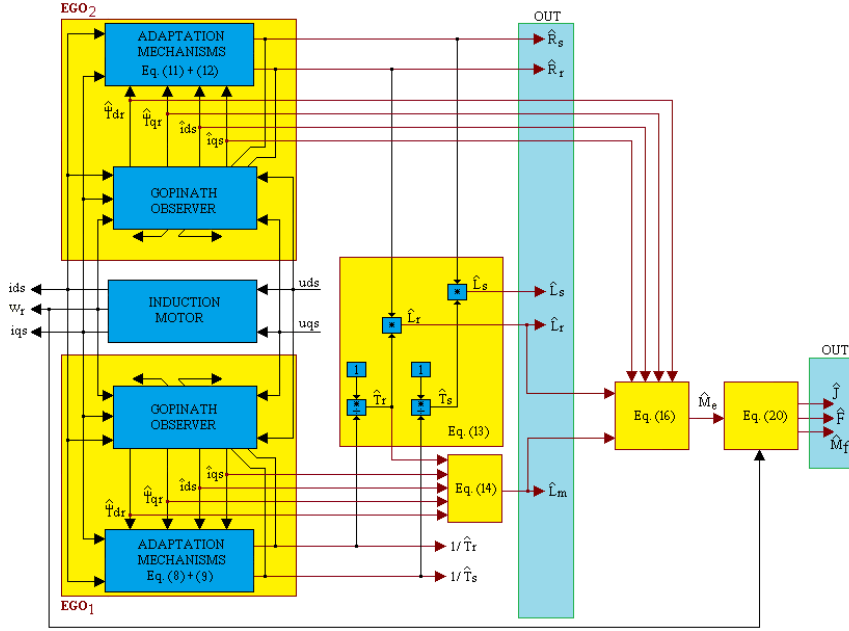


Fig.2. Block diagram of the electrical and mechanical parameters observer.

4. SIMULATION RESULTS

Validation of the estimators presented in this article is done by simulation in Matlab-Simulink.

In this respect, is used an induction motor of 4 [kW], having the electrical and mechanical parameters presented in Table 1.

The parameters presented in Table 1 are determined experimentally using an offline method.

Table 1. Induction Motor Parameters

Name	Value	Name	Value		
R_s	Stator resistance	1.405 [Ω]	F	Friction coefficient	0.002985[N·m·s/rad]
R_r	Rotor resistance	1.395 [Ω]	n_N	Rated speed	1430 [rpm]
L_s	Stator inductance	0.178039 [H]	z_p	Number of pole pairs	2
L_r	Rotor inductance	0.178039 [H]	f_N	Rated frequency	50 [Hz]
L_m	Mutual inductance	0.1722 [H]	U_N	Rated voltage	400 [V]
J	Motor inertia	0.0131[kg·m ²]	M_f	Friction torque	3.4 [N·m]

ELECTRICAL AND MECHANICAL PARAMETERS ESTIMATION
OF AN INDUCTION MOTOR

In the simulation, the parameters of the observer present in Fig. 1, are initialized with the values of the electric parameters of the induction motor given in Table 1.

The simulation is made assuming that the induction motor is preheated. As such, in the initial moment, the rotor resistance is considered with 20% higher than the rated value, while the stator resistance is considered with 15% higher than the rated value. After 10 seconds, the values for rotor and stator resistances are abruptly increased by 25% and 20% from their rated values.

The observer shown in Fig. 2 is tested in the open loop, in the case of direct starting of the induction motor. During the simulation, it is assumed that the stator, rotor and mutual inductances does not change over time.

In the simulation, equations are solved based on the Dormand - Prince method (ode 45), using a relative and absolute error of $\varepsilon = 10^{-6}$.

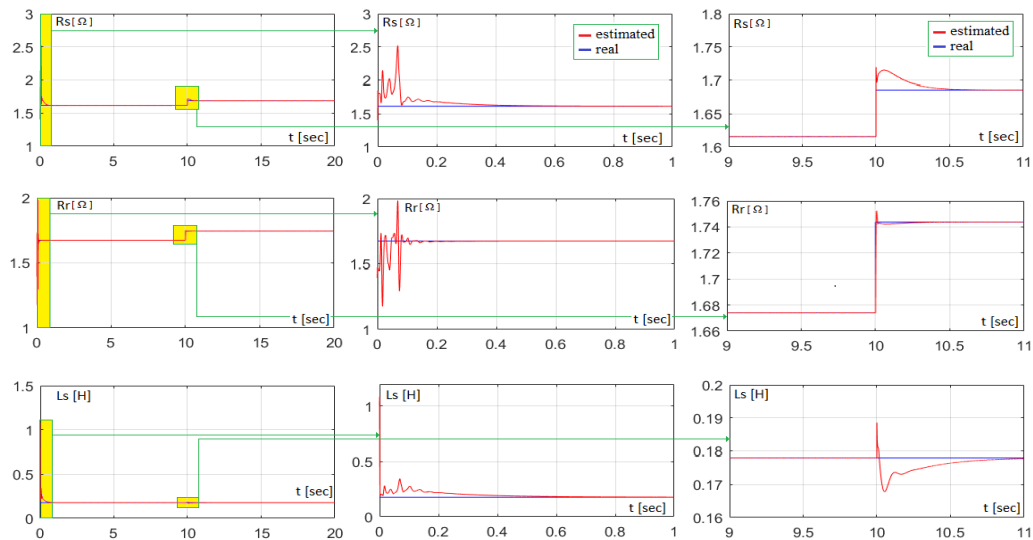
In the simulation, the coefficients of proportionality and integration, in the relations component (8), (9), (11) and (12), are:

$$k_{r_1} = 0.1; k_{i_1} = 40; k_{r_2} = 0.1; k_{i_2} = 30 \quad (22)$$

$$k_{r_3} = k_{r_4} = 1; k_{i_3} = k_{i_4} = 10 \quad (23)$$

In simulation of the observer in Fig. 2, the Gopinath proportional coefficient has the following value: $k = 0.2$. The simulation program in Fig. 2 was run on a numerical computing system that has a Windows 10 operating system installed on 64 bits. The computing system is developed around an I7-4720HQ processor, with a 2.6GHz frequency and an 8GB RAM.

The simulation results are shown in the following figure.



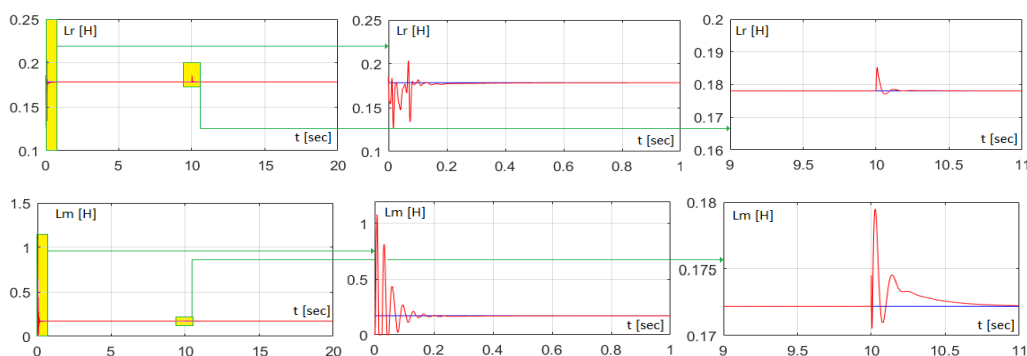


Fig.3. The dynamic performances of the electrical parameters observer of the induction motor.

The transient responses of the observer, have oscillations that are amortizing very quickly. From the graphs in Figure 3, it is noted that the settling time is about 0.4 [sec] when estimating of the stator resistance and stator inductance and much less in the other cases (about 0.2 [sec]). On the other hand, when rotor resistance and stator resistance suddenly increase, it is noted that the settling time is about 0.6 [sec] when estimating of the stator resistance, stator inductance, and mutual inductance.

In simulation test, the induction motor is functioning under load, having at its shaft a resistant torque equal to that of the rated torque of the induction motor (27[Nm]). Simulation of the mechanical parameters estimator of the induction motor shall be made taking into account the following initializations:

$$\theta_0 = [J \quad F \quad M_f]^T ; R_1 = 0.98 \cdot I_3 ; R_2 = 1 ; P_0 = 10^{-6} \cdot I_3 ; T_e = 0.001[\text{sec}] \quad (24)$$

where: I_3 is the third-order unit matrix, and J, F si M_f are equal to values from Table 1.

The simulation results are shown in the following figure.

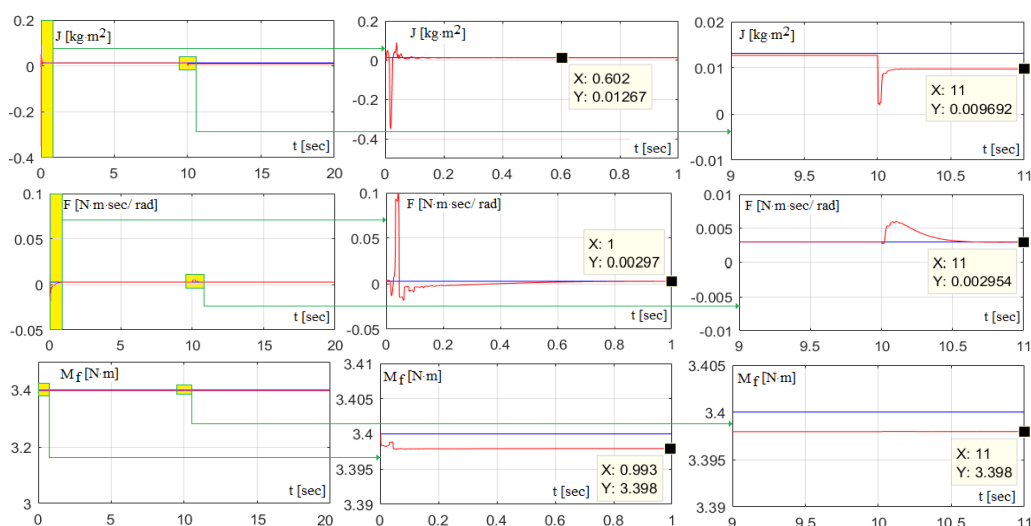


Fig.4. The dynamic performances of the mechanical parameters observer

ELECTRICAL AND MECHANICAL PARAMETERS ESTIMATION OF AN INDUCTION MOTOR

From the graphs of Fig. 4, we can see the sudden variation in stator resistance and rotor resistance affect the dynamic performance of the observer. Stationary estimation errors when starting the induction motor, are maximum 3.3%. After rotor resistance and stator resistance suddenly increase (see time of 10 [sec]), stationary estimation errors are less than 1.1% for friction coefficient and friction torque and the approximately 26%, for motor inertia.

Increasing the dynamic performances of the mechanical parameters observer, can be done by decreasing the sampling time and by better choosing the covariance matrices.

5. CONCLUSIONS

Following the simulation analysis of the observer presented in this article, we can conclude that it has good dynamic performances and can be used successfully instead of existing on-line observers.

The observer analyzed in this article requires an initialization of the electrical and mechanical parameters that can be obtained either through measurements or through an off-line identification.

In order to increase the robustness of the observer presented in the article to the variations in time of the inductances, it is possible to adapt the extended Gopinath observer according to stator, rotor and mutual inductance estimated.

Following the simulation analysis, it was observed that the dynamic performances of the mechanical parameter observer can be improved, either by choosing the appropriate sampling time, or by better choosing the covariance matrices.

REFERENCES

- [1]. **Ayasun S., Nwankpa C.O.**, *Induction motor test using Matlab/Simulink and their integration into undergraduate electric machinery courses*, IEEE Transactions on Education, vol.48, No.1, pp.37-46, 2005.
- [2]. **Boglietti A., Ferraris P., Lazzari M., Profumo F.**, *Induction motor equivalent circuit parameters determination from standard tests made with inverter supply*, Proc. Inst. Elect. Eng. Elect. Mach. Drives Conf., pp. 271–276, 1993.
- [3]. **Bunte A., Grotstollen H.**, *Parameter identification of an inverter-fed induction motor at standstill with a correlation method*, Proc. Europe. Conf. Power Electron. Applicat., vol. 5, pp. 97–102, 1993.
- [4]. **Du T., Brdys M.A.**, *Implementation of extended Luenberger observers for joint state and parameter estimation of PWM induction motor drive*, Proc. Europe. Conf. Power Electron. Applicat., vol. 4, pp. 439–444, 1993.
- [5]. **Holtz J., Thimm T.**, *Identification of the machine parameters in a vector controlled induction motor drive*, Proc. IEEE Industry Applic. Society, pp.601-606, 1989.
- [6]. **Kubota H., Matsuse K.**, *Speed Sensorless Field-Oriented Control of Induction Motor with Rotor Resistance Adaptation*, IEEE Tans. Industry Applications, vol.30, no. 5, pp.1219-1224, 1994.
- [7]. **Loron L., Laliberte G.**, *Application of the extended Kalman filter to parameters estimation of induction motors*, Proc. Europe. Conf. Power Electron. Applicat., vol. 5, pp. 85–90, 1993.

- [8]. **Pana T., Hori Y.**, *Simultaneous Speed Estimation and Rotor Resistance Identification for Sensorless Induction Motor Drives*, Proc. of IPEC, Yokohama, Japan, pp. 316-321, 1995.
- [9]. **Pana T., Stoicuta O.**, *Small Speed Asymptotic Stability Study of an Induction Motor Sensorless Speed Control System with Extended Gopinath Observer*, Journal of Advances in Electrical and Computer Engineering, vol.11, no.2, pp.15-22, 2011.
- [10]. **Pana T., Stoicuta O.**, *Design of a new adaptive observer for sensorless induction motor drive*, Annals of the University of Craiova – Electrical Engineering, pp.73-78, 2010.
- [11]. **Pana T., Stoicuta O.**, *Stability of the Vector Drive Systems with Induction Motors*, Mediamira Publishers, 2016.
- [12]. **Schierling H.**, *Self - commissioning - a novel feature of modern inverter - fed induction motor drives*, Proc. Inst. Elect. Eng. Conf. Power Electronics and Variable Speed Drives, pp. 287–290, 1988.
- [13]. **Stoicuta O., Pana T., Molnar R.**, *Simultaneous estimation of speed and rotor resistance in the sensorless vector control systems with induction motor, based on Extended Gopinath Observer*, Acta Electrotechnica, vol.57, no.3, pp. 427-432, 2016.
- [14]. **Tolyat H.A., Levi E., Raina M.**, *A review of RFO induction motor parameter estimation techniques*, IEEE Trans. on Energy Conversion, vol.18, No.2, pp. 271- 283, 2003.
- [15]. *******, *IEEE Standard Test Procedure for Polyphase Induction Motors and Generators*, IEEE Standard 112, 1996.

INDEX OF AUTHORS

- A**
ANDRIS A., 63
ARAD .S., 81, 89
- B**
BOGANFFY L., 115, 131
BURIAN S., 53, 63
- C**
COLDA C., 63
CSASZAR T., 63
- D**
DARIE M., 63
- F**
FOTAU D., 53
- G**
GABOR D., 27
- J**
JURCA A., 27
- L**
LUPU L., 27
- M**
MAGYARI M., 53
- MARCU M.D., 39
MOLDOVAN L., 53
- P**
PANA L., 15, 39
PATRASCOIU N., 105
PAUN F.A., 27
POPESCU F.G., 15
- R**
RAD M.D. 53
ROSULESCU C., 105
RUS C., 105
- S**
SAMOILA B.L., 45, 81, 89
STOCHITOIU M.D., 35, 45, 97
STOICUTA O., 115, 131
- T**
TIRIAN G.O., 5
- U**
UTU I., 35, 45, 97
- Z**
ZHAO Q., 71

REVIEWERS:

Susana Arad PhD.
Emilian Ghicioi Ph.D
Marius Marcu PhD.
Nicolae Pătrășcoiu PhD.
Liliana Samoila PhD.
Olimpiu Stoicuta PhD.
Ilie Uțu PhD.
Dragoș Păsculescu PhD.
Florin Gabriel Popescu Ph.D